

The Power of the Sea: Tsunamis and Rogue Waves

G14DIS = MATH4001

Mathematics 4th Year Dissertation

2022/23

School of Mathematical Sciences

University of Nottingham

Doug Lawes

Supervisor: Dr. Anna Kalogirou

Assessment type: Review

I have read and understood the School and University guidelines on plagiarism. I confirm that this work is my own, apart from the acknowledged references.

Abstract

This review covers the most prevalent physical models for both rogue waves and tsunamis; namely the Korteweg-de Vries Equation, its two-dimensional analogue the Kadomtsev-Petviashvili Equation, and finally the Nonlinear Schrödinger Equation. The main focal points of this paper are to investigate the efficiency of each model according to predictions, the effect of including realistic parameters such as surface tension, and finally finding the optimal angle of intersection of two solutions and their resulting amplification and probability of wave occurrence. Solutions to these equations will appear in two different forms, the first being the line-soliton solutions representing long and straight wavefronts which intersect to cause large amplitude regions, which will be the basis for the maximal angle portion; and the second solution forms called the lump-soliton solutions, which are more localised solitary humps in space that can be portrayed using varying representations as will be shown here, and will be the focal point of the surface tension portion. Methods which will be used to attain these solutions vary from analytical analysis, numerical analysis using the Fourth Order Runge-Kutta method, and further nuanced methods such as Hirota's Bilinear Method for solving non-linear PDE's. The latter of those methods is found to be the best form to represent solutions and so reach the goals of the report, in that the amplification term is isolated, so the maximal angle can be attained for the KP equation, and corroborated with an equivalent method for the NLS equation. It is also ideal for representing surface tension, where incorporating tension as a force is shown to be insufficient, while certain solution ansatz for Hirota's method provide a better match to wave tank experiments. The report will end with an overview of the most popular statistical models for rogue wave occurrences, most notably the Benjamin-Feir Index that arises from the Nonlinear Schrödinger Equation, its application to the excess kurtosis parameter, and the different probability distributions that apply to rogue waves,.

Contents

1	Introduction	3
2	Modelling Waves	6
2.1	Vorticity Equation	7
2.2	Potential Flow Theory	8
2.3	Linearisation and the Dispersion Relation	10
3	The KdV Equation	14
3.1	Non-dimensionalisation	14
3.2	Multiple Scales	16
3.3	Standard Form and Surface Tension	18
3.4	Solitons	20
3.5	KdV Using Runge-Kutta	31
3.6	Hirota's Bilinear Method for KdV	39
4	The KP Equation	49
4.1	Derivation	49
4.2	Line-Soliton Solutions for the KP Equation	51
4.3	Choosing Appropriate Soliton Vectors	55
4.4	Angle of Maximum Amplification	65
4.5	Breather Solitons	74
4.6	Application of KdV-Type Systems to the Real World	83
5	The Nonlinear Schrödinger Equation	86
5.1	Linear Schrödinger Equation: The Inverse Scattering Transform	89
5.2	Rogue Waves as NLS Solutions	90
5.3	Statistical Analysis	94
5.4	Probability Distributions	95
5.5	Benjamin-Feir Index for One-Dimensional NLS	97
5.6	Benjamin-Feir Index for Two Interacting NLS Solitons	100

5.7 Two-Dimensional NLS	102
6 Conclusions	105
A Modifications to Referenced Code	108
A.1 KdV Solitons Using Fourth Order Runge-Kutta (MatLab)	108

1 Introduction

Tsunamis and rogue waves are waveforms caused by different physical phenomena, such as earthquakes, volcanic eruptions and changes in wind direction, to name a few. Tsunamis are long waves that propagate under the water's surface, and travel far distances without changing shape along the way. These waves are relatively shallow away from the coastline, but they "break" against angled beachfronts, where conservation of mass causes the underwater wave to increase considerably in amplitude, which is called wave shoaling. Rogue waves on the other hand, are narrower, more localised instabilities which propagate on the water's surface, and are caused by the superposition of wind-generated waves. The exact definition of a rogue wave involves considering other waves in the same locale and time, where it is specifically a wave that reaches heights of over twice the mean of the largest waves around it. This, coupled with being propagated on the water's surface, makes rogue waves far more dangerous than tsunamis in deep-water environments, which gives sufficient reason to create physical and statistical models to predict when and how these waveforms will occur.

To motivate the idea of how research in this field is profoundly important, models such as these can be used to predict what events, such as the Boxing Day Tsunami of 2004, would look like in outer-sea environments, and can potentially be used in correlation with coastal management initiatives to mitigate the effect of these events. In the case of rogue waves, the most famous example of the Draupner wave, that occurred at the Draupner Oil Platform in the North Sea, was detected and cited in many sources to have had an amplitude of over 20 metres tall in a sea state with a significant wave height (top 4th standard deviation of waves) of 12 metres, which can be very dangerous for the crew manning the platform if they are unaware of when a rogue wave may strike. Therefore models such as these are vital to the engineering of safe and permanent deep-sea structures.

The aim of this report is to investigate the most common mathematical methods used to model these events to gain a greater understanding of them and how to detect situations when and where they are likely to arise. This is done by introducing the most widely used, rather than most effective, models and investigating their shortcomings to provide motivation for further exploration of more niche models for different circumstances.

In an ideal world, one could take general equations in fluid dynamics, such as conservation of mass on a moving boundary, Euler's equation for inviscid (non-viscous) water flow, and apply these onto a general rotational system which takes all external forces into account. However, this would yield an overly general modelling system that may be too difficult to solve using current methods, and goes into unnecessary detail for a given scenario.

Therefore, for a problem as complex as large-scale fluid simulations it is more efficient to break the problem into smaller chunks by taking the defining equations mentioned above and applying a series of assumptions to it to reduce the model to one of a specific scenario, and to gradually peel back the layers and mix and match certain assumptions until an equation relevant to the problem's environment is achieved. The most notable assumptions of this kind are the irrotationality and flat-based system assumptions which are used in the main models to be investigated in the following report, namely the Korteweg-De Vries (KdV) Equation in one spatial dimension, which is the most one of the most famous, yet simplest equations available in the literature. This is then expanded by extending it to two-dimensions by deriving, modifying, then expanding upon it with two further models, known as the Kadomtsev-Petviashvili (KP) Equation as the two spatial-dimension analogue, and certain solutions to the Nonlinear-Schrödinger (NLS) Equation, also in one spatial dimension, but will be extended to two using a system of coupled equations. The primary assumptions used specifically for the KdV system in this paper are the scale ratios of properties of the waves, where wave amplitude is considered to be much smaller than wave depth, called a shallow wave amplitude approximation, and wave depth being much smaller than wavelength, which is the long wavelength approximation. Systems in this paper also use a flat impermeable base and assume irrotationality to simplify the models, despite these being mostly unrealistic assumptions for real world applications. Extensions such as surface tension and dispersion relations are also investigated to give further insight, and solutions for the KdV equation will be found first analytically, then to incorporate surface tension it will be solved numerically using a series of Fourier transforms and the Fourth Order Runge-Kutta method, which gives solutions for the shape of the waveform, known in this field as solitons. Finally, the solutions for KdV and KP will be found using a new analytical method based on a solution ansatz with Hirota's Bilinear Method to solve the equation for

the case of two interacting waves, which produce an interacting soliton referred to as a Lump Soliton. It will be found that when applying a specific solution ansatz in the Hirota method, it produces more realistic surface tension effects according to wave-tank simulations than can be seen by incorporating surface tension using the derived form.

The latter of these methods will then be explored further when solving the KP equation, where interacting solitons for the KP Equation are shown to yield not only the rogue wave solutions expected, but singularity solutions, which are investigated outside of a realistic wave context but give further motivation into how solutions to the KdV and KP equations interact and when the equations differ from reality with specific choices of parameters.

The above solutions are all known as line solitons, since they appear as long straight lines in space that resemble the shape of tsunami waves. To convert these to isolated rogue wave solutions, as they are known to appear spontaneously, it will be shown that one can instead take a specific solution ansatz with periodicity for the KP Equation, and by taking the period to infinity this gives an accurate solution for a rogue wave, called the Breather Wave solution. However, KdV systems aren't applicable in all scenarios, sometimes even to situations which closely match the assumptions of this model, such as the condition of having a flat impermeable base in a shallow water system, and so alternative models such as the NLS Equation here or the Benney-Luke Equations (o.e.) must be used to compare which gives the most accurate solution. Regarding the use of alternate models, the prior introduction of the Hirota method allows for an analytical approach to find the angle of intersection of two waves that gives the maximum amplification, and so this method will be compared to the coupled NLS equation to test whether they correlate well.

To end, it is prudent to accompany an introduction to physical models with an introduction to the statistical models that form the basis of our current methods of predicting the occurrences of rogue waves in particular across many different seas. In this vein, certain predictive parameters have been widely explored in the context of rogue waves, with the most widely-accepted and prevalent being the Benjamin-Feir Index, which is derived from the NLS Equation, and states that if the scale of wave steepness to spectral density correlate well then a rogue wave is likely in that sea state. This parameter will be explored in its relation to the excess kurtosis,

otherwise known as the skew from the standard gaussian distribution, to measure when rogue waves are most likely.

The overall outcome of this report will be to provide a framework to work from for both modelling and predicting rogue waves and tsunamis, and the content covered provides the most used examples in both of those problems, and suggests possible extensions to each according to their shortcomings.

The structure of the report will begin with a section introducing the general background and approach needed to begin wave models, then it will focus on the derivation for the KdV model, with some reference to the Boussinesq model, before leading into surface tension inclusion and a mixture of analytical and numerical line soliton solutions. Afterwards, the KdV model will be extended to the KP equation, with both the line and lump soliton solutions as mentioned prior. The physical models will then be finalised with reference to the NLS equation and its relevant solutions to this field, which forms part of the basis for statistical modelling with the Benjamin-Feir Index resulting from the equation, which will be investigated alongside certain forms of the Weibull distribution in the final section of the report.

2 Modelling Waves

The basis for the derivations of wave modelling systems relies on a consistent set of steps that derive solution forms and relations. The following is a derivation originating from a velocity potential, but other methods without this are available as detailed in short after. The following method is motivated towards deriving the Korteweg-De Vries equation in one-dimensional space, before it can be expanded to two-dimensions in the Kadomtsev-Petviashvili equation, or to deep water systems in the Nonlinear Schrödinger Equation. In regards to future variables, we define x , y , and z to be the spatial variables, with x moving right from the perspective, z down, and later will use y directed out of the page (as per standard convention). A time variable, t , is also used, alongside a velocity vector v , with components u , v and w .

The general derivation will be following the work in books [1, 3] in particular, until the inclusion of surface tension.

2.1 Vorticity Equation

A good start to the derivation is to define vorticity and to show that example solutions that satisfy incompressibility also satisfy irrotationality.

The derivation begins by recalling the conservation of mass ($\frac{\partial \rho}{\partial t} + \nabla \cdot p\mathbf{v} = 0$, from the equation mass = volume \times density, and use Reynold's Transport Theorem) and momentum ($\rho[\frac{\partial \mathbf{v}}{\partial t} + (\mathbf{v} \cdot \nabla)\mathbf{v}] = \mathbf{F} - \nabla\mathbf{P} + \nu\Delta\mathbf{v}$, from force = mass \times acceleration on a moving time boundary) equations, but for KdV the system is simplified down to

$$\nabla \cdot \mathbf{v} = 0$$

$$\frac{\partial \mathbf{v}}{\partial t} + (\mathbf{v} \cdot \nabla)\mathbf{v} = \frac{1}{\rho_0}(\mathbf{F} - \nabla\mathbf{P}) \quad (2.1)$$

Since viscosity is negligible on inertial pressure scales, and density is assumed to be a constant $\rho(x, t) = \rho_0$. The other terms refer to fluid velocity $\mathbf{v}(x, t)$, pressure \mathbf{P} and external force \mathbf{F} .

Now supposing that the force is predominantly gravitational, so that $\mathbf{F} = (0, 0, -g\rho)$; then one can write the force as a potential $\mathbf{F} = -\nabla U$ then all terms on the right hand side can be grouped under the grad operator, and using $(\mathbf{v} \cdot \nabla)\mathbf{v} = \frac{1}{2}\nabla(\mathbf{v} \cdot \mathbf{v}) - \mathbf{v} \times (\nabla \times \mathbf{v})$ one can substitute that into the above equation and take the curl ($\nabla \times$) of it to give $\frac{\partial \omega}{\partial t} - \nabla \times (\mathbf{v} \times \boldsymbol{\omega}) = 0$, where $\boldsymbol{\omega} = \nabla \times \mathbf{v}$ for shorthand. Then finally use $\nabla \times (\mathbf{F} \times \mathbf{G}) = (\mathbf{G} \cdot \nabla)\mathbf{F} - (\mathbf{F} \cdot \nabla)\mathbf{G} + (\nabla \cdot \mathbf{G})\mathbf{F} - (\nabla \cdot \mathbf{F})\mathbf{G}$ to get

$$\frac{\partial \boldsymbol{\omega}}{\partial t} = (\boldsymbol{\omega} \cdot \nabla)\mathbf{v} - (\mathbf{v} \cdot \nabla)\boldsymbol{\omega} \quad (2.2)$$

In lieu of using the material derivative notation.

This is the vorticity equation, which describes how the rotationality parameter $\boldsymbol{\omega}$ varies with time from an initial state, which we will use to show that we can sustain a system with no rotationality at any time.

2.2 Potential Flow Theory

Now one approach, as on page 100 in [1], is to define a velocity potential $\phi(x, y, t)$ as in $\mathbf{v} = \nabla\phi$ to construct the boundary conditions, and uses asymptotic expansions from there to derive the KdV equation. We do this since taking the curl of the velocity potential to get the rotationality means taking the curl of the grad operator, which is 0, so the solution is initially irrotational and since the velocity potential can also be plugged into the vorticity equation 2.2 for $\omega = 0$ as a solution, one can observe a property that no change in vorticity ω can occur, so solutions remain irrotational permanently. In relation to real world dynamics, this is unrealistic as there is rarely a case without some vorticity, but it is usually negligible for purely surface wave models when compared to the other defining characteristics, so models can safely ignore it.

Substituting this potential approximate solution into the incompressibility condition 2.1 gives the Laplacian, by divergence of the grad operator

$$\nabla \cdot \nabla\phi = \nabla^2\phi = 0 \quad (2.3)$$

This is the defining equation that will be carried forward throughout the calculations, but we require boundary conditions to solve it.

Now, assuming the system has a flat, impermeable base at $z = -h$, such that the upper limit of the flow is $z = \eta(x, y, t)$ around $z = 0$, as shown in:

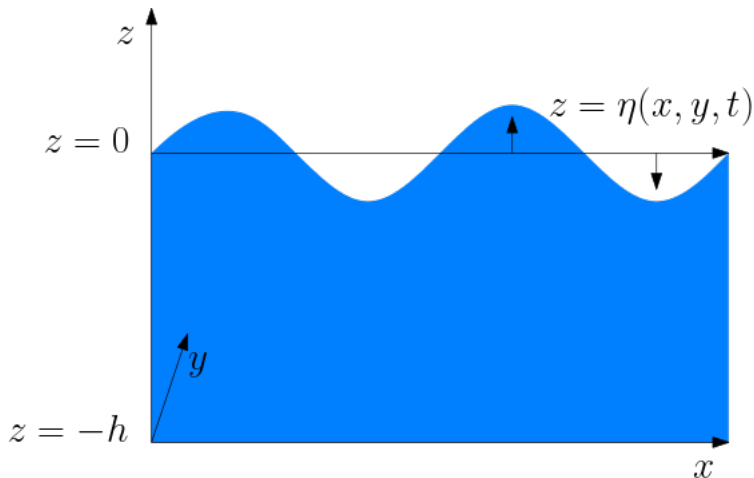


Figure 1: Plot of height (z) against x spatial dimension

Then from this, impermeability implies

$$\mathbf{u} \cdot \hat{\mathbf{z}} = w = \frac{\partial \phi}{\partial z} = 0 \quad (2.4)$$

At the base, which could be extended to being a no-slip condition by including that fluid particles cannot move horizontally when negligibly close to the base, but this is an unnecessary assumption for our system.

The change to using a velocity potential also means the second equation in 2.1 can be written as each term underneath the ∇ operator, by the commutivity of grad and derivatives.

$$\frac{\partial \phi}{\partial t} + \frac{1}{2}||v||^2 + \frac{\mathbf{U} + \mathbf{P}}{\rho_0} = v \times \omega \quad (2.5)$$

On the free surface at $z = \eta$, where the second and right hand side terms come from the prior vector identity $(v \cdot \nabla)v$, where taking the dot product of v on the left side eliminates the right hand side term, and one notes that $u \cdot \nabla H$ for H as the above term means H is conserved along streamlines.

Therefore integrating this out leaves a spatially independent term $f(t)$, which can be eliminated by adding a spatially independent term to ϕ , which is permitted by $\mathbf{v} = \nabla\phi$ only retaining spatial terms. Next, assuming that buoyancy is the dominant force means $\mathbf{F} = -\nabla(\rho_0 g z)$, with reference pressure $\mathbf{P} = 0$ to give

$$\frac{\partial \phi}{\partial t} + \frac{1}{2}||\nabla\phi||^2 + g\eta = 0 \quad (2.6)$$

Which is the Bernoulli boundary condition.

The final relation is the conservation of $z - \eta$, so taking the material derivative simply gives

$$w = \frac{\partial \phi}{\partial z} = \frac{\partial \eta}{\partial t} + \mathbf{v} \cdot \nabla \eta \quad (2.7)$$

which is the Kinematic boundary condition on the free surface.

In summary, the boundary conditions shown above, and as they appear in [1], are as follows:

$$\text{Incompressibility: } \nabla^2 \phi = 0$$

$$\text{No Penetration: } \frac{\partial \phi}{\partial z} = 0$$

$$\text{Bernoulli: } \frac{\partial \phi}{\partial t} + \frac{1}{2} \|\nabla \phi\|^2 + g\eta = 0$$

$$\text{Kinematic: } w = \frac{\partial \phi}{\partial z} = \frac{\partial \eta}{\partial t} + \mathbf{v} \cdot \nabla \eta$$

The goal from this point onwards is to find an equation with dependent variable η to represent the shape of the waveform, which we will achieve by asymptotic expansions of the wavespeed-adjacent parameter ϕ . To do this, one must change to a non-dimensional system, but firstly it is possible to derive interesting relations between the time and spatial parameters using Fourier modes, which will be a recurrent transformation in the following material.

2.3 Linearisation and the Dispersion Relation

The prior system can be simplified when examined at the leading order of asymptotic expansions, so starting with $\phi(x, y, \eta, t)$ Taylor expanding in powers of η around $z = 0$ and then subbing into equations 2.6 and 2.7 for small perturbations $\eta \ll 1$ and $\|\nabla \phi\| \ll 1$ to give $\frac{\partial \phi}{\partial t} = -g\eta$ and $\frac{\partial \eta}{\partial t} = \phi_{0z}(x, y, t)$ around $z = 0$, where ϕ_0 refers to the leading order of the asymptotic expansion.

Now one can try a converting the solution to Fourier modes using $\phi = C(k, l, z, t)e^{ikx+ily}$ where k and l refer to scalings in the x and y directions respectively in Fourier space, and can be grouped together under $\kappa^2 = k^2 + l^2$. Substituting this solution into the Laplace equation gives the solution $C = C'(k, l, t) \cosh[\kappa(z + h)]$ which is translated so that the sinh component that would've resulted from the substitution is necessarily 0 by the no slip condition on $z = -h$.

Next, assuming η takes a similar exponential form to ϕ and substituting that into equations 2.6 and 2.7 gives equations involving hyperbolic trigonometric terms, which can be combined by taking derivatives and substituting one equation into the other to give $\frac{\partial^2 D}{\partial t^2} + g\kappa \tanh(\kappa h)D = 0$

where $D(k, l, t)$ is the coefficient of the exponent in the general solution for η , similar to that of the general solution to ϕ .

Finally, assuming $D(k, l, t) = D(k, l, 0)e^{-i\omega t}$, which uses separation of variables to take the time part out, gives the dispersion relationship ([1])

$$\omega^2 = g\kappa \tanh \kappa h \quad (2.8)$$

Where the size of $g\kappa$ determines whether this models shallow or deep water systems. This also has a leading order expansion of $\omega^2 = gh\kappa^2$, which is the wavespeed for a shallow system, which will be revisited.

2.3.1 Properties of the Dispersion Relation

As an aside to the main models, the dispersion relation equation 2.8 describes how the wave frequency mode ω varies in terms of the wavenumber mode k in the x direction through the Fourier transformation. Using the aforementioned dispersion relationship, where $\frac{\omega}{k} = \sqrt{gh}$, one can note that this has dimensions of MT^{-1} , so is velocity. This is what is known as the phase velocity, which is the velocity of the wavefront in the direction of motion (horizontal on a wave diagram). To calculate this, one can simply divide the dispersion relationship by κ (two-dimensional analogue to the aforementioned k wavenumber, as above) to give

$$\frac{\omega}{\kappa} = \sqrt{\frac{g \tanh \kappa h}{\kappa}} \quad (2.9)$$

However there is another velocity of concern, known as the group velocity. Take, for example, the method given in book [58] that follows the sum of two cosine waves, $a_1 \cos(\chi_1) + a_2 \cos(\chi_2)$ where a_i are amplitudes and $\chi_i = k_i x - \omega_i t + \alpha_i$ for phase shift α_i . Now the sum can be simplified to the form $a \cos(\chi - \theta)$ for shift θ collecting the α_i 's and $\chi = kx - \omega t$ for k and ω as the average of the k_i 's and ω_i 's, by using the trigonometric identity $\cos(A) + \cos(B) = 2 \cos\left(\frac{A+B}{2}\right) \cos\left(\frac{A-B}{2}\right)$. Now book [58] follows by writing each χ_i as a displacement from χ with terms Ω_i to find the new parameters a and θ for a new modulated wave system with $\Omega_1 - \Omega_2 = \chi_1 - \chi_2$, where the individual waves move with a velocity given by the average

ω 's and k 's in $\frac{\omega}{k}$, but that the envelope moves with a velocity given by $\frac{\omega_1 - \omega_2}{k_1 - k_2} = \frac{d\omega}{dk}$, which is coined the group velocity, which defines how the sum of the waves evolves as time progresses. This is relevant in sea states where the context is waves are formed by the superposition of many underlying wavefronts that move at different rates. This becomes clear in the scenario where the component waves have the same amplitudes ($a_1 = a_2$), and so the superposition wave equation becomes

$$2a_1 \cos\left(\frac{1}{2}(\Delta kx - \Delta \omega t)\right) \cos(kx - \omega t).$$

The two terms, called phase and group velocities, refer to the velocities of points stationary in horizontal displacement and displacement from the wave equilibrium respectively. In real world terms this is similar to the difference between a surfer and a buoy, where both move with velocity imparted by the waves, but in different directions. To calculate the group velocity, the dispersion relation can therefore be differentiated in terms of κ to give the change in frequency depending on wavenumber (group velocity moving vertically), giving

$$\begin{aligned} \frac{\partial \omega}{\partial \kappa} &= \frac{\partial}{\partial \kappa} \sqrt{g\kappa \tanh \kappa h} = \frac{g}{2\sqrt{g\kappa \tanh \kappa h}} (\tanh h\kappa + h\kappa \operatorname{sech}^2 h\kappa) \\ &= \frac{g \tanh \kappa h}{2\sqrt{g\kappa \tanh \kappa h}} \left(1 + h\kappa \frac{1 - \tanh^2 h\kappa}{\tanh h\kappa} \right) = \frac{\sqrt{g \tanh \kappa h}}{2\sqrt{\kappa}} \left(1 + h\kappa \frac{\cosh^2 h\kappa - \sinh^2 h\kappa}{\sinh h\kappa \times \cosh h\kappa} \right) \\ &= \frac{c_{\text{phase}}}{2} \left(1 + 2h\kappa \frac{1}{\sinh 2h\kappa} \right). \end{aligned}$$

When investigating waves of relevant magnitude to this paper, an assumption will be made in section 3.1 that waves are shallow compared to their wavelength, and have wavespeed \sqrt{gh} for water depth h . This is of the order $\frac{h}{\lambda} < 0.05$.

This assumption is exclusively valid for shallow waves however, as deep waves have a similar relation for when $h > \frac{\lambda}{2}$ for λ as the wavelength, which follows $\sqrt{\frac{g\lambda}{2\pi}}$ for the deep water phase velocity, and half that for the group velocity. This difference means that water particles act more oscillating around the equilibrium level than travelling with the wave, which means the resultant speed of the wave is lower. Therefore, plotting the general wavespeed against the water depth, scaled by the wavelength, for both phase and group velocities (using their inter-

mediate functions found above) gives a visualisation of shallow and deep water approximations relative speeds, and one can rescale the wavespeed by respective shallow and deep approximations to get a gradient close to 0 in their respective regions, since they have constant values there, but interesting relations elsewhere. For example, when scaling wavespeed by the shallow wavespeed approximation (taking the limit as h tends to 0), one gets the following figure:

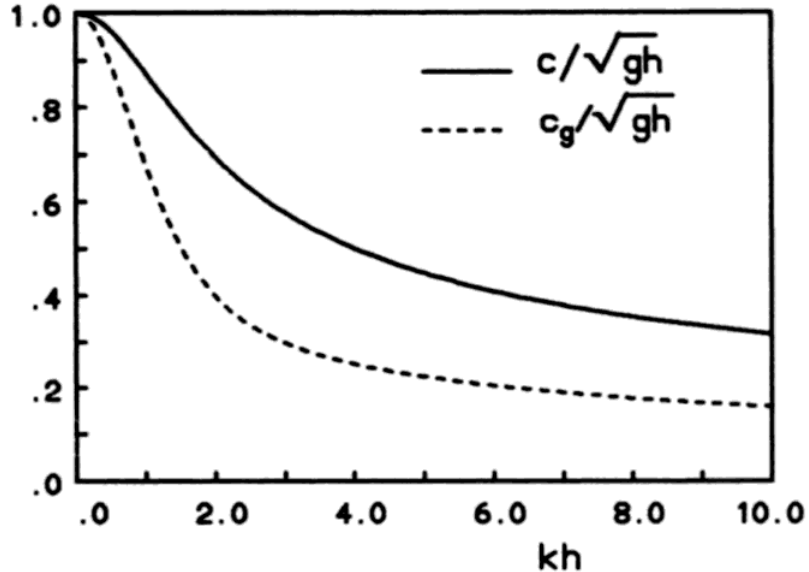


Figure 2: Plot from book [58] of depth-to-wavelength ratio against wavespeed with shallow water scaling

Where the velocities are equal to the shallow water velocity where $h \ll \lambda$, but increasing κh increases this ratio of depth to wavelength, and so this clearly shows how the phase velocity is greater than the group velocity for all water depth ratios, but that group velocities are proportional up to a limit until the ocean depth increases to a certain proportion of the wavelength, where the wavespeed starts relatively levelling off, while phase velocities remain less affected.

This is an example of how water depth has a substantial effect on the velocity of water waves, both in propagation and in amplitude, which will feature more in comparisons between the shallow-water KdV-like systems when compared to the deep-water Nonlinear Schrödinger equation.

3 The KdV Equation

From now on, assumptions will be made that pertain only to the KdV derivation and extensions (such as the modified mKdV and Benjamin-Bona Mahoney equations), but the general method can and will be applied in the derivation of the KP equation later.

3.1 Non-dimensionalisation

To proceed, one must choose appropriate scalings for each variable. As suggested in [1], these can be

$$x = \lambda_x x', \quad y = \lambda_y y', \quad z = hz', \quad t = \frac{\lambda_x}{c_0} t', \quad \eta = a\eta', \quad \phi = \frac{\lambda_x g a}{c_0} \phi'$$

where $c_0 = \sqrt{gh}$ is the shallow water wavespeed, λ is the wavelength parameter and a is a dimensional amplitude parameter. The prime notation will be omitted for brevity. This allows for the relative sizes of each variable to be compared, and leads into the three defining restrictions of the KdV equation, given by

$$\begin{aligned} \text{Amplitude } \ll \text{Depth : } \epsilon &= O\left(\frac{a}{h}\right), \\ \text{Propagation } \lambda \ll \text{Transverse } \lambda : \quad \delta &= O\left(\frac{\lambda_x}{\lambda_y}\right), \\ \text{Depth } \ll \text{Wavelength : } \mu &= O\left(\frac{h}{\lambda_x}\right) \end{aligned} \tag{3.1}$$

which are assumptions that these are shallow waves that propagate further in the x direction than y , but that they are of small amplitude (relative to water depth) allows for us to assume that each parameter is very small. The second point also allows us to negate waves in the y direction and assume they are unidirectional, which we will remove later but provides a simpler

system of equations to solve. This overall leads to the system of equations:

$$\text{Laplace: } \epsilon\phi_{xx} + \phi_{zz} = 0, \quad -1 < z < \epsilon\eta$$

$$\text{No Penetration: } \phi_z = 0, \quad z = -1$$

$$\text{Bernoulli: } \phi_t + \frac{\epsilon}{2} \left(\phi_x^2 + \frac{1}{\epsilon} \phi_z^2 \right) + \eta = 0, \quad z = \epsilon\eta$$

$$\text{Kinematic: } \epsilon(\eta_t + \epsilon\phi_x\eta_x) = \phi_z, \quad z = \epsilon\eta$$

As now z has been re-dimensionalised to be at a minimum at $z = -1$.

Notably we will also assume that small terms such as nonlinearity and dispersion are of the same order of magnitude for our calculations, which is portrayed by the relation $\epsilon = \mu^2$ from now on. The choice of a quadratic relation is a general one used for KdV systems, and will be revisited later, but for now the primary concern is that they are a similar order of magnitude. Now taking an asymptotic expansion of ϕ in powers of small parameter epsilon by $\phi = \phi_0 + \epsilon\phi_1 + O(\epsilon^2)$, and substituting into the Laplace equation gives $\phi_{0zz} = 0$ at leading order, where ϕ_0 is the leading order term of ϕ . This implies $\phi_0 = A + B(z+1)$ for some A and B as functions of x and t . However, writing it in this form allows for substituting the no penetration condition to say $B = 0$ necessarily.

The same can be repeated for order ϵ , where $\phi_{1zz} = -A_{xx}$ to get $\phi_1 = -A_{xx} \frac{(z+1)^2}{2}$, where constant terms are grouped with the leading order term. This shows the start of an expansion for ϕ that can be substituted first into the Bernoulli condition above to get

$$\eta = -A_t + \frac{\epsilon}{2}(A_{xxt} - A_x^2)$$

which gives the leading order relation $\eta' = -A_{t'}$ which will be used later to convert from the speed-adjacent parameter A to a spatial parameter η . Repeating for the Kinematic condition gives

$$\epsilon\eta_t + \epsilon^2\eta_x A_x = -\epsilon A_{xx}(1 + \epsilon\eta) + \frac{\epsilon^2}{3!} A_{xxxx}$$

both up to the first two orders of ϵ .

This gives two equations relating the leading order term of ϕ and η , so can substitute the Bernoulli equation into the Kinematic equation, reduce to leading orders and rearrange to give an equation only dependent on A , called the Boussinesq equation ([1]):

$$\text{Boussinesq: } A_{tt} - A_{xx} = \epsilon \left(\frac{A_{xxtt}}{2} - \frac{A_{xxxx}}{6} - 2A_x A_{xt} - A_{xx} A_t \right) \quad (3.2)$$

Where the first two terms can be grouped into $\frac{A_{xxxx}}{3}$ term by observing the equation at $O(1)$, $A_{tt} = A_{xx} + O(\epsilon)$, and substituting that back into equation 3.2.

This is a fourth order equation in the parameter A , which is the leading order component of ϕ , which itself was the velocity potential of v . This means the equation still needs to be converted to the spatial parameter η .

Using the substitution $\frac{\partial A}{\partial x} = u$, one can take an x derivative of the Bernoulli equation and substitute it into the Kinematic equation to simplify the terms and get some relations $\eta_x = -u_t + O(\epsilon)$ and $\eta_t = -u_x + O(\epsilon)$. These can be used to find the conversion parameter between u and η to be $u = -\int_{-\infty}^x \eta_t dx'$, which shows how the equation itself will contain unknown integrals, and hence becomes quite difficult to solve. Milewski ([26]) continued with the Bernoulli equation, and found solutions to be of the form $u_x = a \operatorname{sech}^2(\kappa(x - ct))$ for κ as the wavenumber parameter and wavespeed c given by $c^2 = 1 - 4(B - \frac{1}{3})\kappa^2$ for parameter $B = \frac{\gamma}{h^2}$ called the Bond number that relates to low ($B < \frac{1}{3}$) and high ($B > \frac{1}{3}$) surface tension in relation proportional to depth squared. We will revisit this later for the introduction to surface tension for the KdV equation.

We will however not consider the Boussinesq model further, and will instead take the unidirectional equivalent model for the KdV equation, which gives a much simpler defining equation and provides a similar solution form to the Boussinesq equation.

3.2 Multiple Scales

Further assuming an asymptotic expansion now for A in powers of ϵ and subbing that into the modified equation 3.2, gives the wave equation at leading order, which means it retains

the general solution $A_0 = F(\xi, T) + G(\zeta, T)$ for $\xi = x - t$, $\zeta = x + t$ and $T = \epsilon t$ as a time rescaling.

This change of variables also changes the derivatives, as can be shown using the chain rule $\partial_t = -\partial_\xi + \partial_\zeta + \epsilon \partial_T$ and $\partial_x = \partial_\xi + \partial_\zeta$. This can be subbed into the modified equation 3.2 with the asymptotically expanded A to get the equation:

$$-4A_{1\xi\zeta} = 2(F_{\xi T} - G_{\zeta T}) + \frac{1}{3}(F_{\xi\xi\xi\xi} + G_{\zeta\zeta\zeta\zeta}) + 3 \left(F_\xi F_{\xi\xi} + \frac{1}{3}F_{\xi\xi}G_\zeta - \frac{1}{3}G_{\zeta\zeta}F_\xi - G_\zeta G_{\zeta\zeta} \right) \quad (3.3)$$

For A_1 as the coefficient of $O(\epsilon)$ in the asymptotic expansion of A . This equation can be integrated to get the KdV style equations in dimensional form. However, integrating this gives rise to secular terms (terms in the expansion at a higher order of ϵ that cause a singularity in the solution as they grow with time), and so by making the coefficients of these terms equal to 0, this gives rise to two KdV style equations.

$$2F_{\xi T} + \frac{1}{3}F_{\xi\xi\xi\xi} + 3F_{\xi\xi}F_\xi = 0 \quad (3.4)$$

$$-2G_{\zeta T} + \frac{1}{3}G_{\zeta\zeta\zeta\zeta} + 3G_{\zeta\zeta}G_\zeta = 0 \quad (3.5)$$

For KdV, we only deal with motion in one dimension, and so only require the first of the above equations which is for right moving waves, but one could equally take only the left moving wave equation in isolation and achieve an equivalent KdV equation.

The final step is to re-dimensionalise the right moving equation given above by reversing the changes of relevant variables, which were $\xi = x' - t'$ and $T = \epsilon t'$ by re-introducing the prime notation.

Using $F_{\xi t'} = -F_{\xi\xi} + \epsilon F_{\xi T}$ and $F_{\xi x'} = F_{\xi\xi}$, both using chain rule, equation 3.4 becomes

$$2(F_{\xi t'} + F_{\xi x'}) + \epsilon \left(\frac{1}{3}F_{\xi x' x' x'} + 3F_\xi F_{\xi x'} \right) = 0$$

Remembering that F is the right moving part of the travelling wave solution for the leading order component of the linear term in the asymptotic expansion of the velocity potential ϕ .

Now using the relation $\eta' = -A_{t'}$ found in the initial non-dimensionalisation using the Bernoulli

equation, this gives $\eta' = F_\zeta$, and can use the previous set of rescalings defined at the start of section 3.1 and the chain rule on derivatives to transform the equation into

$$2 \left(\frac{\lambda_x \eta_t}{c_0 a} + \lambda_x \frac{\eta_x}{a} \right) + \epsilon \left(\frac{\lambda_x^3}{3a} \eta_{xxx} + \frac{3\lambda_x}{a^2} \eta \eta_x \right) = 0$$

Then multiplying through by $\frac{a}{\lambda_x}$ and reversing the approximation $\epsilon = O(\frac{a}{h})$ also used in 3.1 gives the non-linear KdV equation ([1])

$$\frac{1}{c_0} \eta_t + \eta_x + \frac{h^2}{6} \eta_{xxx} + \frac{3}{2h} \eta \eta_x = 0 \quad (3.6)$$

This is the generic dimensional form of the KdV equation, which can be solved as it is to give sufficient solutions, but it isn't the most common form of presenting the KdV equation. This is because it can be written more succinctly in non-dimensional form, which gives equally as viable solutions, and will be explored in the next section.

3.3 Standard Form and Surface Tension

Incorporating surface tension causes a change in the Bernoulli boundary condition 2.6, with the term $\frac{T}{\rho} \nabla \cdot \frac{\nabla \eta}{\sqrt{1+|\nabla \eta|^2}}$ added to the right hand side since it is an inclusion of an extra force component to the existing gravitational force $\mathbf{F} = -\nabla(\rho_0 g z)$. The term T is the surface tension coefficient, and ρ refers to the density. Expanding the derivative and keeping only terms that are relevant up to $O(\epsilon)$ gives the added term as $\frac{T}{\rho} (\eta_{xx} + \eta_{yy})$, where following the same method from section 2.3 onwards gives the same outcome but with a coefficient (often referred to as γ) that incorporates the original $\frac{h^2}{6}$ coefficient in equation 3.6 with an added $\frac{-T}{2\rho g}$ term.

Therefore, the final form for the dimensional KdV equation ([1]) is

$$\frac{1}{c_0} \eta_t + \eta_x + \gamma \eta_{xxx} + \frac{3}{2h} \eta \eta_x = 0 \quad (3.7)$$

for $\gamma = \frac{h^2}{6} - \frac{T}{2\rho g} = \frac{h^2}{6}(1 - 3\hat{T})$ with $\hat{T} = \frac{T}{\rho g h^2}$. Setting $\gamma > 0$ gives low surface tension, and is when the \hat{T} term is close to 0 ($< \frac{1}{3}$) and high surface tension is when $\gamma < 0$, so when \hat{T}

increases (above $\frac{1}{3}$).

This can be simplified to a standard form of the KdV equation by applying a moving coordinate $\zeta = x - c_0 t$, $t = t'$, and the chain rule with $\partial_x = \partial_\zeta$ and $\partial_t = \partial_{t'} - c_0 \partial_\zeta$ to eliminate the $\partial_x \eta$ term using the chain rule expansion of the η_t term, since these terms become $\frac{1}{c_0} \eta_{t'} - \frac{c_0}{c_0} \eta_\zeta + \eta_\zeta = \frac{1}{c_0} \eta_{t'}$ (a dimensionalisation that retains this term will be referenced later, but in most cases it is removed for brevity). Next, a simple non-dimensionalisation of the displacement term η using $\eta = k_1 u$ and $\zeta = k_2 \zeta'$ leads to

$$u_{t'} + \left(\frac{h^2 c_0}{6k_2^3} - \frac{T c_0}{2\rho g k_2^3} \right) u_{\zeta' \zeta' \zeta'} + \frac{3c_0 k_1}{2hk_2} uu_{\zeta'} = 0 \quad (3.8)$$

Where the coefficients of each term can be set to whatever constant is required for that form, as long as it is consistent among them. Thus, to get the KdV equation with a dependence on the surface tension term γ , one possibility is to set $\frac{h^2 c_0 \rho g - 3T c_0}{6k_2^3 \rho g} (= \frac{\gamma c_0}{k_2^3}) = 1$ to find rescaling parameters k_i which achieve the aim, and set the coefficient of the triple-spatial derivative term accordingly. This means that the sign of γ affects the choice of parameter k_2 , and hence also affects the coefficient of the non-linear term. Therefore setting the other coefficient to be $\frac{3c_0 k_1}{2hk_2} = 6(1 - \psi)$ for $\gamma > 0$ (low surface tension) means when setting $\gamma < 0$ (high surface tension) that the coefficient changes sign. Therefore $k_2 = \sqrt[3]{\gamma c_0}$ to give the completed KdV system

$$u_{t'} + 6(1 - \psi)uu_{\zeta'} + u_{\zeta' \zeta' \zeta'} = 0 \quad (3.9)$$

With rescaling parameters $\zeta = \sqrt[3]{\gamma c_0} \zeta'$ and $\eta = \frac{4(1-\psi)h\sqrt[3]{\gamma c_0}}{c_0} u$.

Setting $\psi = 0$ results in the standard KdV equation with no surface tension, and for the case of $\gamma < 0$, choosing a $\psi = \hat{\psi} > 1$ will make these effects more pronounced the larger the magnitude of $\hat{\psi}$, since $\gamma < 0$ means $k_2 < 0$ where k_1 is unaffected, so $\psi > 1$ to make $1 - \psi < 0$. A standard value for ψ with surface tension included is $\psi = 2$ to make the coefficient -6 , however we will consider the case of increasing ψ up to 1 only in certain cases. The biggest takeaway from this, is that no surface tension originates from $\psi = 0$, and increasing ψ leads to increasing amounts of surface tension, therefore gradually reducing the size of the coefficient for the uu_x term should in theory represent increasing the amount of surface tension

in the system, which will be important later for numerical solution forms of the KdV equation. An alternate form of surface tension inclusion arises from moving the surface tension defining coefficient to the third-order spatial term, such as in paper [37] where they define the KdV equation under the reference frame $\zeta = x - ct$ to be

$$\eta_t + \frac{3c_s}{2h}\eta\eta_\zeta + \frac{1}{6}c_sh^2\left(\frac{1}{3} - B_0\right)\eta_{\zeta\zeta\zeta} = 0$$

for $B_0 = \frac{\gamma}{\rho gh^2}$, where this γ is relating to the surface tension as before, but is not the same expression, since increasing γ will increase the amount of surface tension, as will be seen later. Notably also, paper [37] quotes the change in the prior dispersion relation when applying surface tension as $\omega^2 = \left(gk + \frac{\gamma k^2}{\rho}\right) \tanh(kh)$ by adding the tension term to the Bernoulli condition from the start, which will be useful for later formulation of solutions using a method known as Hirota's Bilinear Method.

3.4 Solitons

The equation derived above has no purpose if not to be solved for specific boundary conditions. Luckily, the KdV equation yields analytical solutions, known as solitary wave solutions, which give the exact movement of the flow. Using a non-dimensional system similar to 3.9 (but with a simpler surface tension parameter) of the form

$$u_t \pm 6uu_x + u_{xxx} = 0 \quad (3.10)$$

with solutions found by using a moving frame of reference with

$$u(x, t) = f(x - ct) = f(\zeta) \quad (3.11)$$

where, for brevity, the variable $\zeta = x - ct$, is continued.

Next, following the method described in [8] but including the surface tension case, substituting this into the KdV system gives a system of ζ derivatives when using the chain rule with $\partial_t = -c\partial_\zeta$ and $\partial_x = \partial_\zeta$, and hence integrating that system with respect to ζ in the same step

gives

$$-cf \pm 3f^2 + \frac{d^2 f}{d\zeta^2} = A_1 \quad (3.12)$$

as is seen in paper [8], where the integral of $6ff'$ is done with integration by parts. This notably uses complete derivatives in the new variable, and A_1 is a constant of integration independent of ζ , and so is independent of space and time.

Then, to simplify further, one must multiply through by a factor of $\frac{df}{d\zeta} = f'$ so that the product rule can be used. Integrating with this change gives

$$-c\frac{f^2}{2} \pm f^3 + \frac{(f')^2}{2} = A_0 + A_1 f \quad (3.13)$$

Now for a solitary wave solution, $f(\zeta = 0) = 0$, the constants A_i are both = 0, which leaves the system

$$(f')^2 = f^2(c \mp 2f) \quad (3.14)$$

and can be solved by taking the positive root of both sides and using separation of variables with the integral of 1 in terms of ζ on the right-hand side and

$$\int (cf^2 \mp 2f^3)^{-\frac{1}{2}} df \quad (3.15)$$

on the left-hand side, which requires a substitution using a dummy variable s of

$$f = \frac{c \operatorname{sech}^2 s}{2} \quad (3.16)$$

to get a neater solution form in the end.

This substitution means $c \mp 2f = c(1 \mp \operatorname{sech}^2 s) = c \tanh^2 s$ for the negative (no surface tension) case by substitution and trigonometric identities. For the positive (including surface tension) case, one must instead use a dummy variable of $f = -\frac{c \operatorname{sech}^2 s}{2}$, which will be accounted for in the following by the \pm notation. Notably, it is difficult to perform this step for intermediary values of ψ mentioned earlier, so for these we will investigate another solution form that allows the gradual shift of the non-linear coefficient.

By also noting that by the definition, the derivative of f in terms of s is $\mp c \frac{\sinh f}{\cosh^3 f}$, and so performing a change of variables in the integral gives

$$\int \frac{\mp 2}{\sqrt{c}} \frac{\sinh f}{\operatorname{sech}^2 s \tanh f \cosh^3 f} ds \quad (3.17)$$

where all hyperbolic trigonometric terms cancel out to leave just $\frac{\mp 2}{\sqrt{c}}$ in the integrand. Finally executing this integral gives

$$\mp \frac{2}{\sqrt{c}} s = \zeta + x_0 \quad (3.18)$$

using integration constant x_0 , and substituting back in for s , gives

$$f(\zeta) = \frac{c}{2} \operatorname{sech}^2 \frac{\sqrt{c}}{2} (\zeta + x_0) \quad (3.19)$$

for moving variable $\zeta = x - ct$.

Substituting this back into the non-dimensional u form yields the solution:

$$u(x, t) = \pm \frac{c}{2} \operatorname{sech}^2 \left(\frac{\sqrt{c}}{2} (x - ct + x_0) \right) \quad (3.20)$$

With \pm in front due to the symmetry of the sech^2 function, where the negative, or depressive, case will be investigated later in the context of high surface tension systems.

Now regarding the low surface tension case, this equation is in non-dimensional form, so to get the dimensional form, e.g. for $\gamma > 0$ (low surface tension), take the previous non-dimensional form in equation 3.4 and rescale using $\zeta = l_1 \zeta'$, $T = l_2 T'$ and $F_\zeta = l_3 F'_\zeta$ where the prime notation denotes the dimensional form. This gives a KdV type equation with coefficients $\frac{2l_1}{l_2 l_3}$ and $\frac{1}{3l_1^2 l_3}$ for the time and triple spatial dimension derivative terms respectively. Therefore equating these coefficients and setting them equal to $\frac{1}{2}$, which is the rescaling required for equation 3.9, and the reverse of the other rescalings used prior $\zeta = x - t$ and $T = \epsilon t$, and of those in section 3.1, to give the solution given at the start as

$$\eta(x, t) = \frac{ca}{3} \operatorname{sech}^2 \left(\frac{\sqrt{c}}{2} \left(\frac{x}{\lambda_x} - \left(1 + \frac{c\epsilon}{6} \right) \frac{c_0 t}{\lambda_x} \right) - \frac{x_0}{\lambda_x} \right) \quad (3.21)$$

for a as the rescaling parameter of η .

Now using the relations from section 3.1 of

$$\epsilon = O\left(\frac{a}{h}\right), \quad \mu = O\left(\frac{h}{\lambda_x}\right), \quad \text{and} \quad \mu^2 = \epsilon$$

gives the final form [1]

$$\frac{\eta}{h} = \frac{c\epsilon}{3} \operatorname{sech}^2\left(\frac{\sqrt{c}}{2h}\sqrt{\epsilon}\left(x - \left(1 + \frac{c\epsilon}{6}\right)c_0t\right) - x_0\right) \quad (3.22)$$

for approximate wavespeed $c_0 = O(\sqrt{gh})$ but variable. Therefore one can read off the amplitude of the wave by the coefficient of the sech term, which is notably dependent on the wavespeed parameter c , and can be plotted for specific choices of the depth h , typical wave amplitude a in the parameter $\epsilon = \frac{a}{h}$ and the constant of integration x_0 that represents the wave position at $t = 0$.

Therefore choosing these to be $h = 1000$, $\epsilon = 0.01$, $c_0 = \sqrt{gh} \approx 100$ and a simple translation $x_0 = -5000$ gives

KdV Soliton with $h = 1000$, $\epsilon = 0.01$ and $x_0 = -5000$

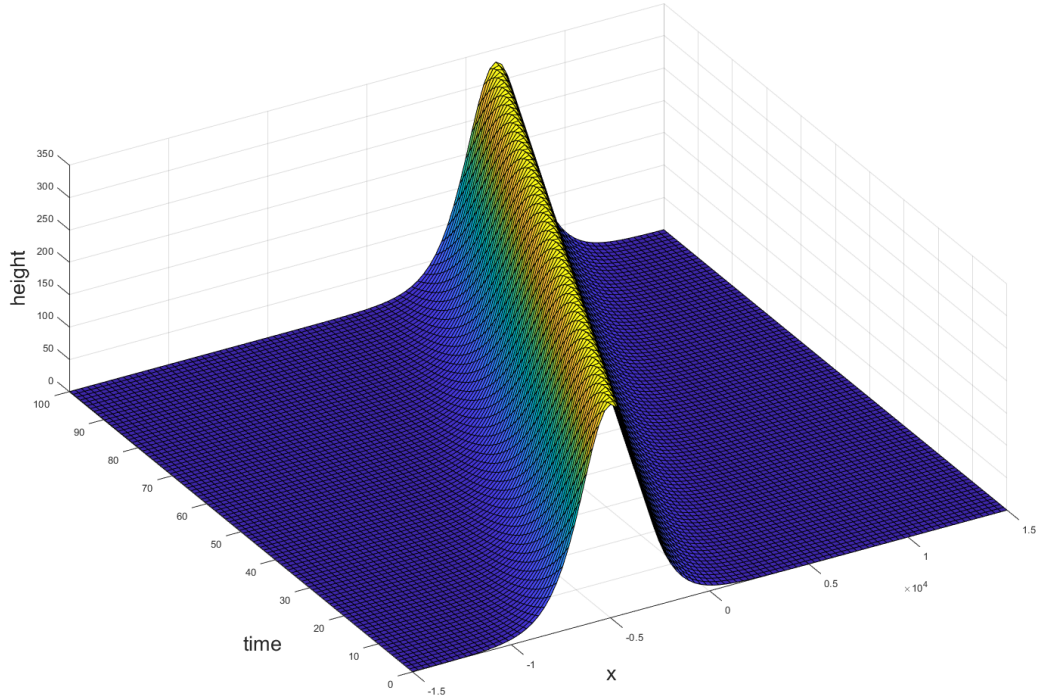


Figure 3: KdV Surface plot of spatial dimension x , time and height of the wave

Which shows how the wavefront evolves as time increases. Notably, the envelope of the wave before and after the peak is a smooth transition with the equilibrium, which isn't exactly what is expected for a typical wave, where there is usually a dip caused by the surface tension, but it is still a worthwhile representation of tsunami wave formations.

The parameters chosen affect different areas of the model, where the choice of wavespeed affects how far the wave travels in a given time, and also faster moving waves have a larger amplitude due to increased force, as is evidenced by the amplitude (the coefficient of the sech^2 function) being solely dependent on wavespeed c . This can be shown in the following representations with increased and decreased wavespeed

KdV Soliton with $h = 1000$, $\epsilon = 0.01$, $c_0 = 150$ and $x_0 = -5000$

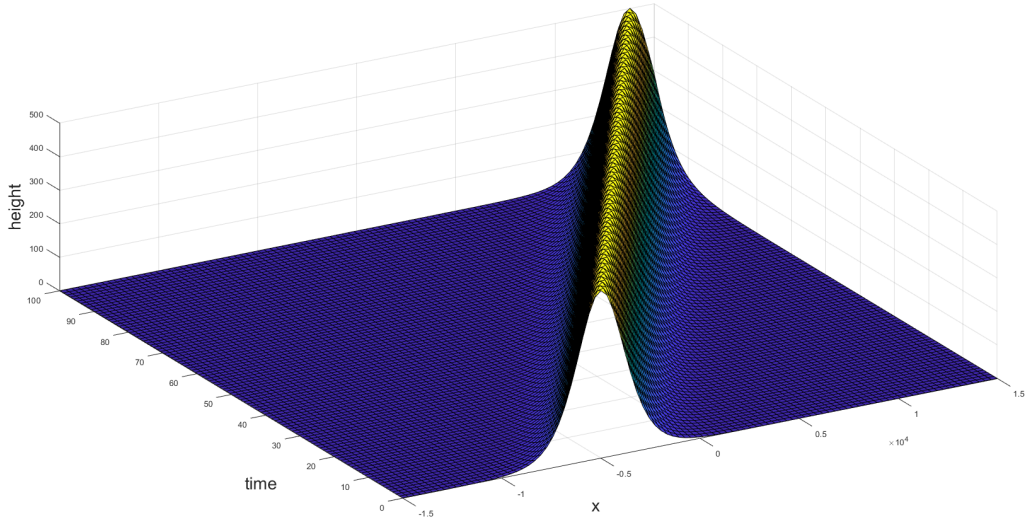


Figure 4: KdV Surface plot with $\frac{3c_0}{2}$

KdV Soliton with $h = 1000$, $\epsilon = 0.01$, $c_0 = 50$ and $x_0 = -5000$

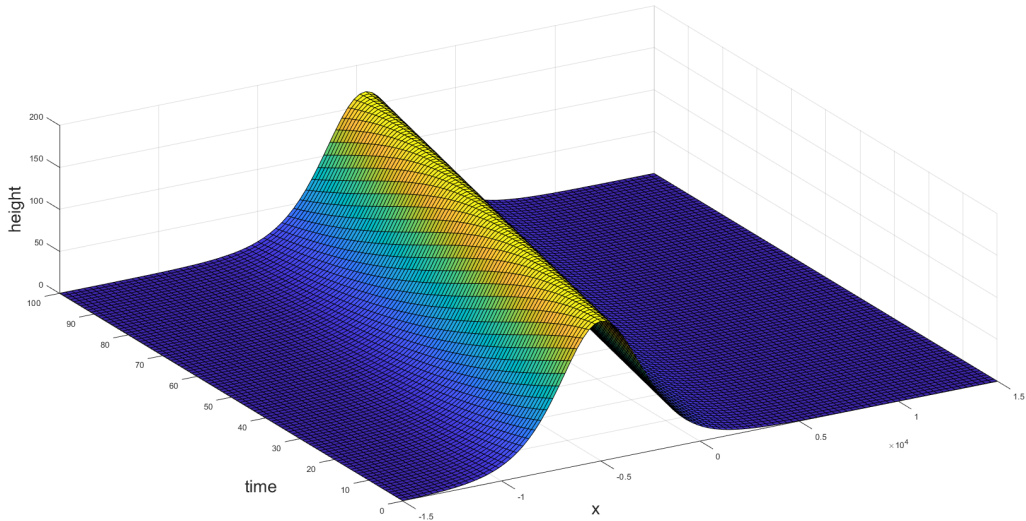


Figure 5: KdV Surface plot with $\frac{c_0}{2}$

Then changing the depth parameter h will affect both wave height and width, as shown by the outer profile of the wave in

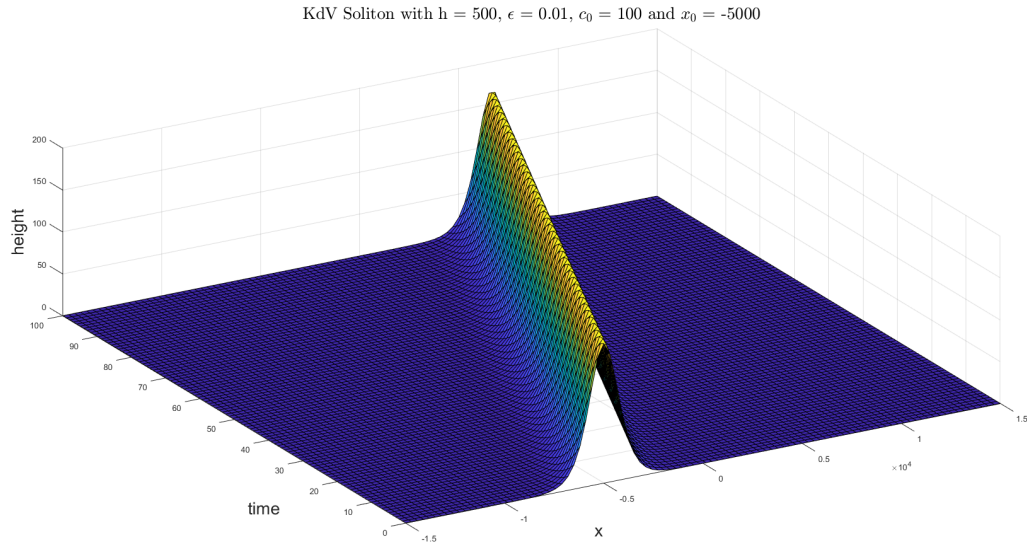


Figure 6: KdV Surface plot with $\frac{h}{2}$

Whereas changing the parameter $\epsilon = \frac{a}{h}$ more directly impacts the height of the wave without affecting the width, leaving

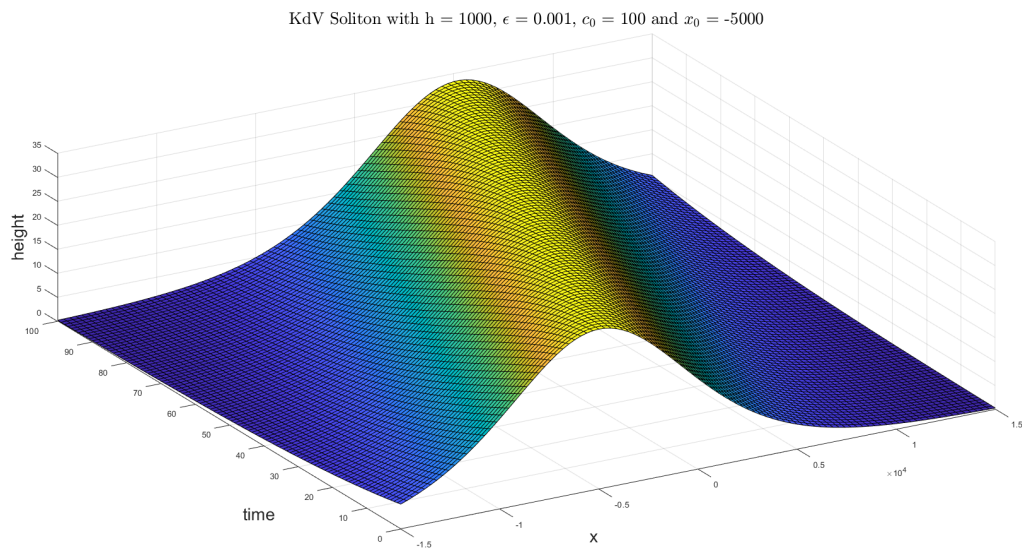


Figure 7: KdV Surface plot with $\frac{\epsilon}{10}$

Which is chosen since ϵ is assumed to be small by the section 3.1 assumption that amplitude

is much smaller than wave depth, and so increasing ϵ could potentially invalidate the model. Lastly, it is prudent to investigate the interactions between multiple solitons, which as stated previously is typically the instability that causes the development of rogue waves, since the constructive interaction of two surface wind waves will trigger a wave that can be taller than the strict sum of the interacting waves. This is contrary to the idea that one can simply take the sum of two solitons and receive an interaction soliton twice the height of the incident solitons, which is the logical result; however, this is a far too simplistic model for the dynamics that take place during this interaction, such as changing the angle bisecting the incident solitons to increase the amplification, and instead we must make modifications to our solution method to make it realistic. This does however show how the interaction region is a much taller waveform when the waves overlap in space, which then dissipates back into the original waveforms at later time with no change to the original waves. This is typical of KdV solutions, and will be observed later when numerical solutions are introduced for interacting KdV solitons.

But first, the soliton form given in equation 3.20 was shown to have a \pm in front of the coefficient due to the incorporation of surface tension by changing the defining non-dimensional KdV equation to $u_t - 6uu_x + u_{xxx} = 0$, which is the standard form for high surface tension. This means the value of γ now dictates the elevation of the wave, where increased surface tension ($\gamma < 0$) results in a depression of the wave (the peak now becomes a trough in the soliton), and vice versa for the reverse, given properties of the function $\text{sech } x$ for varying $x \in \mathbb{R}$. This solution works well for the no surface tension case, but including surface tension effects (changing the sign) doesn't give the solution we expected from the work shown prior in section 3.1 by Milewski ([26]), where they solved the Bernoulli equation and varied their Bond number (surface tension to depth squared ratio) as shown in their result below

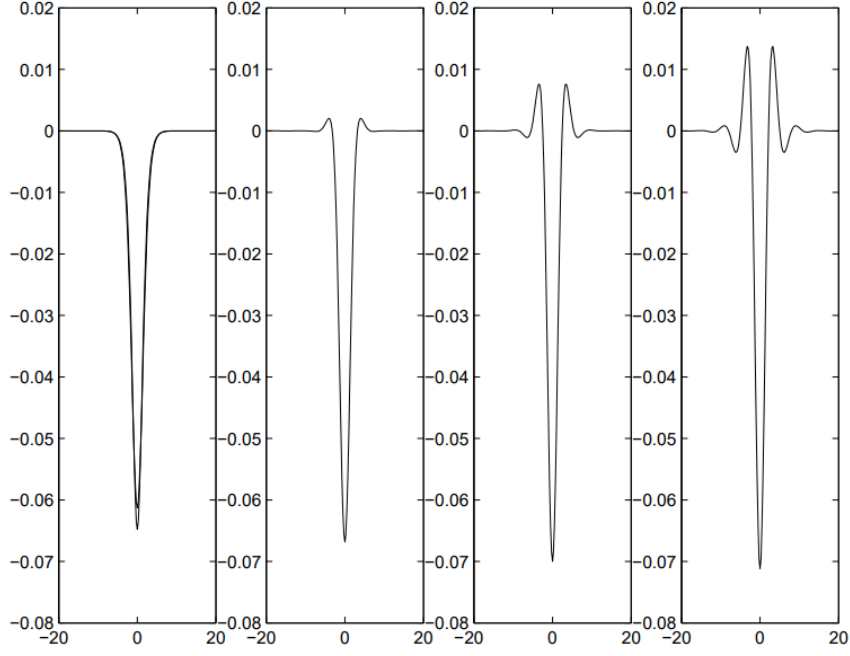


Figure 8: Plots from paper [26] of u_x vs x for varying parameter $B = \frac{\gamma}{h^2}$

First is $B > \frac{1}{3}$, second is $B = \frac{1}{3}$, and latter two are $B < \frac{1}{3}$

which shows how increasing surface tension should transform the solution both into a depressive wave, as shown in our derived soliton, and also changes the shape of the soliton around the leading and succeeding edges of the wave, and ideally introduces some perturbation effects in the farfield, which is the area sufficiently far away from the primary instability. This is also evident in the second formulation of surface tension given in paper [37] cited in section 3.3, where the solitons result in the form

$$\eta(x, t) = \eta_0 \operatorname{sech}^2\left(\frac{x - ct}{L}\right)$$

$$\text{for lengthscale parameter } L = \sqrt{\frac{4(1 - 3B_0)h^3}{9\eta_0}} \quad \text{and wavespeed } c = \sqrt{gh} \left(1 + \frac{\eta_0}{2h}\right)$$

Where plotting solitons in (x, t, h) results in the following plots for the parameters $\rho = 1 \times 10^3$, $\eta_0 = 0.01$, $h = 100 \times \eta_0 = 1$ (so that it satisfies the ϵ assumption), $g = 9.81$ and an increasing constant γ (remembering that the γ used in this representation increases for increasing amounts of surface tension, which is the opposite of the derived γ) gives

Surface Tension KdV for $B_0 = 0.30581$ and $\eta_0 = 0.01$

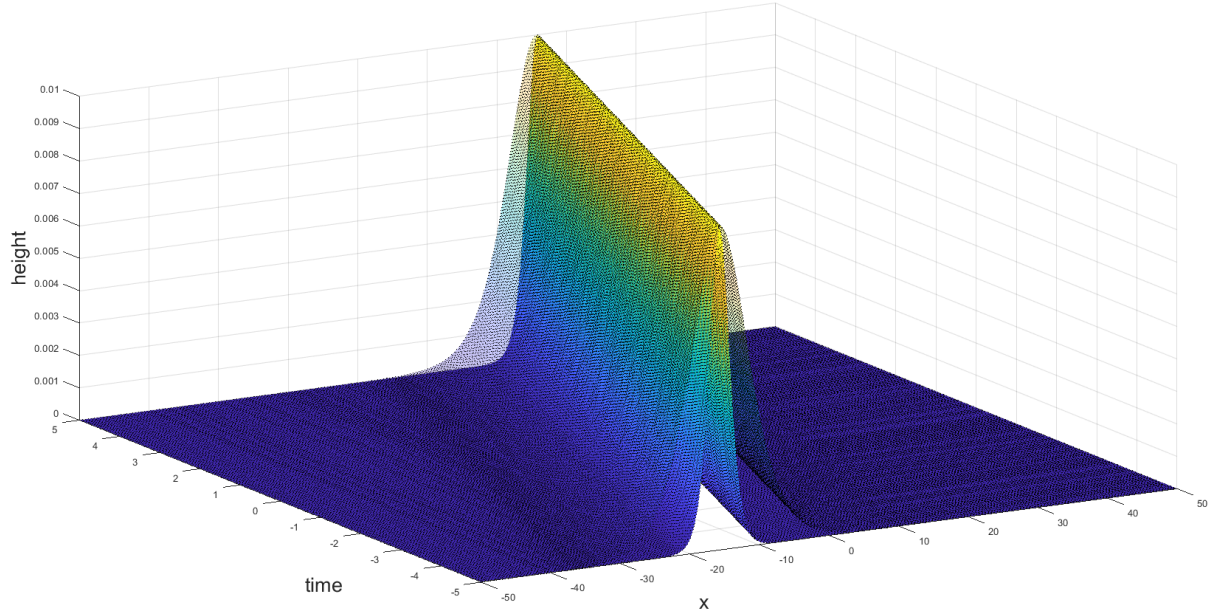


Figure 9: Elevation plot based on analytical solution from paper [37]

Translucent plot is lower value of parameter γ , which means less surface tension in this case

Where one can increase γ until $B_0 = \frac{\gamma}{\rho g h^2} = \frac{1}{3}$, upon which one must change the initial amplitude η_0 to a depressive state as found prior in our derived solution by changing the sign, then γ can be increased further as in

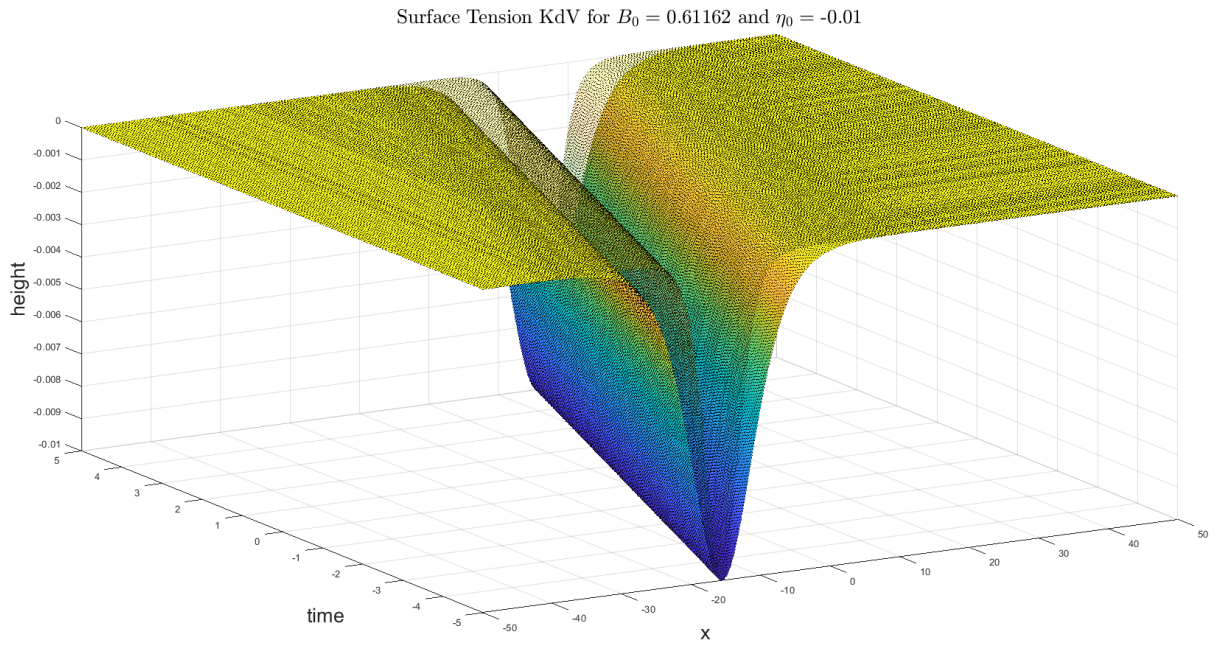


Figure 10: Depression plot based on analytical solution from paper [37]

Translucent plot is lower value of parameter γ , which means less surface tension in this case

The notable thing from these is that regardless of how far γ increases, only the width of the soliton increases, and the front and rear edges remain smooth compared to the farfield, as opposed to the formations caused in real wave tanks with similar values, as shown in [37]

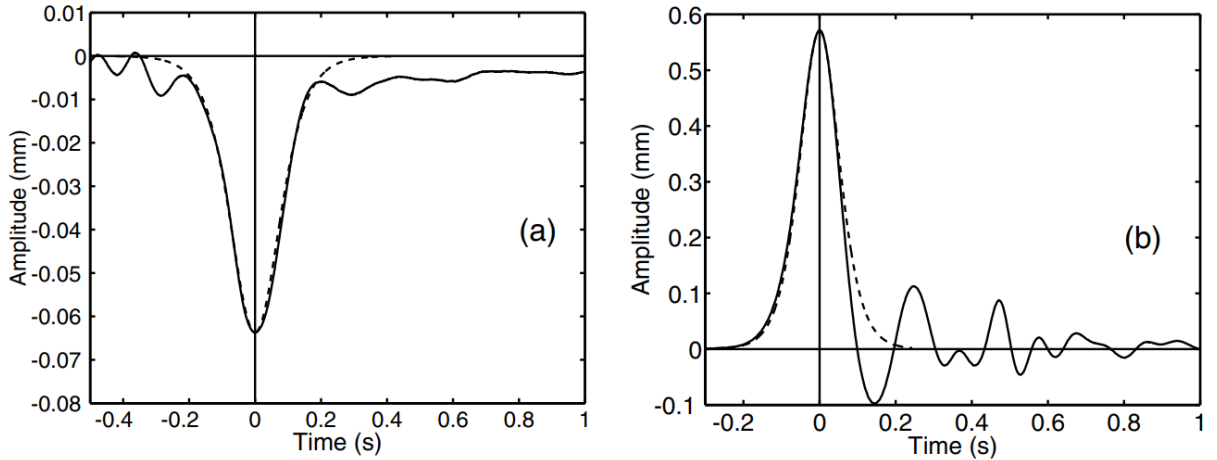


Figure 11: Plot from [37] where the solid lines show the observed data from sensors detecting waves originating from a small-scale wavemaker, and the dotted lines indicate the analytical solution obtained

Therefore in an attempt to recreate these ripple effects caused by increased surface tension, we will introduce a numerical solution instead and investigate how changing the γ parameter affects the wavefront in that case.

3.5 KdV Using Runge-Kutta

Now that the issues of multiple soliton interactions and the incorporation of surface tension have been introduced, the motivation for the following numerical solution is apparent, and will be derived with these goals in mind.

Plotting the multiple-soliton solutions mentioned prior for the low surface tension case can be done by taking snapshots in time and plotting them at different times in the interaction. Taking the constant $x_0 = 0$, the solution takes the form of a travelling wave with horizontal speed c in the positive x direction as shown above. The wavespeed c was chosen arbitrarily for each plot, and the peak is wherever $x = ct + \text{const}$ is. For example, when the peak is at $x = 0$ the waveform has the profile

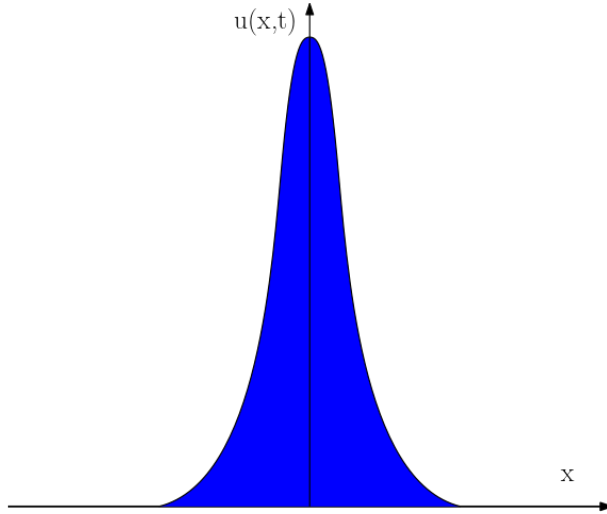


Figure 12: 2D plot of spatial dimension x against wave height at a snapshot $t = t_0$

This isn't necessarily a rogue wave though, since it can take the interaction of two or more incident waves to superpose and form a freak wave. The basis for this interaction can be found using 2-soliton solutions, which is the linear superposition of two different travelling wave solutions with differing speeds, and therefore heights, which combine to create larger waves, and hence form rogue waves under the right conditions.

A model for these solutions can be found on page 112 of [2], which shows a numerical solution to a KdV type equation $u_t + (\frac{1}{2}u^2)_x + u_{xxx} = 0$, which is inherently stiff (unstable for most step sizes) due to the final linear term, so is converted to Fourier space using the implied Fourier transform $u = e^{ikx}$ to remove spatial derivatives to give $\hat{u}_t + 3ik\hat{u}^2 - ik^3\hat{u} = 0$ with an integrating factor substitution which removes the linear term to make the system solvable (non-stiff partial differential equation).

It does this by using an integrating factor of the coefficient for the linear term in the form e^{-ik^3t} , multiplying through by it in the above equation and using a substitution of $\hat{U} = e^{-ik^3t}\hat{u}$ such that the time derivative term becomes $\hat{U}_t = -ik^3\hat{U} + e^{-ik^3t}\hat{u}_t$, which cancels with the linear term to give $\hat{U}_t + 3ie^{-ik^3t}k\hat{u}^2 = 0$. The final form of this equation can be seen in the below application of Runge-Kutta. Changing this method to solve the form of KdV prior in equation 3.4, this method takes the sum of two soliton initial conditions in the form

$$3K^2 \operatorname{sech}^2 \frac{K}{2}(x + x_0)$$

as derived in the previous section but for a parameter $K(c)$ and uses the Runge-Kutta method to approximate the solution, which is given by

$$u_{n+1} \approx u_n + k_1 * \frac{1}{6} + k_2 * \frac{1}{3} + k_3 * \frac{1}{3} + k_4 * \frac{1}{6}$$

for $k_1 = f(u_n)$, $k_2 = f\left(u_n + \frac{k_1}{2}\right)$, $k_3 = f\left(u_n + \frac{k_2}{2}\right)$, $k_4 = f(u_n + k_3)$

with $\frac{\partial U}{\partial t} = f = -3ie^{-ik^3t}k\mathcal{F}((\mathcal{F}^{-1}(e^{ik^3t}U))^2)$

with equation 3.4 and for Fourier transform \mathcal{F}

(3.23)

which differs from the solution that uses the moving variable ζ . Using this system, one can plot a general intersection of two solitons with a suitably large difference in wavespeeds, such as in

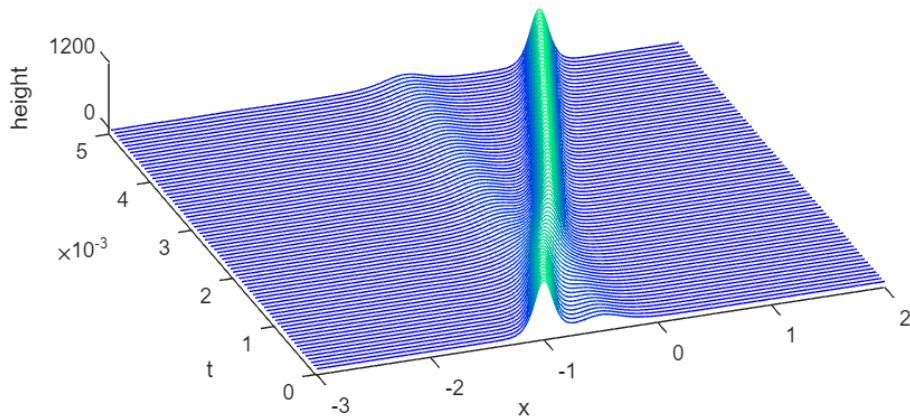


Figure 13: Surface plot of (x,t,h) with wavespeed parameter $K = 18$ and 8

Which shows the waves merging and then splitting back into individual waves afterwards. This is typical behaviour for a KdV model, for which waves will intersect and then continue on afterwards without change. A time snapshot of this just after the interaction looks like

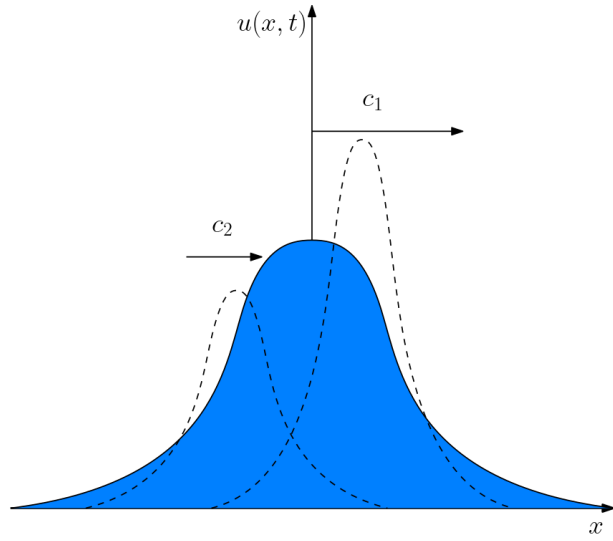


Figure 14: 2D Merge Interaction plot of x against h at time just after intersection, with dotted lines indicating how each wave will re-develop

Another interaction is caused when the parameters are close, which is when the wavespeed ratio of the two waves is below a threshold value, which produces a Bounce-Exchange Interaction, as it is termed in paper [10], where it differs from the prior interaction by the waves never merging into one waveform and instead moving through each other, similar to the motion of the cue and target balls in billiards, as shown by

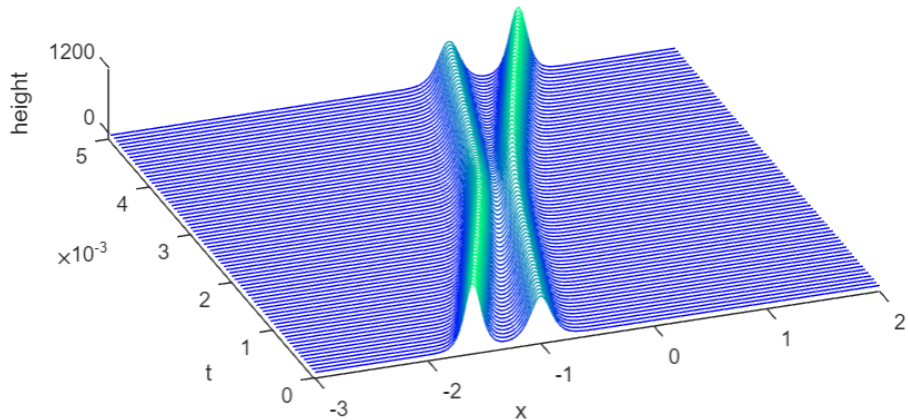


Figure 15: Surface plot of (x,t,h) with wavespeed parameter $K = 20$ and 16

Where the waves meet and exchange shapes after the interaction. This in turn, modelled just after the interaction, looks like

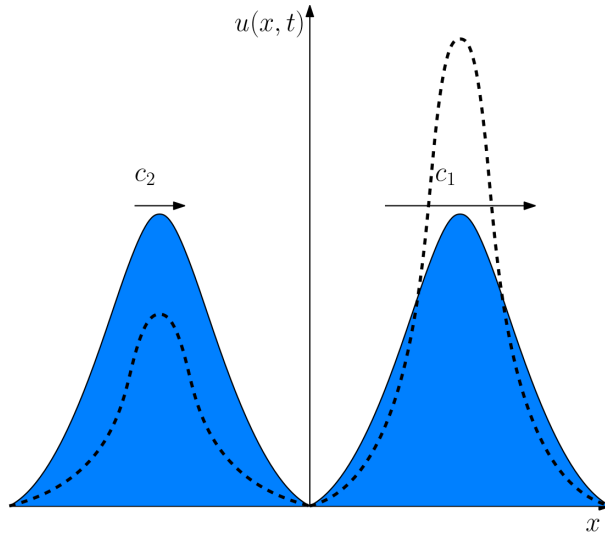


Figure 16: 2D Bounce Interaction plot of x against h at time just after intersection, with dotted lines indicating how each wave will re-develop

Finally, one can model the intersections between three incident soliton solutions, such as in

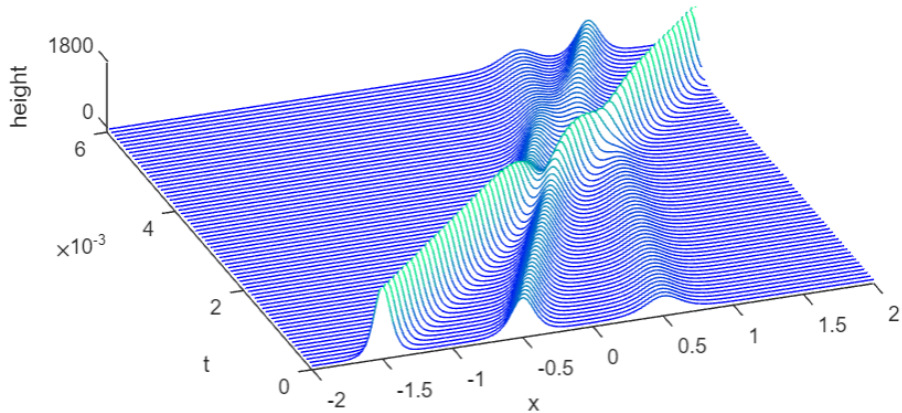


Figure 17: Surface plot of (x,t,h) with wavespeed parameter $K = 25, 18$ and 12

showing both of the above interactions with three different wavespeeds.

One major issue is shown as a result of the above solutions, in that the interaction region of the KdV solutions shows a dip in amplitude. This would be highly irregular for a real world constructive wave interaction, and hence these solutions apply to the KdV system, but not exactly to the waves that we want to investigate. To solve this issue, I will introduce another solution form known as Hirota's Bilinear Method, which outputs both of the solitary wave

solutions (solitons), and also the term corresponding to the interaction region, and so the effects of amplification can be observed.

But first, there is still the issue of including surface tension, which can be done by using the result found previously in 3.3 that inclusion of surface tension is a scale between the positive coefficient of the $+6uu_x$ term, and the negative coefficient of the $-6uu_x$ term, and so decreasing the magnitude of that coefficient towards 0, as shown in the modified code in section A.1, should begin to show the effects of inclusion of surface tension. The code by default uses $uu_x = (\frac{1}{2}u^2)_x$, so decreasing this $\frac{1}{2}$ coefficient towards 0 should display the beginnings of characteristics of surface tension, as seen below for the single soliton case

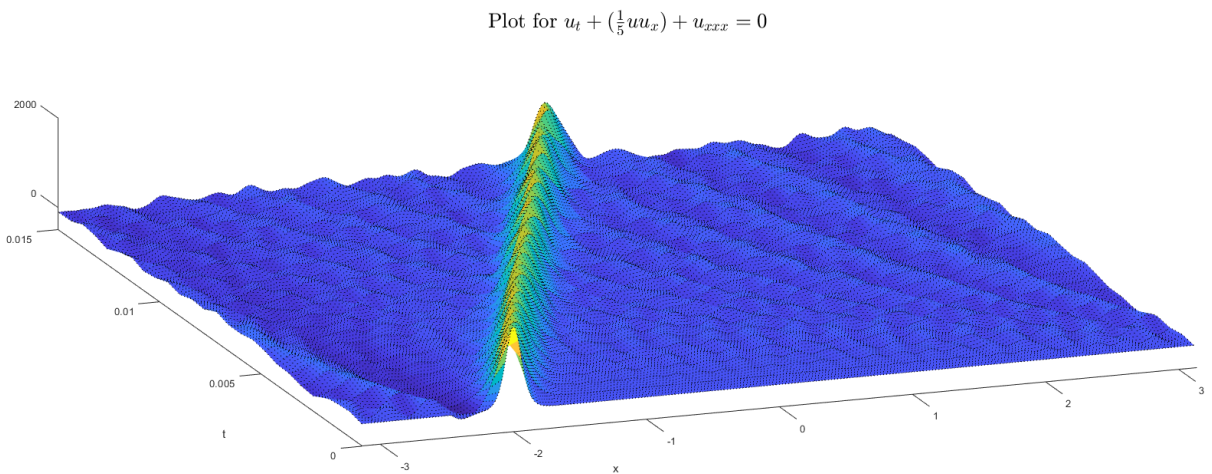


Figure 18: Surface plot of (x,t,h) with wavespeed parameter $K = 25$ for $u_t + (\frac{1}{5}u^2)_x + u_{xxx} = 0$

which shows how compared to the prior figures using the numerical solution that the area adjacent in space to the propagating solitons, remembering that they are propagating in the same direction at different speeds, is itself interacting with them as they travel, where the ripples change shape as time increases. This is as to be expected in more realistic wave scenarios where the presence of a large wave has a physical effect on the water surrounding it, and so this model is more accurate than the last, but still doesn't truly reflect the findings of Milewski in paper [26] where the far-field remains largely unaffected relative to the near-field edges of the soliton.

Decreasing the coefficient further shows surface tension beginning to overpower the line soli-

tons, as shown in the below comparison between the two-soliton interaction with a small change in the coefficient of 0.1 between the figures

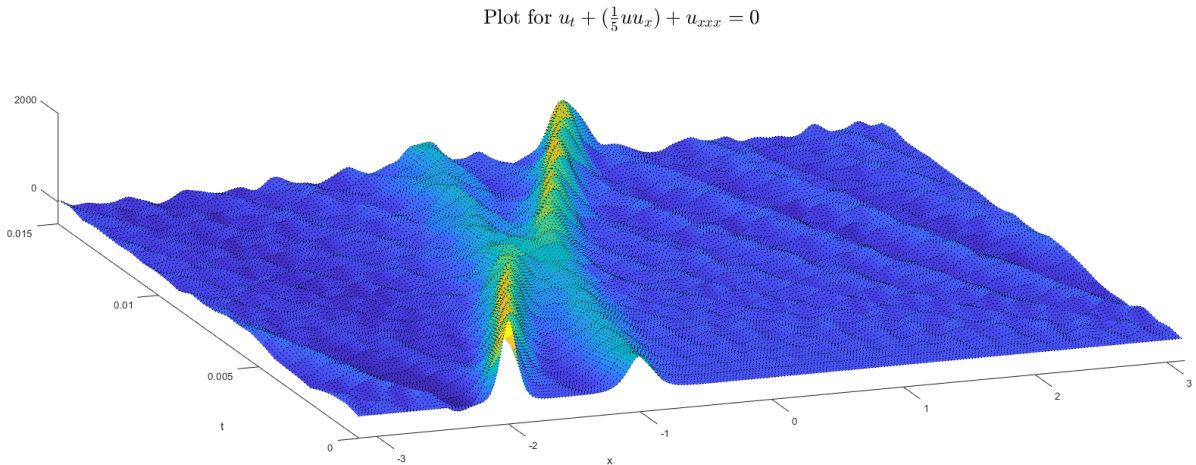


Figure 19: Surface plot of (x,t,h) with wavespeed parameters $K = 25$ and 16 for $u_t + (\frac{1}{5}u^2)_x + u_{xxx} = 0$

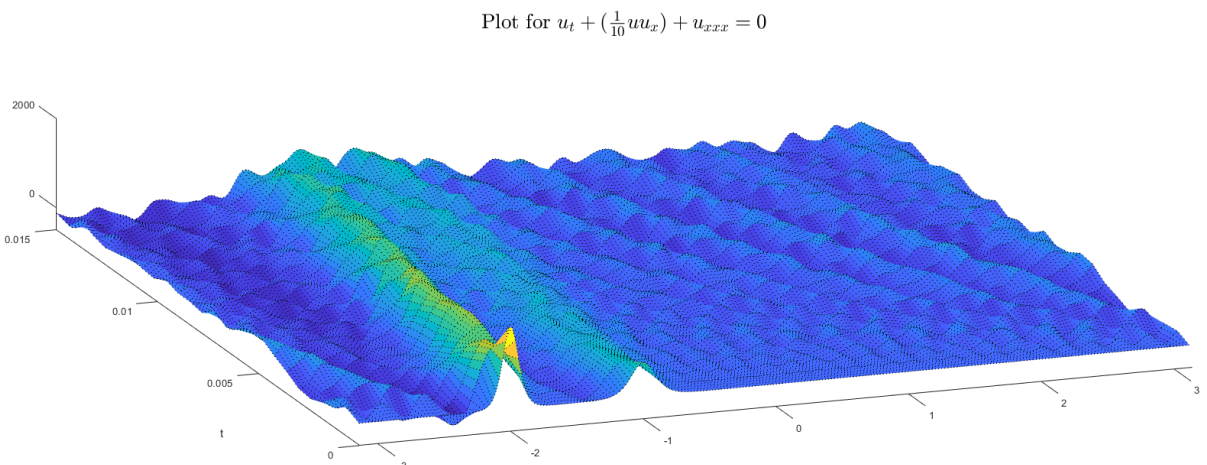


Figure 20: Surface plot of (x,t,h) with wavespeed parameters $K = 25$ and 16 for $u_t + (\frac{1}{10}u^2)_x + u_{xxx} = 0$

Where notably plotting for multiple interacting solitons doesn't change the ripple pattern, which is another unrealistic effect of this solution as we would expect the presence of another significantly-sized soliton to have its own surface tension effects.

This is obviously a less realistic outcome due to the generated ripples being of a similar amplitude to the wave that caused them. Therefore finally increasing the wavespeed, and hence amplitude according to section 3.4, and decreasing the coefficient just a bit more to 0.08 results in an unrealistic sea state where the ripples are magnified alongside the interacting solitons when plotted on a larger time scale

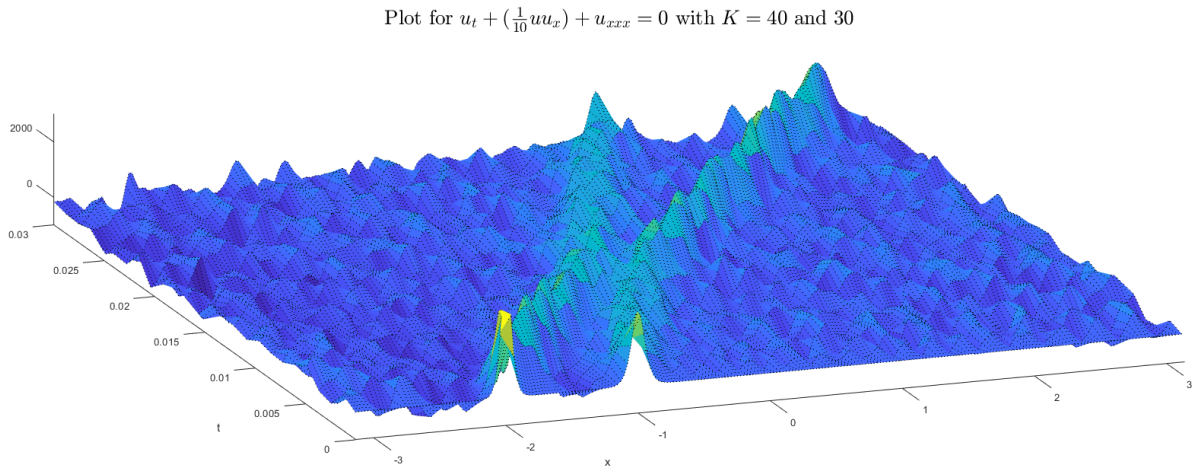


Figure 21: Surface plot of (x,t,h) with wavespeed parameters $K = 40$ and 30 for $u_t + (0.08u^2)_x + u_{xxx} = 0$

To effectively increase the parameter ψ all the way to 2 (to give a $-6uu_x$ term in the KdV equation), another method could be used by modifying the method used in [2] with equation $u_t + (\frac{1}{2}u^2)_x + u_{xxx} = 0$ to incorporate surface tension by reversing the sign of the uu_x term, which here results in $u_x - (\frac{1}{2}u^2)_x + u_{xxx} = 0$ and then one can reverse time and take the negative reciprocal of the equation to get $u_t + (\frac{1}{2}u^2)_x - u_{xxx} = 0$, which means the same numerical method as before can be used but this time the integrating factor would be $e^{ik^3 t}$, and so the substitution would be $\hat{U} = e^{ik^3 t} \hat{u}_t$ to give $f = -3ie^{ik^3 t} k \mathcal{F}((\mathcal{F}^{-1}(e^{-ik^3 t} U))^2)$ so only the exponential terms change sign. However, this method seems to have difficulty working with the Runge-Kutta formulation, so additional numerical solvers that can handle this shift or additional modifications to this method provide an avenue for further research in this field. To finish the solution forms for the KdV system, we ideally would like a solution form that has a constructive interaction region, and one that can show the same surface tension effects

as capillary action on the Boussinesq equation, and we will find this by using Hirota's Bilinear Method in the following sections.

3.6 Hirota's Bilinear Method for KdV

Hirota's Bilinear Method is one of a variety of methods that can be used to find soliton solutions for nonlinear PDE's. Other notable methods include the Darboux transformation, the Inverse Scattering transform and the Bäcklund transformation, to name a few, but the main advantage of using Hirota's method is that it is simpler to use and formulate as solutions for the KdV equation.

This method solves nonlinear PDE's analytically as long as the PDE can be transformed into a Bilinear form, which is a transformation where a function in two or more parameters, e.g. x and t in this case, can be written such that taking one to be fixed leaves a linear equation in the other. So to this effect, Hirota defined a new differential operator that must be satisfied as

$$D_x^m D_t^n ab = \left(\frac{\partial}{\partial t} - \frac{\partial}{\partial t'} \right)^m \left(\frac{\partial}{\partial x} - \frac{\partial}{\partial x'} \right)^n a(x, t)b(x', t') \quad (3.24)$$

evaluated at the point $x = x'$ and $t = t'$, and applied it onto the PDE in question by using a dependent variable transformation, e.g. in this case as suggested by [12] we use

$$u(x, t) = 2 \frac{\partial^2}{\partial x^2} \log f(x, t) = 2 \frac{ff_{xx} - f_x^2}{f^2} \quad (3.25)$$

This choice of dependent variable transformation is specifically chosen to satisfy the statement: "the leading derivative should go together with the nonlinear term" (paper [45]) in reference to its degree in x , and so since the standard form has a third-order derivative term, so is order $3 + O(u)$ for $O(u)$ meaning the degree of function u in derivatives of x , and the non-linear term is $1 + 2 \times O(u)$. That means the order of u in derivatives of x should be set to 2 to satisfy the equality, and so another variable w which is order 0 in x is introduced such that $w_{xx} = u$. Now substituting this w into the standard KdV equation, integrating w.r.t. x (with no integration constant due to u losing constant terms in w by differentiation) and introducing a new variable with degree 0 by default, which happens for functions of variables

such as setting $w = R \log(F)$ as suggested in paper [45]. This leads to a fourth order equation in F when subbed into the KdV equation, and so we pick R such that it reduces the order of the equation to as simple a system as possible, which here is $R = 2$ to reduce the equation to second order.

Another method used to find the coefficient R is detailed in paper [30] for a modified form of the soon-to-be introduced KP equation by substituting $u = R(\log(f)_{xx})$ for $f = 1 + e^{kx+my-\omega t}$ into the KdV (and later KP) equations and simplifying to get $R = 0$ or 12 , where 0 is the trivial solution so we take $R = 12$ in that circumstance. Regardless, when subbed into the KdV equation, given by $u_t + 6uu_x + u_{xxx} = 0$, this reparameterisation leads to the following form called the bilinear equation for the solution f

$$f(f_{xt} + f_{xxx}) - (f_x f_t + 4f_x f_{xxx} - 3f_{xx}^2) = 0 \quad (3.26)$$

This form is rearranged from the order of the original KdV equation so that the left bracket represents the linear terms in f 's with respect to derivatives (ignoring the f without derivatives for now which will be explained later), and the right representing terms non-linear with respect to derivatives of f .

Now applying this back to Hirota's differential operator results in the following [27]

$$(D_t D_x + D_x^4)f \cdot f = 0$$

Defining the derivatives according to that stated at the start of the method, and shows the difference in order (of ϵ) between the two brackets once more using the differential operator D , but this form is more instructional for the purpose of the method.

This is now simplified further using a combination of the first and second brackets on the function f to different orders of magnitude, where we define f to be an asymptotic expansion in powers of some bookkeeping parameter ϵ (not a small parameter and not related to $\epsilon = \frac{a}{h}$) and functions f_i that represent the Fourier modes of each soliton order. These f_i are the crux of the Hirota Bilinear Method, in that each of them represents the effects of the number of solitons interacting in the system, so starting from order 1 for one soliton solutions this gives

f as $f = 1 + \epsilon f_1$ since only 1 soliton is interacting. Adding on powers of f_i will increase the number of interacting solitons in the system, where f_2 represents the Fourier mode for the interaction between two single solitons, and f_1 must now be the sum of the distinct parts of the single solitons. The functions f_i each have coefficients in the form of the bookkeeping parameters ϵ , and so they can be found by grouping coefficients of ϵ together and setting them equal to 0, e.g. for $O(\epsilon^1)$, all of the nonlinear and squared terms in the second bracket are at least order 2, and all that remains is

$$(1)(f_{1xt} + f_{1xxx}) = 0$$

which is solved by assuming the first f_1 function to be a linear superposition of N-soliton solutions in Fourier space ([12])

$$f_1 = \sum_{i=1}^N e^{k_i x - \omega_i t + \delta_i}$$

for wavenumber k and wave frequency ω , where the single soliton case comes from setting $N = 1$, and gives at $O(\epsilon)$ the relationship between the Fourier modes in time and space, known as the dispersion relation, by $0 = -\omega_i k_i + k_i^4$, and hence $\omega = k^3$. When increasing the number of solitons interacting, this f_1 term will increase to include the Fourier representation of the other isolated solitons, and the higher order f_i terms will contain the information for the interaction regions of i solitons in space.

This is shown to yield a one-soliton solution by Hirota in their book ([28]), where taking $f = 1 + e^{k_1 x - \omega_1 t + \delta_1}$ and substituting back into $u = 2 \frac{\partial^2}{\partial x^2} \log f$ gives solutions of the form

$$u = \frac{2K^2 e^{k_1 x - \omega_1 t + \delta_1}}{(1 + e^{k_1 x - \omega_1 t + \delta_1})^2} = \frac{K^2}{2} \operatorname{sech}^2 \frac{k_1 x - \omega_1 t + \delta_1}{2}$$

so outputs a singular sech^2 function, as we expected given the solution forms found prior, which validates the choice of ansatz used above, at least for the one soliton case.

Plotting this will give the same solution type as seen previously

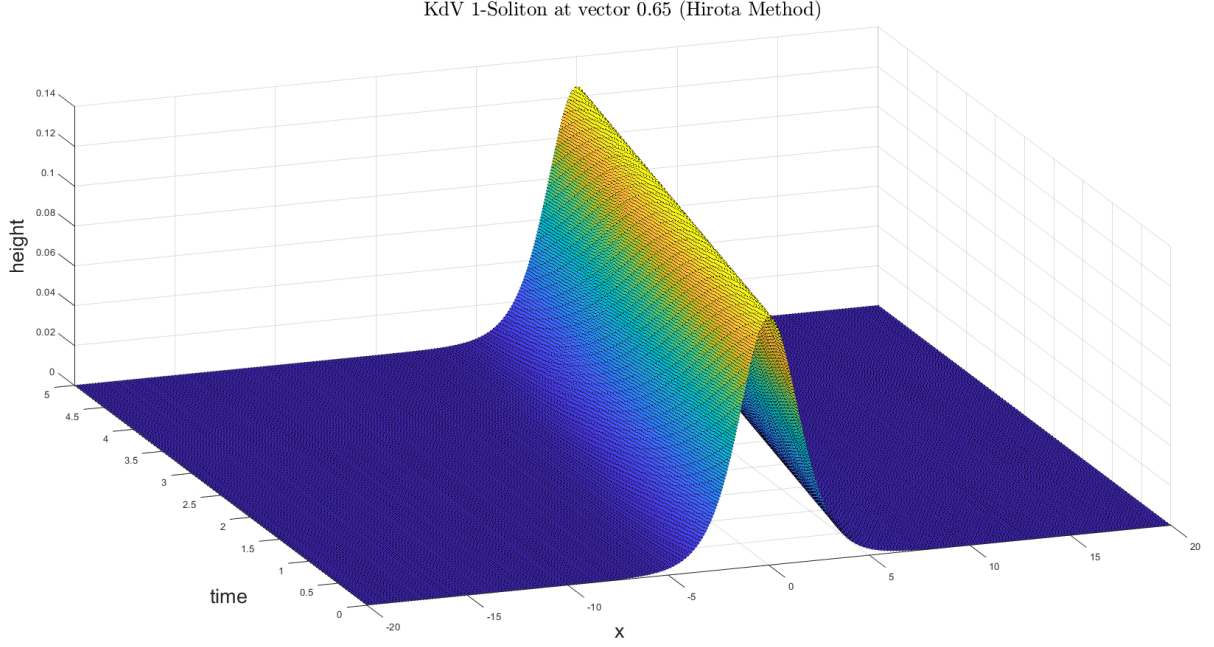


Figure 22: Surface plot of (x,t,h) with Fourier mode $k = 1$ Using Hirota's Bilinear Method

Which shows a generic elevation singular soliton travelling slowly in the positive x direction in time, excluding surface tension effects.

Now for the two soliton case, extending this to $O(\epsilon^2)$ gives $f = 1 + \epsilon f_1 + \epsilon^2 f_2$, and thus the left hand side becomes ([12])

$$(1 + \epsilon f_1 + \epsilon^2 f_2)(\epsilon f_{1xt} + \epsilon^2 f_{2xt} + \epsilon f_{1xxx} + \epsilon^2 f_{2xxx}) \rightarrow f_1 f_{1xt} + f_{2xt} + f_{2xxx} \quad (3.27)$$

to order ϵ^2 , and the right becomes simply

$$f_{1x} f_{1t} + 4 f_{1x} f_{1xxx} - 3 f_{1xx}^2 \quad (3.28)$$

Where the latter suggests the solution form for f_2 using a combination of the aforementioned Fourier expansions for f_1 , e.g.

$$f_2 = \sum_{i,j}^N A_{ij} e^{(k_i + k_j)x - (\omega_i + \omega_j)t + (\delta_i + \delta_j)}$$

$$A_{ij} = \frac{(k_i - k_j)^2}{(k_i + k_j)^2}$$

for $j > i$ as indices from the Fourier expansion, and the coefficient A_{ij} is found as the output when equating statements 3.27 and 3.28 with this solution form.

Now using

$$f = 1 + \epsilon f_1 + \epsilon^2 f_2 = 1 + \epsilon e^{k_1 x - \omega_1 t} + \epsilon e^{k_2 x - \omega_2 t} + \epsilon^2 \frac{(k_1 - k_2)^2}{(k_1 + k_2)^2} e^{(k_1 + k_2)x - (\omega_1 + \omega_2)t}$$

with the same dispersion relation as found for order ϵ in the one soliton case (as adding an $O(\epsilon^2)$ term will not change this) and substituting this as the two soliton interacting solution into the solution form $u = 2 \frac{ff_{xx} - f_x^2}{f^2}$ gives solutions which look like

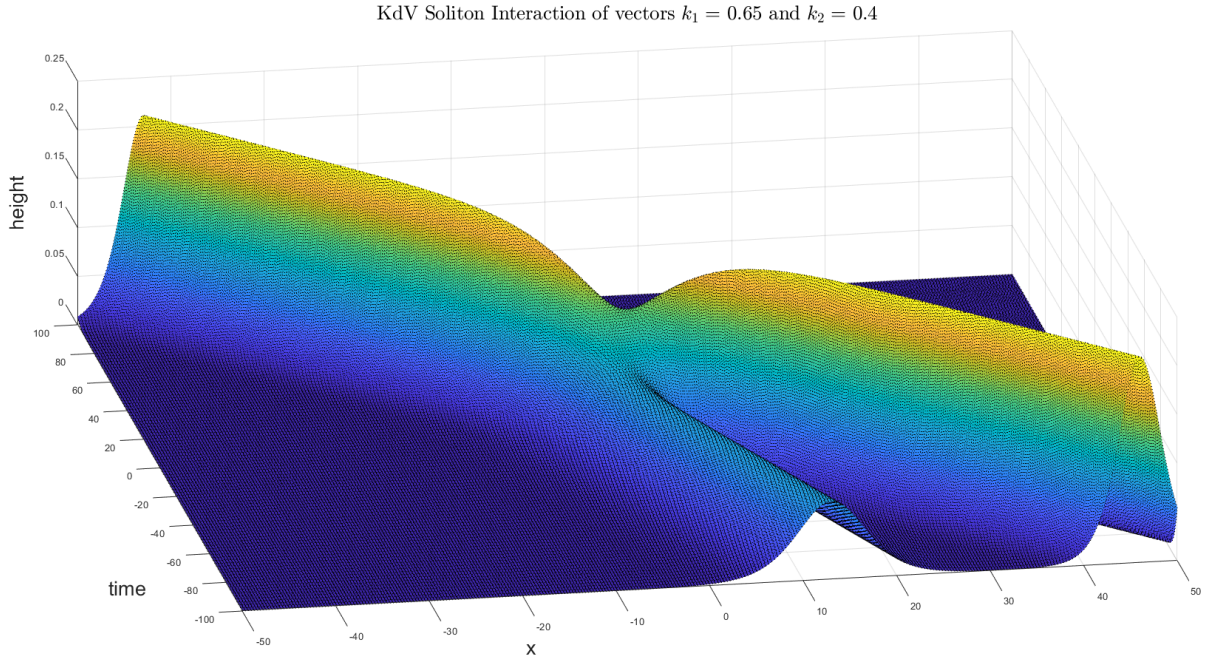


Figure 23: Surface plot of (x,t,h) with vectors $k_1 = 0.65$ and $k_2 = 0.4$

Notably, this solution form still retains the destructive interference that was present for all three of the prior methods of plotting solitons for the KdV model. This referred to on page 505 of paper [29] as a positive phase shift scenario, where phase shift is defined as $\Delta_{12} = -\log(A_{12})$, which will be derived in full later following the KP equation introduction, where incident waves of significantly different amplitudes result in a positive phase shift (since

$0 \leq A_{12} < 1$), which means the resulting wave in the interaction doesn't exceed the height of the largest incident wave. The opposite is for $A_{12} \geq 1$, where the incident waves are of similar height, and so the resultant wave reaches heights greater than the sum of the incident solitons, partially due to conservation of mass in the system. Making a specific choice of these vectors k_1 and k_2 allows the coefficient A_{12} to become larger relative to the size of the ϵ coefficients, however for this form of the KdV equation with $A_{12} = \frac{(k_1-k_2)^2}{(k_1+k_2)^2}$ it is difficult to make $A_{12} \approx 1$ without using the superposition of very slow and very fast moving waves, and so a change must be made in the defining state to make the modification of A_{12} easier, however this lays the groundwork for how constructive and destructive interference is portrayed in KdV solutions, and what one needs to do to achieve a realistic solution, given that the superposition of multiple wave solitons must increase in amplitude by conservation of mass and the impermeable base at a constant height $= -h$ as shown previously in

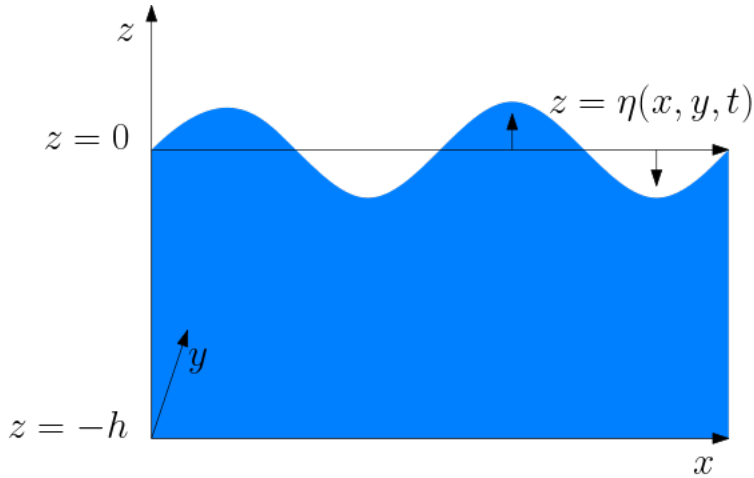


Figure 24: Plot of height (z) against x spatial dimension

Despite the goal to seek constructively interfering solitons, destructively interfering solitons can occur in realistic situations as long as vectors are moving in perpendicular directions and meet at specific phase. However, even opposite moving waves will meet at a point and reach a much larger height, again due to conservation of mass of the water converging at one point in space, hence negative growth in the interaction region is always unrealistic, but is a property of most KdV solutions.

Lastly, the form of the KdV solution as the sum of the two incident waves and the third

resultant interaction soliton isn't the only representation found for the interaction when using Hirota's Bilinear method. As per the previous statement in section 3.4 about simply taking the solution as a sum of incident solitons, this is actually possible with specific forms of the Hirota Bilinear solution, such as in [25], where they decomposed the solution u found using Hirota's Bilinear Method into one which is the sum of two solutions, e.g. $u = u_1 + u_2$. This leads to a modified form of the KdV equation, known as the Interacting KdV Equation, as such

$$\frac{\partial}{\partial t}u_i + 6(u_1 + u_2)\frac{\partial}{\partial x}u_i + \frac{\partial^3}{\partial x^3}u_i = 0$$

for $i = 1, 2$. Which looks like

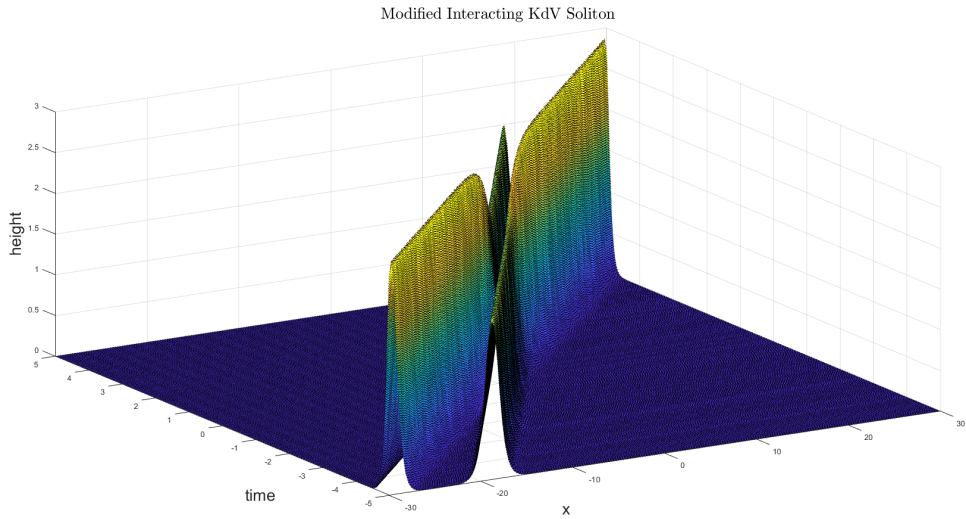


Figure 25: Surface plot of (x,t,h) with vectors $k_1 = 1$ and $k_2 = 1.2$

Showing the prior bounce-exchange interaction. Properties of these solutions u_i are that they are singular solitons in the farfield solution, which means when they aren't close, u_1 and u_2 act like normal KdV solitons, which suggests that these are the original soliton solutions with their contributions to the interaction soliton contained within. The specific functions this yields for both solitons won't be explored further here, but provides motivation for one of the many different forms of representation of solutions that can appear when using Hirota's Bilinear Method.

3.6.1 Including Surface Tension

Next, incorporating surface tension into the Hirota Bilinear Method requires substituting the solution ansatz $u(x, t) = R \frac{ff_{xx} - f_x^2}{f^2}$ into the KdV equation with a decreasing coefficient for the non-linear term, with the limit of this given in section 3.3 as $u_t - 6uu_x + u_{xxx} = 0$.

Now by the same method used prior, it is found in sources such as paper [4] that the coefficient R is again either 0 or 2, so taking $u(x, t) = 2 \frac{ff_{xx} - f_x^2}{f^2}$ and the same expansion for f results in the addition of surface tension, which again only causes an increase in the width of the soliton in the space-time plot, instead of providing the Milewski dynamics as expected. This is a common issue among KdV solutions that use the exponential form of f of

$$f = 1 + \epsilon \sum_{i=1}^N e^{k_i x - \omega_i t + \delta_i} + O(\epsilon^2)$$

Therefore, to achieve oscillations in the farfield, one could instead try using a dissipating periodic solution ansatz in the Hirota method, where the periodic oscillations away from the central soliton will form a similar shape to that of the wave tank experiments in paper [37]. This is what is done in paper [46], which analyses soliton solutions for a modified form of the KdV equation called the perturbed-KdV equation in the general form

$$u_t + \alpha u_x + \beta uu_x + \gamma u_{xxx} = 0$$

Which is simply a possible non-dimensionalisation of the the previously derived form of the dimensional KdV equation

$$\frac{1}{c_0} \eta_t + \eta_x + \gamma \eta_{xxx} + \frac{3}{2h} \eta \eta_x = 0$$

But without using the simplification using a decomposition to cancel out the u_x term; so now includes an extra spatially dispersive term u_x which is referenced as the Coriolis effect. We will choose specific values of $\alpha = 1$, $\gamma = 1$ and $\beta = \pm 1$ to fit the prior notions of including and excluding surface tension used previously, despite not re-deriving the surface tension coefficient ψ for this form of the non-dimensional KdV.

This has the effect of changing the coefficient R used prior in $u(x, t) = R \frac{ff_{xx} - f_x^2}{f^2}$ to be $R = \frac{12\gamma}{\beta} = 12$. They then suggested an ansatz in general form for the function f that uses a periodic term in the form

$$f = \begin{bmatrix} 1 & x & t \end{bmatrix} \begin{bmatrix} a_{1,1} & a_{1,2} & a_{1,3} \\ a_{2,1} & a_{2,2} & a_{2,3} \\ a_{3,1} & a_{3,2} & a_{3,3} \end{bmatrix} \begin{bmatrix} 1 \\ x \\ t \end{bmatrix} + \omega \cos(p_1 x + p_2 t + p_3) + \sigma$$

For constants $a_{i,j}$, p_1 , p_2 , p_3 and σ , where the product $X^T A X$ shown above is the suggested form for the singular lump-soliton solution, which expands to a polynomial in parameters x and t , and works since it only needs to satisfy the Bilinear form of the perturbed KdV equation, which here is found to be

$$ff_{xt} - f_x f_t + \alpha ff_{xx} - \alpha f_x^2 + \gamma ff_{xxxx} - 4\gamma f_x f_{xxx} + 3\gamma f_{xx}^2 = 0$$

And so as long as the ansatz f is differentiable at least once in t and four times in x , which polynomials are and eventually reach 0, then the ansatz is sufficient to apply to the Hirota Bilinear Method. Now subbing that solution form f into the Bilinear form, grouping coefficients of x , t and cos terms and setting them to 0 as a trivial solution results in achieving specific values for the constants mentioned above which can be found in paper [46]. The resulting specific choice of f results in ([46])

$$\begin{aligned} f = \sigma + a_{1,1} + a_{2,1}t + (a_{1,2} + a_{3,1})x + a_{2,2}xt \pm \frac{(a_{1,2} + a_{3,1}) \cos(p_1(x-t) + p_1^3 t + p_3)}{p_1} \\ + t((3p_1^2 - 1)(a_{1,2} + a_{3,1}) - a_{2,1} - a_{2,2}x) \quad (3.29) \end{aligned}$$

Which when subbed into $u = 12 \log(f)_{xx}$ gives the following periodic surface plot

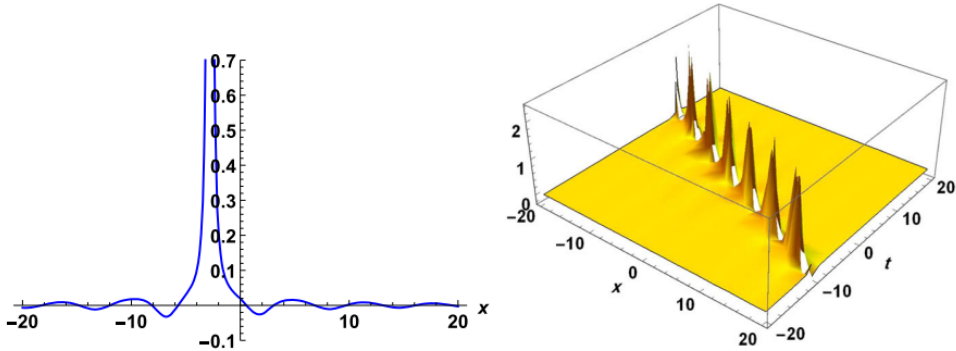


Figure 26: Surface and 1D plot from paper [46] of $u_t + 6uu_x + u_{xxx} = 0$ solved using Hirota's Method with periodic f

Notably for this solution, the function f contains no reference to the coefficient of the non-linear term β , and the only reference to this parameter is in the definition of the coefficient R which includes a $\frac{1}{\beta}$ term; therefore increasing the parameter ψ for this system will again result in a change from an elevation to a depressive soliton. However, this solution also correctly portrays the desired effects of farfield oscillations, with decreasing intensity as distance from the instability increased, so it is likely that the current representation used for incorporation of surface tension is not what causes the oscillatory effects seen in paper [26], but the periodicity of the function f can be what causes it.

Regarding this periodicity, it leaves an unrealistic portrayal for rogue waves, which are typically more isolated and defined by size relative to the waves around them, so logically one would need to take the periodicity of this function to ∞ to achieve this, but this particular solution form isn't easily amenable to changing the factors p_i to allow a singular solution. Alongside this it is also difficult to discern between the spontaneous lump-soliton and the persistent line-soliton; which are different solution types when viewed in two-spatial dimensions. Thus we will improve on this by now including transverse variations in the form of the KP equation and determine the terms that define surface tension for that form of the equation, and compare it to the results here and from papers [26] and [37].

4 The KP Equation

To fix the issues of the KdV equation, the KP equation was introduced as an extension to the KdV equation in the transverse direction, and is the second of the main models used for tsunamis and rogue waves. This extra dimension results from not discounting changes in the y -direction in the derivation of the KdV equation, and means surface plots of KP solutions are typically in three spatial dimensions, rather than in x , h and t as seen prior for the KdV equation.

4.1 Derivation

Continuing from the derivation for the dispersion relationship in section 3.1 (using source [1]), including transverse variations requires instead setting $\lambda_y = O(\lambda_x)$, and so the y terms in the non-dimensionalisation are not removed, and can now say $\delta \approx 1$ and that μ is the same parameter for x and y variations; however, the shallow wave and small amplitude assumptions remain, leaving

$$\text{Laplace: } \epsilon\phi_{xx} + \epsilon\phi_{yy} + \phi_{zz} = 0, \quad -1 < z < \epsilon\eta$$

$$\text{No slip: } \phi_z = 0, \quad z = -1$$

$$\text{Bernoulli: } \phi_t + \frac{\epsilon}{2} \left(\phi_x^2 + \phi_y^2 + \frac{1}{\epsilon} \phi_z^2 \right) + \eta = 0, \quad z = \epsilon\eta$$

$$\text{Kinematic: } \epsilon(\eta_t + \epsilon\phi_x\eta_x + \epsilon\phi_y\eta_y) = \phi_z, \quad z = \epsilon\eta$$

and carried through using the same method as the KdV form.

Regarding the change in surface tension, extending the Bernoulli equation 2.6 to include the multi-dimensional form of the surface tension component, which is different now due to use of ∇ in its definition, means the dispersion relationship equation 2.8 becomes $\omega^2 = (g\kappa - \frac{T}{\rho}\kappa^3) \tanh \kappa h$ as stated in book [1] for T as the same surface tension coefficient and κ represents the 2-norm average of k and l , the Fourier spatial parameters introduced in the KdV derivation. During the previous derivation, in section 3.1, it was assumed that the wavelength in the transverse (y) direction was much smaller than in the direction of motion (x), and so k is much larger than l , so Taylor expanding the $\tanh \kappa h$ and taking the square root, one

can rearrange the brackets to be $\left(1 + \frac{l^2}{k^2}\right)^{\frac{1}{2}}$, which is essentially $1 + \epsilon$, and so this can be taken at leading order, and converted from Fourier modes, as derived in section 2.3, using the differential relations ω in Fourier space means $i\partial_t$ in real space and k means $-i\partial_x$, which originate from their form in Fourier mode being an exponential to the power $ikx - i\omega t$, so derivatives of this in x and t leave these powers as the coefficients.

Now subbing these terms into the Taylor expanded dispersion relation gives the linear KP equation:

$$\frac{1}{c_0} \eta_{tx} + \eta_{xx} + \frac{1}{2} \eta_{yy} + \left(\frac{h^2}{6} - \frac{T}{2\rho g} \right) \eta_{xxxx} = 0$$

This notably reuses the γ term from the surface tension for the KdV in section 3.3, where setting $\gamma < 0$ gives large surface tension, and is called the KPI equation; whereas setting $\gamma > 0$ gives small surface tension, which is referred to as the KPII equation. Soliton solutions for either can be used for models of KP, with the main differences being the differences in amplitude and the periphery of the soliton having a dip when taking surface tension into consideration in the KPI form.

To get the nonlinear version, moving the transverse term to the right-hand side and integrating once through by x gives equation 3.7 from section 3.3 but with a non-zero right-hand side given by

$$\frac{-1}{2} \int_{-\infty}^x \eta_{yy} dx'$$

since x' is still used at this stage as in the derivation of the KdV equation. Now similarly to what was done in section 3.3, the term γ can be contained within a new parameter σ as a coefficient for the u_{yy} term by reusing $\zeta = x - c_0 t$ and $t = t'$ to eliminate the second term, and so $\partial_x = \partial_\zeta$ and $\partial_t = \partial_{t'} - c_0 \partial_\zeta$ like prior, where the addition of y makes no change, but now we introduce a new term $y = k_3 y'$ such that $\frac{-1}{2} \partial_{yy} = \frac{-1}{2k_3^2} \partial_{y'y'}$, which is allowed since we now have three coefficients to work with and so can introduce a new parameter k_3 that we can relate to the other's using comparisons of these coefficients. So like before the η_x term cancels, and the non-dimensional version of $\frac{-1}{2} \eta_{\zeta\zeta}$ on the right-hand side becomes $\frac{-c_0 k_2}{2k_3^2} u_{y'y'}$ where the k_2 on the numerator comes from the integral form in x (ζ) of the KdV-portion of

the KP equation to give

$$u_{t'} + \left(\frac{h^2 c_0}{6k_2^3} - \frac{Tc_0}{2\rho g k_2^3} \right) u_{\zeta' \zeta' \zeta'} + \frac{3c_0 k_1}{2hk_2} uu_{\zeta'} = \frac{-c_0 k_2}{2k_3^2} \partial_{y'y'} \quad (4.1)$$

So like before, we want to achieve a specific coefficient on now the transverse term, and to do this we will use the k_2 term on the right-hand side to relate the k_3 term to the surface tension term γ . Therefore setting $\frac{-c_0 k_2}{2k_3^2} = 3$, where this choice of constant is arbitrary, as will be seen later with a form of the equation that used the constant equal to 1, but leads to the most generic form of the equation. This means $k_3 = \sqrt{\frac{c_0 k_2}{6}}$, and so depends on the coefficient k_2 , for which we set $k_2 = \sqrt[3]{\gamma c_0}$ again to get the third derivative coefficient to be 1, and neglecting the original surface tension component for this instance means $\frac{3c_0 k_1}{2hk_2} = 6$ and so $k_1 = \frac{4hk_2}{c_0}$ to complete the non-dimensionalisation of ζ , η and y . This means $y = \sqrt{\frac{c_0 k_2}{2\sigma}} y' = \sqrt{\frac{c_0 \sqrt[3]{\gamma c_0}}{6}} y'$, so for $\gamma > 0$ this coefficient is positive, and is low surface tension; whereas it is negative for high surface tension, and the amount increases as the coefficient decreases.

This ultimately leads to the non-dimensional form:

$$\partial_x(u_t + 6uu_x + u_{xxx}) \pm 3u_{yy} = 0 \quad (4.2)$$

Where the latter term is \pm due to the γ term mentioned above, and is positive for when tension is small and so the term $g\kappa - \frac{T}{\rho}\kappa^3$ is positive, and vice versa for negative.

Notably, negating the latter term and derivative leaves the KdV equation derived previously.

4.2 Line-Soliton Solutions for the KP Equation

Since there are no analytical solutions for the KP equation, fluid dynamicists have used a multitude of numerical methods to find N-soliton solutions to the KP equation. The method to be investigated here will be Hirota's Bilinear method extended to two-spatial dimensions, but other methods do exist, such as the tanh-coth method for one-soliton solutions, given by a moving parameter $\xi = x + ry - ct$ used to convert the PDE form of the KP equation to an ODE in derivatives of non-dimensional displacement parameter u . Then introducing $Y = \tanh \mu\xi$ and using the chain rule to convert the aforementioned derivatives of ξ to derivatives of Y

leads to a solution for u as a linear superposition of \tanh and \coth functions, given in paper [11] as

$$u(\mu\xi) = \sum_{k=0}^M a_k Y^k + \sum_{k=1}^M b_k Y^{-k} \quad (4.3)$$

For integer M , which is the transformation to be applied onto the solution u found in the ODE form of the KP equation, where coefficients will be set to 0 to find values for the above constants.

Methods such as these aren't what we want for rogue waves though, since it is only valid for a singular line-soliton, whereas we require an interaction of line solitons to achieve a superposition soliton, which is the primary method of rogue wave generation. This linear superposition of solitons is generally notated simply by $u = s_1 + s_2 + s_{12}$ as before in the initial derivation of Hirota's method, where we will investigate methods of representation for this s_{12} soliton and how the choice of Fourier modes in the incident vectors (k_1, m_1) and (k_2, m_2) affect the length and height of this region.

Alongside this, this paper will only cover Hirota's Bilinear Method applied to the standard form of the KP equation as given in equation 4.2 using the assumptions from the KdV system derivation; however there exist a plethora of different forms such as those researched in papers [30] and [48] of the forms

$$(u_t + uu_x + u_{xxx})_x + 3u_{yy} + g(t)u_{xy} = 0$$

$$\text{and } (u_t + uu_x + u_{xxx})_x + 3u_{yy} + h(t)u_{xx} = 0$$

That describe scenarios of changing depth and width, which provide the first steps as logical extensions to the following research due to their similarity to the current form and amicability to the Hirota solution, but will not be explored further in this paper for the sake of brevity.

4.2.1 Hirota's Bilinear Method for KP

For small surface tension waves, the parameter γ , which was first derived in section 3.3, is small, and hence the coefficient of the u_{yy} term is positive which yields the KPII equation. This gives solutions of a single phase, known as line solitons, which are modelled in [9] by the

general solution

$$u = 2 \frac{\partial^2 F_N}{\partial x^2} \quad (4.4)$$

Where F_N represents the polynomial of exponentials as introduced in section 3.6 again with $R = 2$ like the KdV case in section 3.6. The $N = 1$ solution relates to the simplest one-line soliton, so travels in one direction with no variation in the direction perpendicular to travel, so is essentially the same as the prior KdV solutions. Therefore the more interesting results come from the $N = 2$ solutions of the form

$$F_2 = 1 + e^{\eta_1} + e^{\eta_2} + A_{12}e^{\eta_1+\eta_2} \quad (4.5)$$

Which is derived for the KP extension to the KdV method in section 3.6 as follows.

For the general KP equation given by $\partial_x(u_t + 6uu_x + u_{xxx}) \pm 3u_{yy} = 0$, with keeping ambiguity of surface tension in the final term, means the method proceeds like before in section 3.6 but with slight alterations as stated in paper [11]. The Bilinear form of the equation is found similarly to 3.26 as

$$f(f_{xt} + f_{xxxx} \pm f_{yy}) - (f_x f_t + 4f_x f_{xxx} - 3f_{xx}^2 \pm f_y^2) = 0 \quad (4.6)$$

Which adds y dependent terms whose sign depends on the value of γ from section 3.3. Using a similar decomposition of the above function, and performing the same asymptotic expansion on f yields the same exponential solution form, but with an additional y parameter, e.g. $f_1 = \sum_{i=1}^N \exp(k_i x + m_i y - \omega_i t)$. Similarly to the KdV case, the ω parameter can be written in terms of the k and m parameters using the first order ϵ equation, and hence one-soliton solutions u can be found by taking up to order ϵ^1 in the expansion of f with an omitted ω term, and reversing the dependent variable transformation back to u , which is written as ([11])

$$u = \frac{2\partial^2 \log f}{\partial x^2} = \frac{2k_1^2 e^{\left(k_1 x + m_1 y - \frac{k_1^4 + m_1^2}{k_1} t\right)}}{\left(1 + e^{\left(k_1 x + m_1 y - \frac{k_1^4 + m_1^2}{k_1} t\right)}\right)^2} \quad (4.7)$$

Which can be converted to the original sech^2 form using the identity

$$\text{sech}^2 = \frac{1}{\cosh^2} = \frac{4}{(e^x + e^{-x})^2} = \frac{4}{e^{2x} + 1 + e^{-2x}}$$

and so

$$u(x, y, t) = \frac{1}{2} k_1^2 \text{sech}^2 \left(\frac{1}{2} (k_1 x + m_1 y - \omega_1 t) \right)$$

Which is simply an extension of the original one-soliton KdV solution.

The two-soliton KP solution can be found similarly by extending to $N = 2$ in the definitions of f_1 and f_2 , with the latter being

$$f_2 = A_{12} e^{(k_1+k_2)x+(m_1+m_2)y-(\omega_1+\omega_2)t}$$

to get ([11])

$$f = 1 + \epsilon e^{\theta_1} + \epsilon e^{\theta_2} + \epsilon^2 \frac{3k_1^2 k_2^2 (k_1 - k_2)^2 - (k_1 m_2 - k_2 m_1)^2}{3k_1^2 k_2^2 (k_1 + k_2)^2 - (k_1 m_2 - k_2 m_1)^2} e^{\theta_1 + \theta_2}$$

for $\theta_i = k_i x + m_i y - \frac{k_i^4 \pm m_i^2}{k_i} t$, remembering that

$$u = 2 \frac{f f_{xx} - f_x^2}{f^2} \quad \text{for} \quad f(x, y, t) = 1 + \sum_{n=1}^{\infty} \epsilon^n f_n(x, y, t)$$

This is already a much more useful representation of the A_{12} coefficient than was found in section 3.6, as one can vary the parameter k_2 without worrying about the scale of the parameter since the choice of $(k_1 m_2 - k_2 m_1)^2$ can be made large to balance it. However, in regards to choosing parameters k_i and m_i that make this a constructive interaction, it is difficult to see which vectors provide $A_{12} \approx 1$ in this case. Therefore to plot this we will introduce a simplification on the parameters to simplify the coefficient A_{12} to make our lives easier.

But first, it is instructive to note that this method is a simplification of the method that arises from using the Wronskian representation of the functions f , which is given in paper [34] by

$$u(X, Y, \tau) = 2\partial_{XX} \log K(X, Y, \tau)$$

for K being obtained using the Wronskian

$$K(X, Y, \tau) = \begin{bmatrix} f_1^{(0)} & f_1^{(1)} & \dots & f_1^{(N-1)} \\ f_2^{(0)} & f_2^{(1)} & \dots & f_2^{(N-1)} \\ \dots & \dots & \dots & \dots \\ f_N^{(0)} & f_N^{(1)} & \dots & f_N^{(N-1)} \end{bmatrix}$$

where the same line soliton solutions are obtained by taking the same exponential decomposition for each f_i

$$f_i = \sum_{j=1}^M A_{ij} e^{k_i x + m_i y - \omega_i t}$$

4.3 Choosing Appropriate Soliton Vectors

Plotting of the line-soliton solutions for the KP equation is similar to that of the KdV Hirota solutions; where vectors for the incident waves must be chosen specifically to produce a realistic model for a wavefront, since not all solutions represent real world dynamics.

The following section covers suitable solution vectors, and details certain cases of instabilities that these solution vectors can tend towards that act as limiting cases.

Using the aforementioned Hirota's Bilinear Method, paper [13] provides a basic beginning to plotting the solutions by making a choice of the bookkeeping parameters to be $\epsilon = \frac{a_i}{k_i}$ per incident soliton for a given amplitude factor a_i and x -direction wavenumber in Fourier space k , as shown in

$$f = 1 + \epsilon_1 e^{\eta_1} + \epsilon_2 e^{\eta_2} + A_{12} \epsilon_1 \epsilon_2 e^{\eta_1 + \eta_2}$$

Remembering that this parameter ϵ does not have to be a small parameter, and is instead used for the multiple scales analysis of the Hirota Bilinear form. Then, to simplify the coefficient A_{12} before, paper [47] notes that the complexity arises from the dispersion relation derived at $O(\epsilon)$ in the above derivation, and so for the form of the KPII equation that they are modelling

$$(u_t + 6uu_x + u_{xxx})_x + 3u_{yy} = 0$$

they decompose the vector quantities k and m into subcomponent variables l and n that are defined as $k_i = l_i + n_i$ and $m_i = n_i^2 - l_i^2$, so that the dispersion relation found as

$$\omega = \frac{k_i^4 + 3m_i^2}{k_i}$$

can be reduced to

$$\omega = \frac{(l_i + n_i)^4 + 3(n_i^2 - l_i^2)^2}{n_i + l_i} = 4(l_i^3 + n_i^3)$$

Which massively simplifies the following steps as shown by applying a modified f to the one used above in equation 3.25 as

$$f = \delta_{ij} + \frac{a_i}{l_i + n_j} \exp(k_i x + m_i y - \omega_i t)$$

for Kronecker delta δ_{ij} , and

$$A_{12} = \frac{(n_1 - n_2)(l_1 - l_2)}{(l_1 + n_2)(l_2 + n_1)}$$

Which is a much simpler representation of the constant A_{12} , which gives multiple options for choosing vectors such that $A_{12} \approx 1$ and importantly provides an easier framework to avoid singular situations where $A_{12} < 0$, which has no solutions.

This solution form shares the same resonance attributes as the previously investigated model, but shows relations that the vectors (k_i, m_i) of each soliton must satisfy. Thus the choice of vectors has a profound effect on not only the interaction region, but on whether the system has an output at all.

Now there are four choices to be made for the components l_i and n_i of the incident vectors that will produce the resultant vector in the interaction region, and so choosing an arbitrary example of vectors (l_i, n_i) such as $(1.3, 1.5)$ and $(1.2, 1.0)$ will produce a valid output, but one that has a destructive "bounce interaction" interference region, as shown in

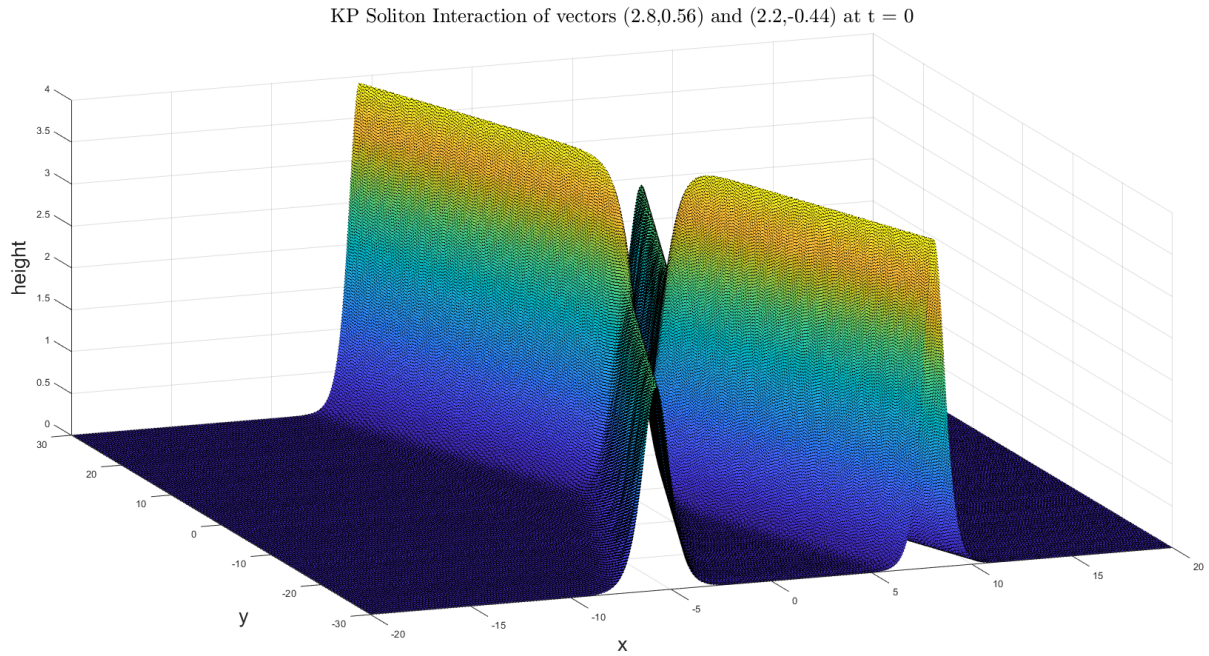


Figure 27: Hirota's Bilinear KP Solution with vectors $(2.8, 0.56)$ and $(2.2, -0.44)$

Where the vectors also cannot be chosen to be of a similar size since the coefficient A_{12} would become negative in that case for all positive l_i and n_i . This destructive interference is due to the choice of vectors producing waves with interaction soliton coefficients $A_{12} \approx 0$. Therefore to produce a wavefront with a positive overlapping region, one must choose vectors such that $A_{12} \approx 1$, and so the interaction region becomes an amplification on the incoming solitons at the interaction point. So making choices of the parameters l_i and n_i to make the vectors (k_i, m_i) equal to $(0.5, 1.5)$ and $(0.5, 2.25)$, for example, gives

KP Soliton Interaction of vectors (0.5,1) and (0.5,2.25) at t = 0

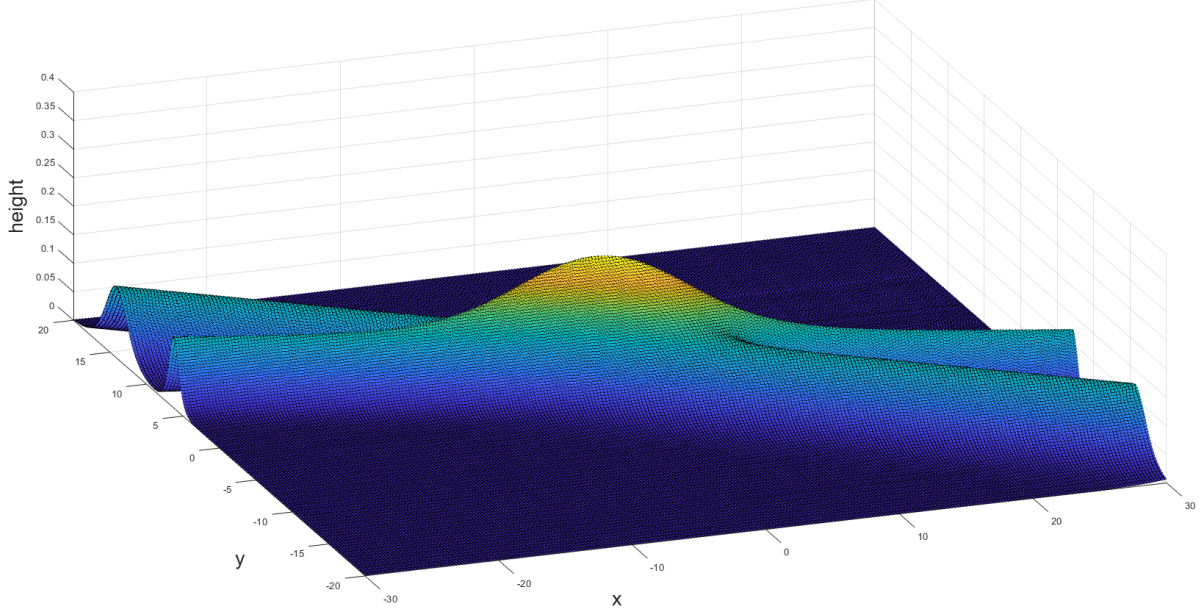


Figure 28: Hirota's Bilinear KP Solution with vectors (0.5, 1.5) and (0.5, 2.25) ($A_{12} \approx 1$)

Which is precisely the goal with Hirota's Bilinear Method for the KdV equation, with the coefficient A_{12} being approximately 1 which gives the overlapping region as positive, while small A_{12} gives a dip. This means the vectors in KP space must be chosen such that $A_{12} = \frac{(n_1-n_2)(l_1-l_2)}{(l_1+n_2)(l_2+n_1)} \approx 1$, and so preferably $(k_1 - k_2)^2 \geq (k_1 + k_2)^2$ according to the previously derived representation for this to be the case (but not necessarily using the notation $k_i = l_i + n_i$ the current form is a modification on the original Fourier modes).

This vector form also allows us to find limiting cases of the function to show which combinations of vectors give unusual wave formations, and to test the limits of the parameters l_i and n_i as they tend towards the aforementioned dangerous singular states. Therefore, setting variables n_i and/or l_i such that A_{12} is exactly equal to 0 causes "Full Resonance" where the last term in the given solution for f disappears, and hence soliton solutions f can be formed from linear combinations of the remaining components. This produces a Triad solution, as described in [13] and as shown below

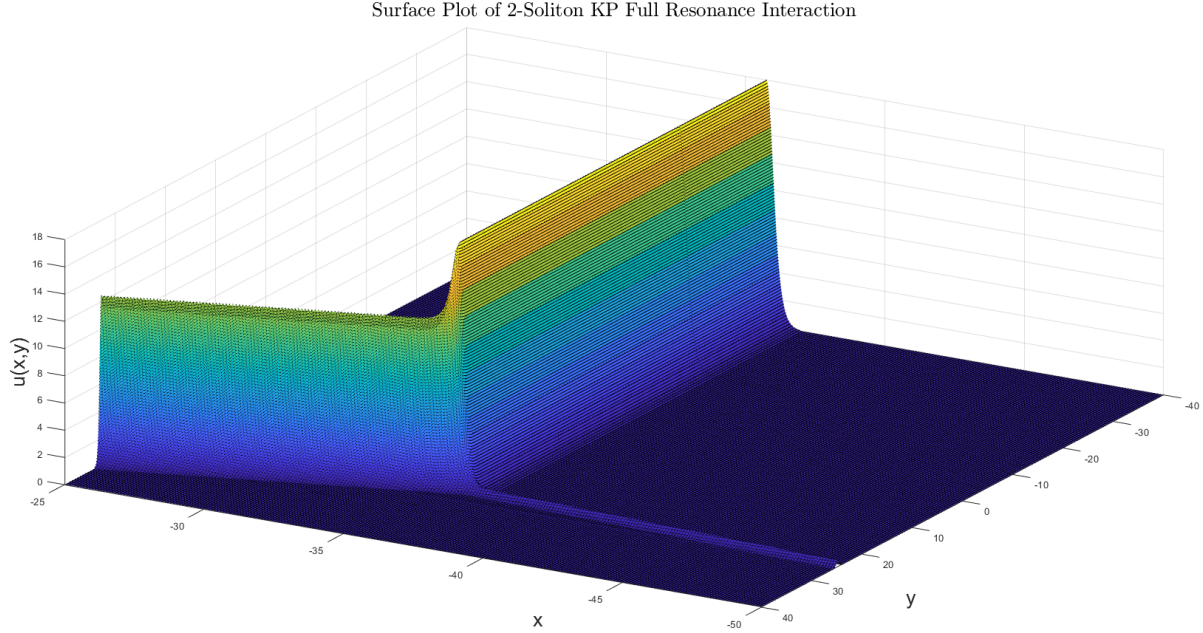


Figure 29: Hirota's Bilinear KP Solution with $A_{12} = 0$

Where the farfield action of the two incident waves is transformed into a singular wave with lower amplitude. This interaction will be explained analytically later using a method of limits on the Hirota's Bilinear solution for term u .

Decreasing A_{12} in this case would lead to singular solutions, which break the system for the given representation. However, increasing A_{12} using a slight perturbation on the n_2 term, e.g. $+e^{-20}$, will gradually decrease the relevance of the interaction region until we reach A_{12} large enough that the interaction region becomes irrelevant and the solution takes the form of an x -type crossover, as shown below

Surface Plot of 2-Soliton KP Partial Resonance Interaction

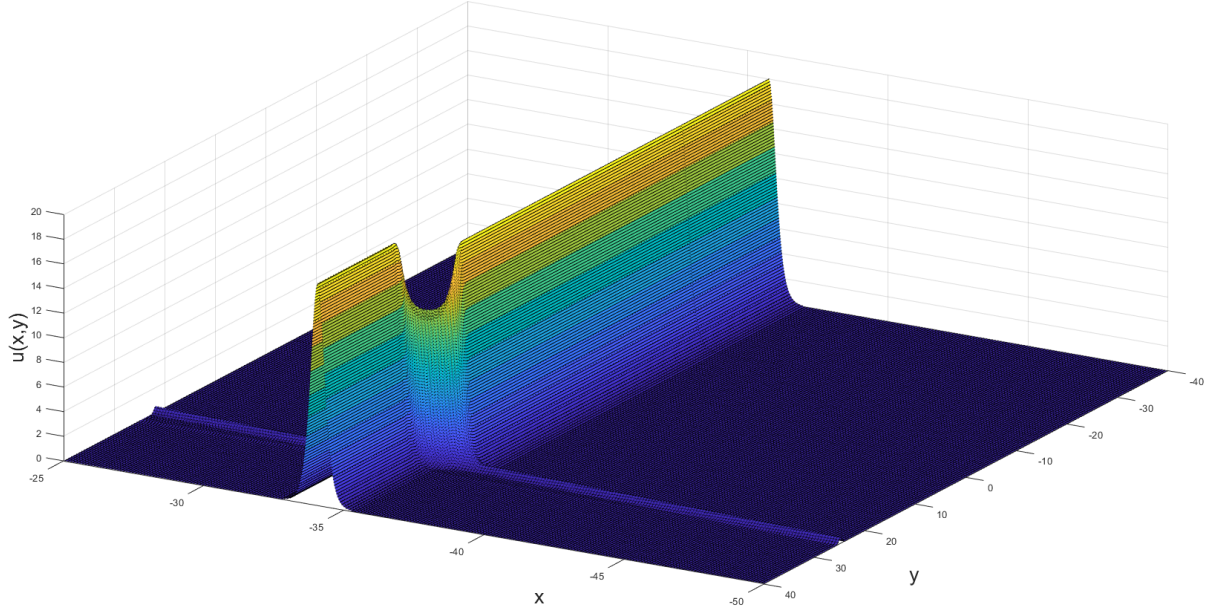


Figure 30: Hirota's Bilinear KP Solution with $A_{12} \approx 0$

Then the amount of intersection of the waves can be modified by changing the size of the additional parameter, e.g. by using $n_2 = 3 + e^{-10}$ gives a narrower intersection since the system is tending towards the two-soliton farfield state at either farfield limit for each soliton. Finally, choosing $n_1 \neq n_2$ and $l_1 \neq l_2$ such as using $(l_1, n_1) = (2, 1)$ and $(l_2, n_2) = (3, 3)$, results in the aforementioned x -type crossover with minimal action at the interface

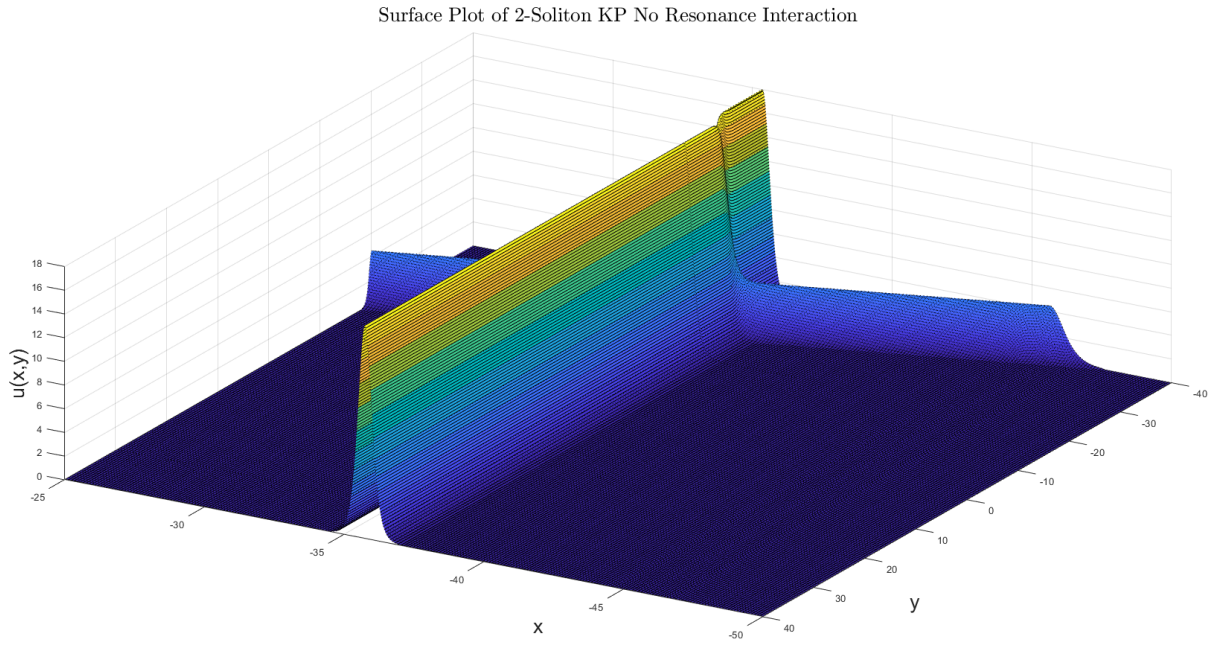


Figure 31: Hirota's Bilinear KP Solution with $A_{12} \neq 0$

This last interaction is the form that will be carried forward in the analysis, since it relates closest to the constructive interference scenario, but the others provide instructive background on other potential KP Hirota solutions.

Now using the above information about when instabilities of the solution occur, the maximal value attainable by the intersection of two waves can intuitively be found by changing the angle of the waves to be closer and observing the maximal height at the origin for fixed time $t = 0$ as long as the system gives a reasonable output. Thus taking the vectors for the prior plot of $(0.6, 1.25)$ and $(0.5, 2.5)$ and shifting the value of m_2 lower (the transverse wavenumber component of the second soliton, the equivalent of reducing n_2 and increasing l_2 by the same linear factor up to a limit) will change the angle of approach of the second soliton, and so with $m_2 \approx 1.59$ being a singularity point (since below this causes the coefficient A_{12} turn < 0) taking the limit to this case should make the vectors tend towards parallel, as shown in the figures below

KP Soliton Interaction of vectors $(0.6, 1.25)$ and $(0.5, 2.5)$ at $t = 0$

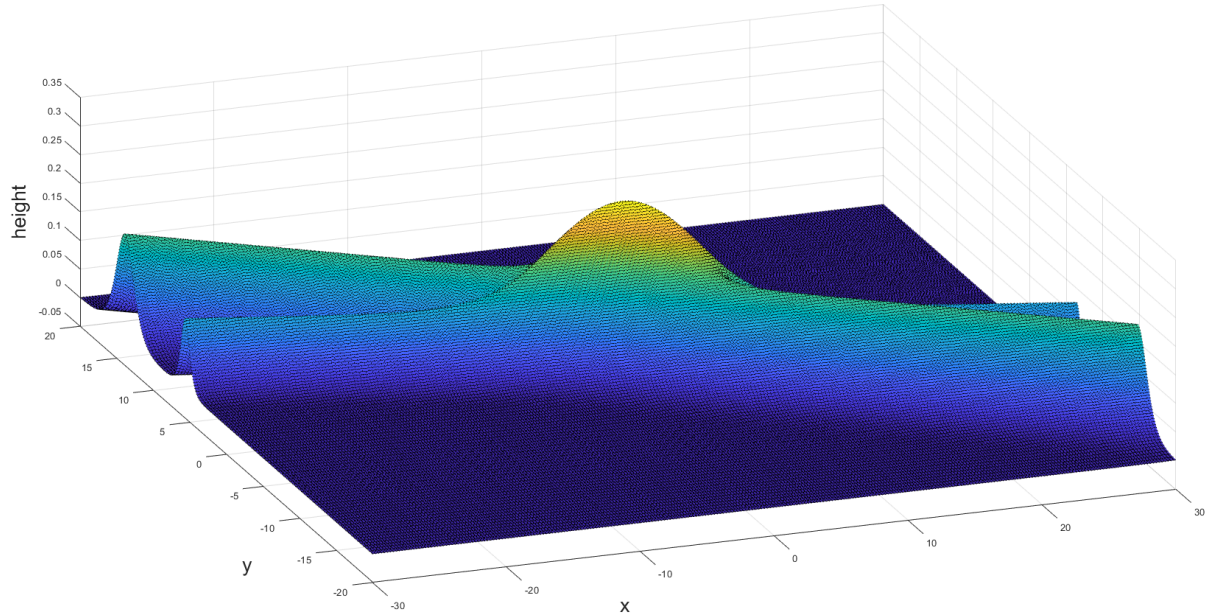


Figure 32: Hirota's Bilinear KP Solution with $m_2 = 2.5$

KP Soliton Interaction of vectors $(0.6, 1.25)$ and $(0.5, 1.7)$ at $t = 0$

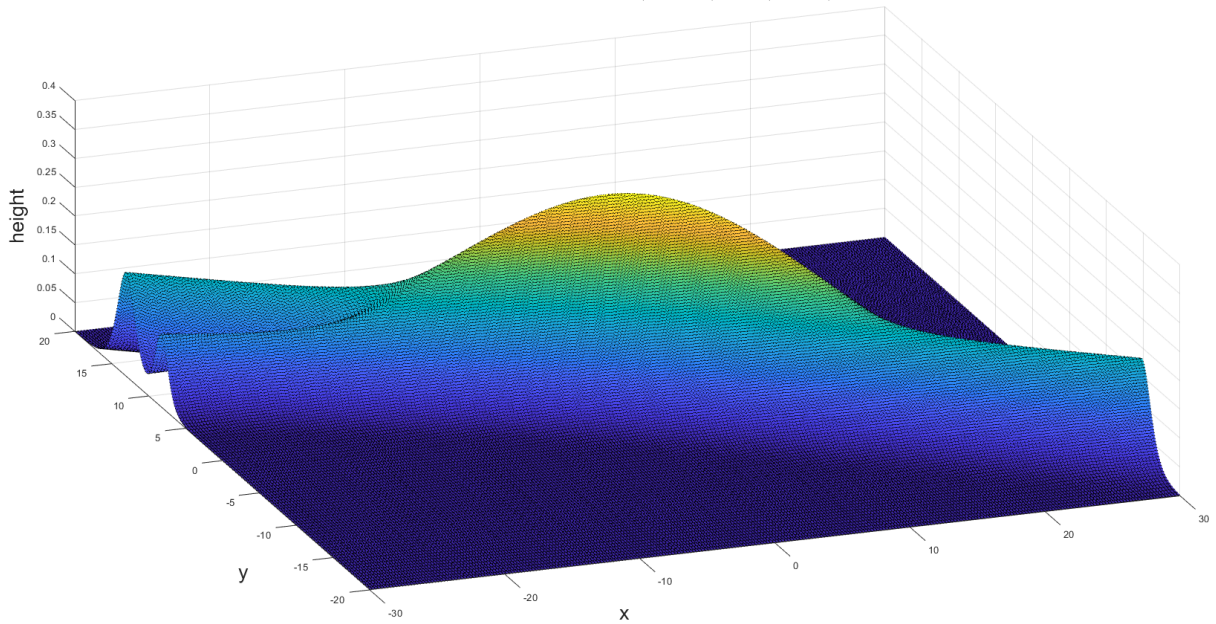


Figure 33: Hirota's Bilinear KP Solution with $m_2 = 1.7$

and finally decreasing the angle further leads to the largest amplitude when the waves are moving closest to parallel (with an instability triggered at $m_2 \approx 1.59$)

KP Soliton Interaction of vectors $(0.6, 1.25)$ and $(0.5, 1.6)$ at $t = 0$

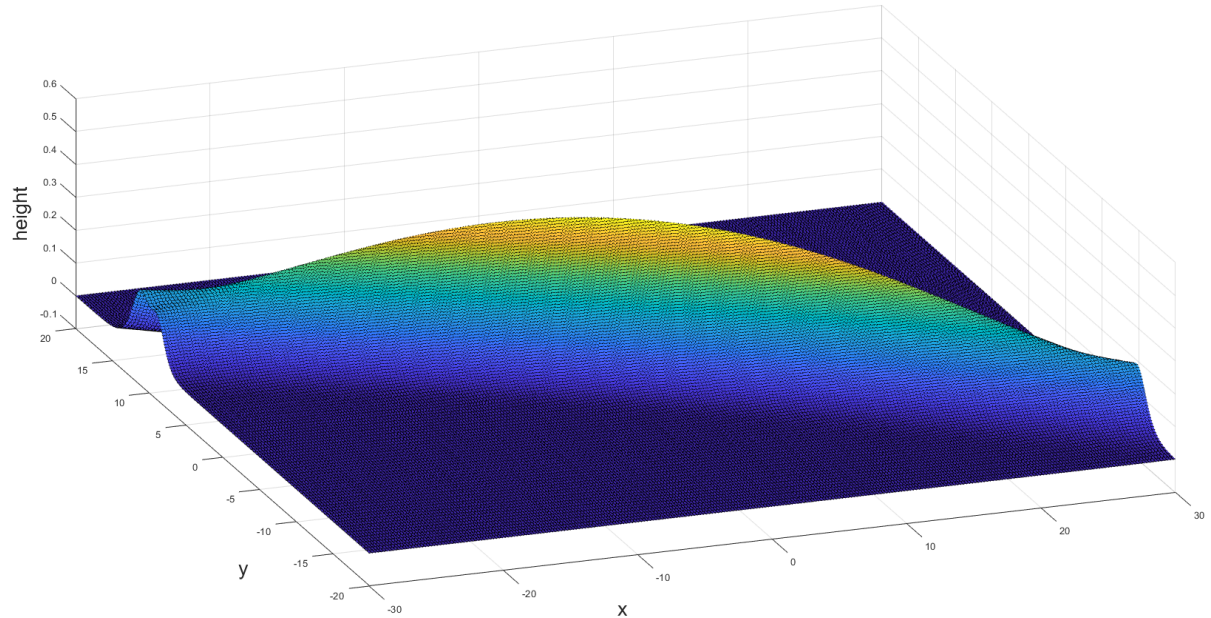


Figure 34: Hirota's Bilinear KP Solution with $m_2 = 1.6$

This shows how for the current model, the maximal amplitude is attained by reducing the angle of intersection towards a limiting angle, as shown in the following plots of the above scenarios where the amplification goes from approximately twice the farfield

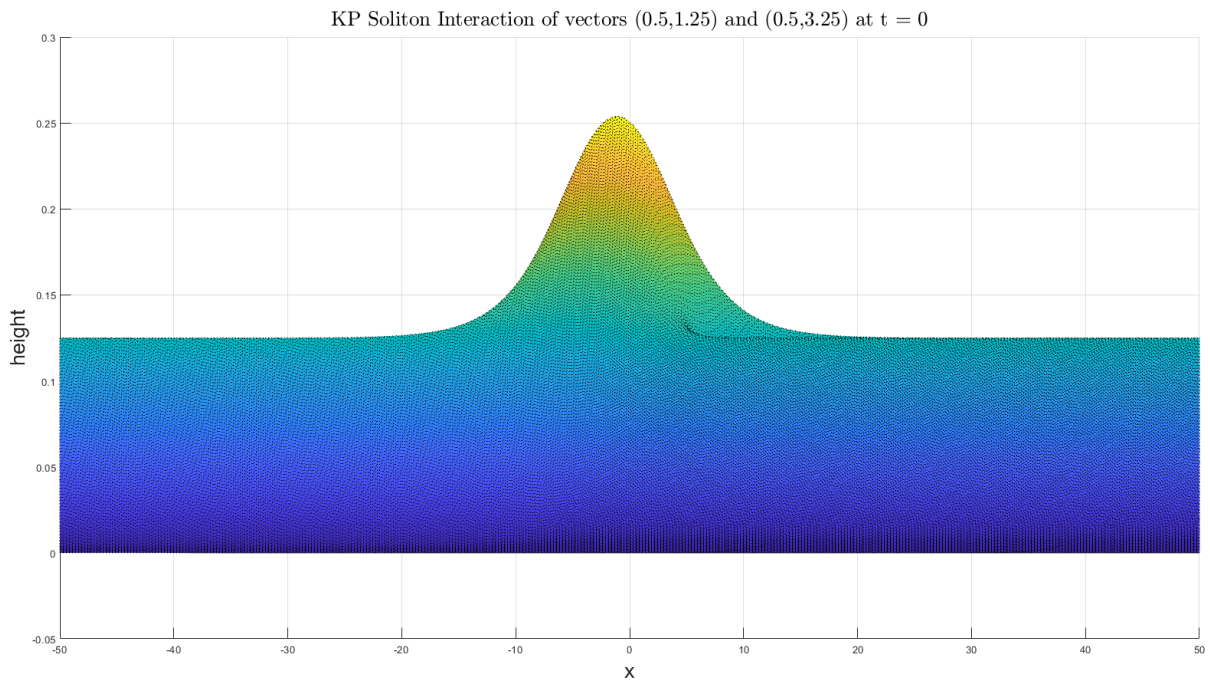


Figure 35: Hirota's Bilinear KP Solution with $m_2 = 2.5$

To around 3 times the farfield amplitude of each incident, equal-height soliton

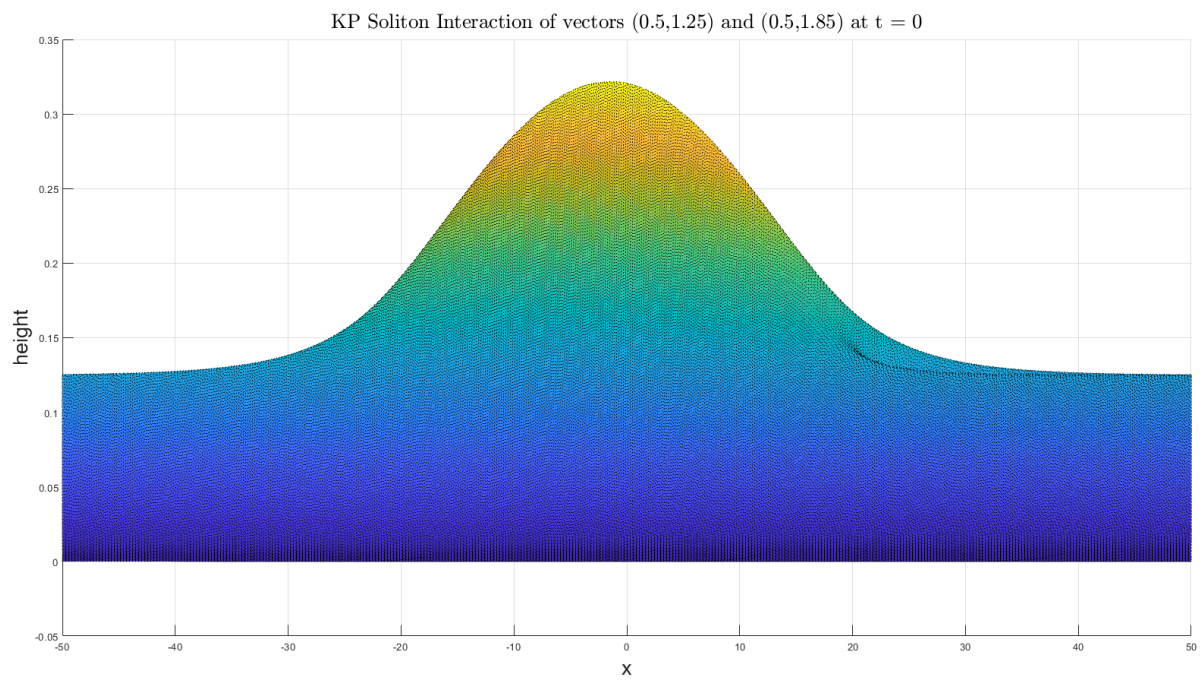


Figure 36: Hirota's Bilinear KP Solution with $m_2 = 1.6$

However upon changing the vector parameters, such as increasing the baseline amplitude of the incident waves and decreasing the angle further, one can achieve an amplification up to 4 times the baseline level, as shown in

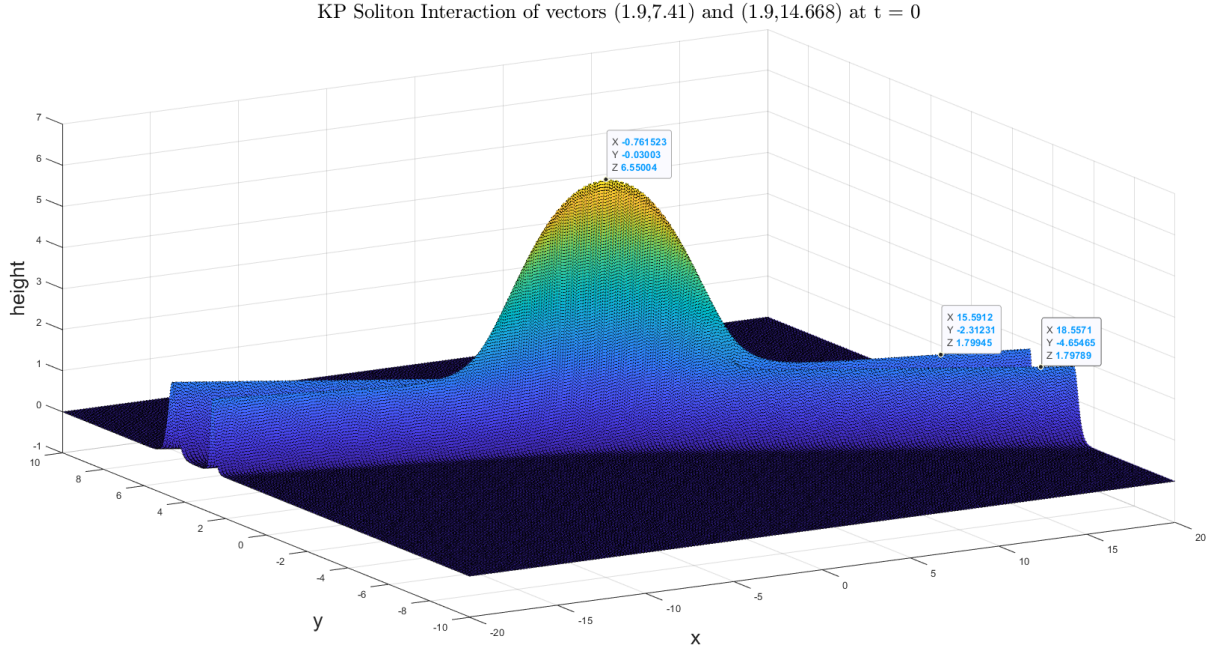


Figure 37: Hirota's Bilinear KP Solution of the above with increased k_i relative to m_i

Which is supported by research, such as is referenced in [34]. This shows how there is a limiting point of the angle bisecting the incident waves such that beyond that limit the coded model as portrayed earlier breaks, and at which the amplification of the interaction region reaches its maximum. This amplification beyond twice the incident solitons is an example of the finer details included in the soliton interaction that simply taking the sum of solitons as at the end of section 3.4 misses. The following pertains to an analytical approach to finding both the maximum angle that achieves this amplification, and the length of the interaction region.

4.4 Angle of Maximum Amplification

The above form of Hirota's Bilinear Method seems to work well for what we want, given that it shows a constructive interference between solitons and exhibits the expected surface tension

effects, but that isn't all of the properties expected of these solutions compared to the real world. For real tsunamis, there exists a field of research on which angle of intersection between solitons results in the greatest amplification at the interface, and hence is the most destructive. Therefore given this, research has found that the angle that produces the largest wavefront is not, in fact, waves moving in parallel, but a small angle referred to generally as α , which will be discussed in this section.

To derive this α , first we must evaluate the current model using Hirota's Bilinear Method. Now using the method of finding Hirota's Bilinear Solution to the standard, but linearised KP equation, uses the dispersion relation $\omega_i = \frac{-k_i^4 - 3m_i^2}{k_i}$, which differs to the prior method since they ([29]) take $\eta = k_i x + m_i y + \omega_i y$ so time works in reverse. Regardless, the two soliton interaction coefficient after performing the same method falls out as

$$A_{12} = \frac{\lambda^2 - (k_1 - k_2)^2}{\lambda^2 - (k_1 + k_2)^2} \quad \text{for} \quad \lambda = \frac{m_1}{k_1} - \frac{m_2}{k_2}$$

This representation is equivalent to a simplified form without the coefficient 3 of the previous form

$$A_{12} = \frac{3k_1^2 k_2^2 (k_1 - k_2)^2 - (k_1 m_2 - k_2 m_1)^2}{3k_1^2 k_2^2 (k_1 + k_2)^2 - (k_1 m_2 - k_2 m_1)^2}$$

and is made since the constant λ representation has been chosen such that the ratio of m_i to k_i can be converted to one parameter in the angle bisecting the two incident waves, as will be derived below.

Now when exploring maximal amplification, we will exclusively look at scenarios of negative phase shift, as defined in section 3.6, where the resultant wave amplitude is greater than the sum of the incident waves. This is because the positive phase shift case results in a destructive wave interaction, and hence will not yield the maximum, or any, amplification above the incident waves.

Regarding the incident waves, what will be considered from now on are waves that travel in the positive x direction (reverse of before), and where the interaction is bisected by the x -axis. Physically, paper [29] portrays this system to look like

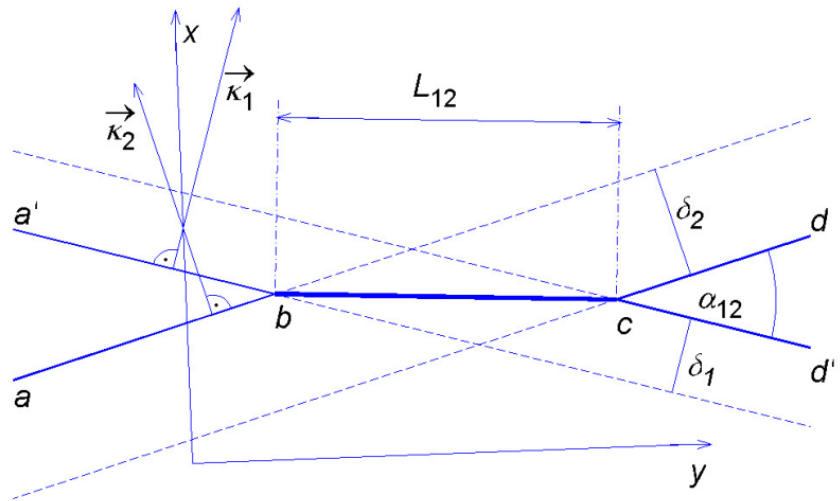


Figure 38: Diagram from paper [29] showing incident soliton vectors, the angle of intersection α_{12} , the length L_{12} of the resultant soliton, and the phase shift parameters δ_i

Where the interaction region becomes a short straight line soliton at the intersection of the wave vectors, similarly to the prior plots in this paper used for decreasing the angle before, where a top-down view more clearly shows the property L_{12} increasing as the angle decreases

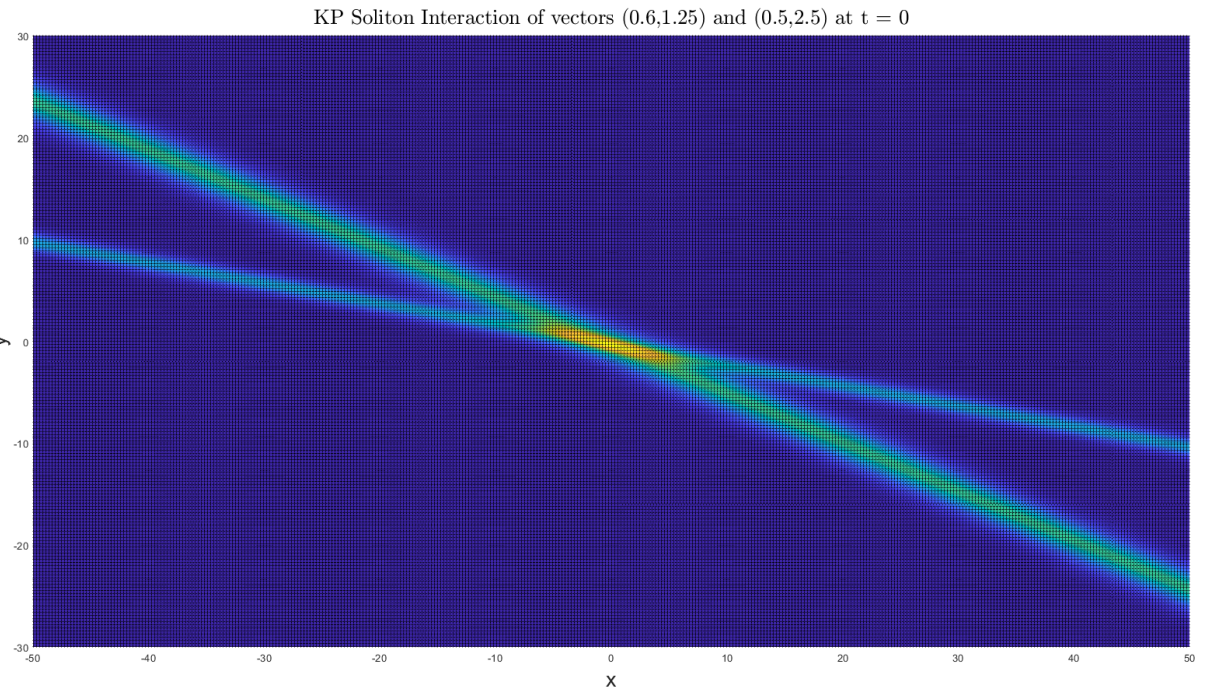


Figure 39: Top-Down View of Hirota's Bilinear KP Solution with $m_2 = 2.5$

and then decreasing the y component of the second vector

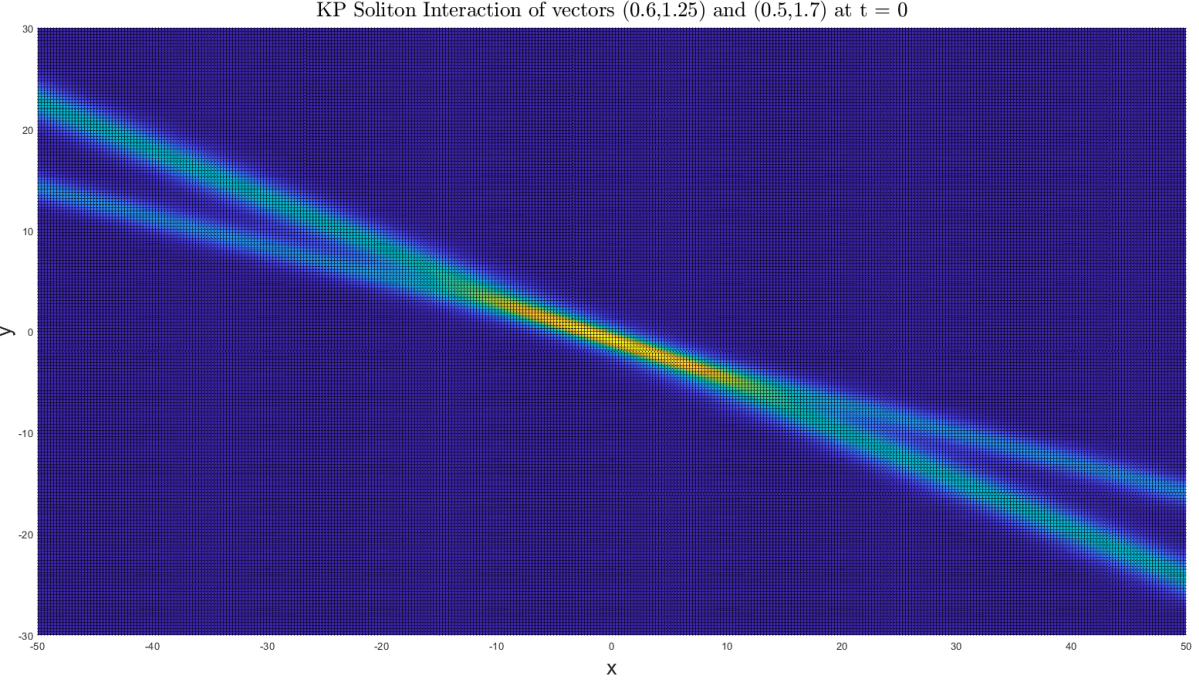


Figure 40: Top-Down View of Hirota's Bilinear KP Solution with $m_2 = 1.7$

Where the annotations show the properties L_{12} and α_{12} that will be investigated and defined here. The presence of this line at the interface means each individual wave is delayed by a specific amount, which is notated in figure 38 by δ_i . This phase shift can be shown using the derived equation by taking the limit as $\eta_i = k_i x + m_i y - \omega_i t$ tends to $\pm\infty$ as shown in paper [38], where taking the surface elevation equation derived using Hirota's method

$$U(\theta_1, \theta_2) = 2 \left(k_1 \frac{\partial}{\partial \theta_1} + k_2 \frac{\partial}{\partial \theta_2} \right)^2 \log \left(1 + e^{\theta_1} + e^{\theta_2} + A_{12} e^{\theta_1 + \theta_2} \right)$$

Then the limit as θ_i tends to $-\infty$ will give the equation

$$U(\theta_i, \theta_j) = 2 \left(k_j \frac{\partial}{\partial \theta_j} \right)^2 \log(1 + e^{\theta_j})$$

Where derivatives in variables that have a negligible contribution to the solution have been omitted, which just leaves the original single-soliton solution for initial soliton indexed by j . However, taking the limit as θ_i tends to $+\infty$ means the terms that tend to infinity (e^∞) can

be grouped and divided through by the divergent portion to give the equation

$$U(\theta_i, \theta_j) = 2 \left(k_i \frac{\partial}{\partial \theta_i} \right)^2 \log \left(e^{\theta_i} \times (e^{-\theta_i} + 1 + e^{\theta_j - \theta_i} + A_{12} e^{\theta_j}) \right) = 2 \left(k_j \frac{\partial}{\partial \theta_j} \right)^2 \log(1 + e^{\theta_j} + A_{12})$$

When applying what is known as Gauge invariance ([38]) to eliminate the e^{θ_i} term. Gauge invariance is the disregarding of a coefficient $\lim_{x \rightarrow \infty} e^x K$ for function K that is kept; which can be done by using $\log(ab) = \log(a) + \log(b)$, and so the unwanted coefficient can be removed and substituted into the equation u independently to get

$$2 \left(k_1 \frac{\partial}{\partial \theta_1} + k_2 \frac{\partial}{\partial \theta_2} \right)^2 \log(e^{-\theta_i}) = 2 \left(k_1 \frac{\partial}{\partial \theta_1} + k_2 \frac{\partial}{\partial \theta_2} \right)^2 (-\theta_i)$$

For large θ_i , and so since there is no θ_j dependence, taking the derivatives in terms θ_i results in

$$= 2 \left(k_i \frac{\partial^2}{\partial \theta_i^2} \right) (-\theta_i) = 2k_i \frac{\partial}{\partial \theta_i} (-1) = 0$$

And so the exponentially large coefficient term in θ_i can be ignored.

This shows how now there is an extra contribution of $\log(A_{12})$, which is exactly where the previous $\Delta_{12} = -\log(A_{12})$ phase shift parameter from section 3.6 comes from. The effect of this on the height of the interaction soliton is that $A_{12} < 1$ results in the shift being positive, and so the waves are shifted away from each other, hence also leading to the dip as the waves are displaced away from the overlapping region, and vice versa for $A_{12} > 1$ where there is negative shift, and so the waves are shifted into each other's path and superpose while being displaced by a phase shift δ_i .

This can be applied to the specific cases examined before, where taking $A_{12} = 0$ in the $+\infty$ case leads to the individual limiting processes tending to 0, but for $\theta_1 - \theta_2$ as a constant value, taking $\theta_1 + \theta_2$ to $+\infty$ can be done by repeating the same method but by taking a factor of $e^{\frac{1}{2}(\theta_1 + \theta_2)}$ out instead of just e^{θ_i} after setting the A_{12} term to 0, and results in the equation ([38])

$$U(\theta_i, \theta_j) = 2 \left(k_1 \frac{\partial}{\partial \theta_1} + k_2 \frac{\partial}{\partial \theta_2} \right)^2 \log(1 + e^{\theta_i - \theta_j})$$

Which is why the prior examination of the $A_{12} = 0$ singularity had the shape

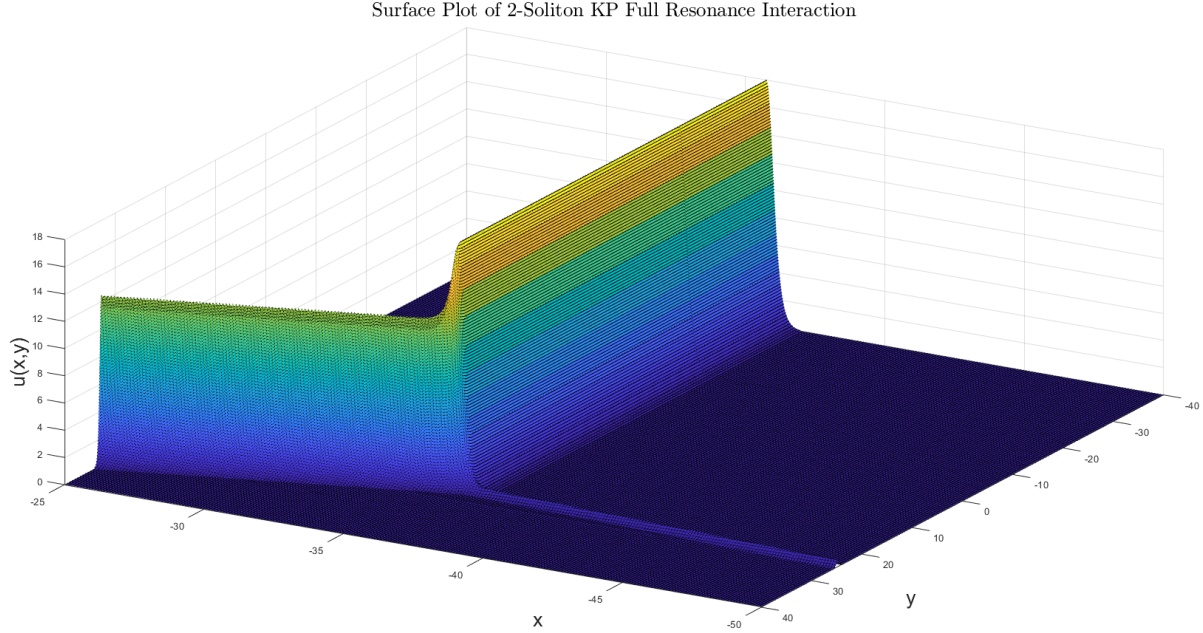


Figure 41: Hirota's Bilinear KP Solution with $A_{12} = 0$

Since the solution tends towards a soliton with equation $u = \frac{(k_1-k_2)^2}{2} \operatorname{sech}^2\left(\frac{1}{2}(\theta_1 - \theta_2)\right)$ at the farfield $\theta_1 + \theta_2$ tending to $+\infty$, and so the smaller resultant soliton points in the direction of $\theta_1 + \theta_2$ and continues on as a singular soliton, without reforming into the incident solitons. This is still an unrealistic case for rogue wave models, but is important to note as it defines the divide between real solutions for the KP equation with $A_{12} > 0$ and singular solutions that break the system for $A_{12} < 0$.

We will now take the incident waves to be of equal amplitude, due to the definition of negative phase shifts given above suggesting this as the limiting case that yields the greatest amplification; and the result of this is that the wave vectors become (k, m) and $(k, -m)$ such that $\lambda = \frac{2m}{k}$, and so by the definition of the vectors k , m and the angle α_{12} , this can be turned into an equation depending only on α_{12} (the angle between solitons 1 and 2) using trigonometric identities on the bisected form of α shown in

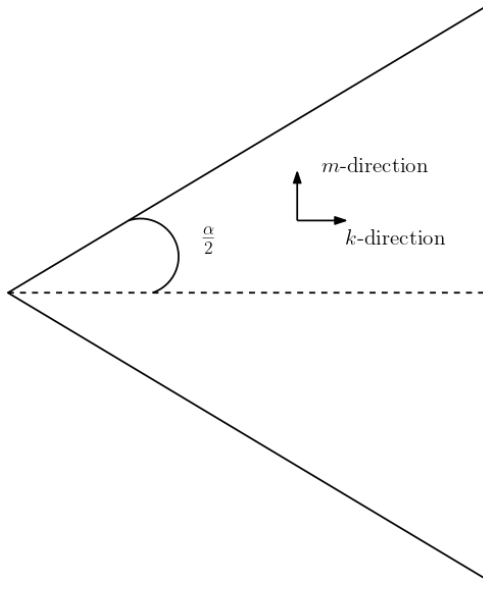


Figure 42: Bisected Angle of Figure 38

with the right angle separating the two waves to get $\lambda = \frac{2m}{k} = 2 \tan\left(\frac{\alpha_{12}}{2}\right)$, and so $\alpha_{12} = 2 \arctan\left(\frac{\lambda}{2}\right)$ for λ as the parameter in wavenumbers derived from the term A_{12} , which then leaves $A_{12} = \frac{4 \tan^2\left(\frac{\alpha_{12}}{2}\right) - (k_1 - k_2)^2}{4 \tan^2\left(\frac{\alpha_{12}}{2}\right) - (k_1 + k_2)^2}$ as given in paper [35], and $= \frac{m^2}{m^2 - k^4}$ after simplification of the form given prior with the specific choice of vectors for equal height incident solitons.

The length of the interaction L_{12} , otherwise known as the width of the resultant rogue wave superposition vector s_{12} , can be mathematically obtained using the above representation by taking the parallelogram formed from the phase shifts of the vectors $\kappa_i = (k_i, m_i)$, and so one can find the resultant vector by taking the sum of the vectors κ_i , normalising it using length $= \kappa_1 \times \kappa_2$, and finally scale by the phase shift parameter, defined in section 3.6 as $\Delta_{12} = -\log(A_{12})$; which gives

$$L_{12} = \frac{|\kappa_1 + \kappa_2|}{|\kappa_1 \times \kappa_2|} |\Delta_{12}|$$

for $\kappa_1 + \kappa_2 = (k_1 + k_2, m_1 + m_2)$

And when taking equal height incident vectors as we are, this becomes $(2k, 0)$, and since $\kappa_1 \times \kappa_2$ for vectors κ_1 and κ_2 is the same as taking the determinant of the matrix

$$\begin{bmatrix} k_1 & m_1 \\ k_2 & m_2 \end{bmatrix} = \begin{bmatrix} k & m \\ k & -m \end{bmatrix}$$

that means the absolute values give $L_{12} = \frac{\sqrt{4k^2}}{2km} |- \log A_{12}| = \frac{\log(A_{12})}{m}$.

Returning to the maximum amplification, the function f can be written in terms of the parameter λ , which we found to be dependent on the angle α above, such as in paper [35] where they define f using a transformation on the following original form $f = 1 + e^{\theta_1} + e^{\theta_2} + A_{12}e^{\theta_1+\theta_2}$ by taking a factor of $e^{\frac{\theta_1+\theta_2}{2}}$ out of each term in f and applying the cosh simplification to the two single-soliton contributions to get ([38])

$$f = 2 \cosh\left(\frac{1}{2}(\theta_1 - \theta_2)\right) + \sqrt{A_{12}} \left(e^{-\frac{1}{2}(\theta_1 + \theta_2) - \log(\sqrt{A_{12}})} + e^{\frac{1}{2}(\theta_1 + \theta_2) + \log(\sqrt{A_{12}})} \right)$$

Where the latter two terms in the bracket are the constant 1 and the A_{12} contribution respectively. This can then be simplified further using a second cosh function to group the latter terms and substituted into the equation for the Hirota solution form $u = 2 \frac{\partial^2}{\partial x^2} \log(f)$ to get (paper [35])

$$\begin{aligned} u(x, y, t = 0) &= 2 \frac{\partial^2}{\partial x^2} \log[\cosh\left(\frac{1}{2}\left(k_1\left(x + \frac{1}{2}y\lambda\right) - k_2\left(x - \frac{1}{2}y\lambda\right)\right)\right) \\ &\quad + \sqrt{A_{12}} \cosh\left(\frac{1}{2}\left(k_1\left(x + \frac{1}{2}y\lambda\right) + k_2\left(x - \frac{1}{2}y\lambda\right) - \Delta_{12}\right)\right)] \\ &\quad \text{and in [38]} \\ &= \frac{1}{f^2} [\sqrt{A_{12}} k_1^2 \cosh(\theta_2 + \log(\sqrt{A_{12}})) + \sqrt{A_{12}} k_2^2 \cosh(\theta_1 + \log(\sqrt{A_{12}})) + \\ &\quad \frac{1}{2}((k_1 - k_2)^2 + A_{12}(k_1 + k_2)^2)] \end{aligned} \tag{4.8}$$

Which incorporates the term $\lambda(\alpha)$ from before. This overtly shows how the first two terms relate to the contributions of the individual θ_i 's, while the latter term relates to the superposition amplitude, which is what the maximum amplification is dependent on. Paper [38] verifies this by further repeating the farfield limits to find its contribution is 0 at either extreme, so these results will be assumed for the sake of the following argument. This leaves the amplitude as

$$a_{12} = \frac{(k_1 - k_2)^2 + A_{12}(k_1 + k_2)^2}{2f^2}$$

Which can be simplified using the choice of vectors used above in (k, m) and $(k, -m)$ and by taking the maximal value of $\frac{1}{\cosh} = 1$ to get ([29])

$$a_{12} = \frac{2A_{12}k^2}{(1 + \sqrt{A_{12}})^2}$$

Now to attain the maximum amplification, one must simply find the α_{12} which maximises this function, using the resulting values from A_{12} . This can be found by expanding the square on the denominator and dividing through by A_{12} to find $a_{12} = \frac{2k^2}{\frac{1}{A_{12}} + \frac{2}{\sqrt{A_{12}}} + 1}$, and so taking the limit as A_{12} tends to ∞ will give the maximal amplification as $2k^2$, which occurs when the denominator of $A_{12} = \frac{4\tan^2(\frac{\alpha_{12}}{2}) - (k_1 - k_2)^2}{4\tan^2(\frac{\alpha_{12}}{2}) - (k_1 + k_2)^2}$ is minimised, so

$$4\tan^2\left(\frac{\alpha_{12}}{2}\right) \approx 4k^2$$

and so $\alpha_{12} = 2\arctan(\pm k)$ will give the maximal amplification of the system, where the \pm is the result of swapping the ordering of the vectors, since arctan is symmetric. This makes sense, since inputting the k portion of the vector will give the ideal angle, and from which one can reverse engineer the corresponding choice of m .

Paper [29] provides an alternative form of this angle which depends on the initial soliton heights given by $\frac{k^2}{2}$ and the ocean depth h

$$\alpha_{12} = 2\arctan\left(\sqrt{\frac{3\eta}{h}}\right)$$

Then they provide an example of a typical wave scenario of $\eta = 1.8$ metres and $h = 50$ metres to give an ideal angle of 36° , which represents a typical rogue wave scenario, and so this angle should be relatively consistent for most equivalent rogue wave models. Therefore this will later be compared to another wave scenario in a different model to test the reproducibility of results between methods.

4.5 Breather Solitons

For the KP equation, as stated prior, inclusion of surface tension comes from taking the general form in equation 4.2, and modifying the final transverse term similarly to the changes made to the non-linear term in the KdV equation, where we change it to

$$\partial_x(u_t + 6uu_x + u_{xxx}) + 3\sigma u_{yy} = 0$$

for some parameter

$$\sigma = \begin{cases} +1 & \text{for low surface tension} \\ -1 & \text{for high surface tension} \end{cases}$$

However this parameter acts very differently to the KdV parameter ϕ defined before, since choosing the case of $\sigma = +1$ results in the line soliton solutions seen prior above and for the KdV equation, but choosing $\sigma = -1$ results in a completely different soliton form known as the Lump or Breather Wave soliton.

We do this because the above system of interactions between line-soliton solutions for the KP equation gave realistic looking solutions for multiple wave collisions, but isn't the only solution form to the KP equation that can give rogue wave like results. The next solution form also requires using a different ansatz to the above method detailed in Hirota's method for line-soliton solutions.

This method starts similarly but now we begin with $\sigma = -1$ to give the high surface tension equation, referred to in most literature as the KPI equation.

$$\partial_x(u_t + 6uu_x + u_{xxx}) - u_{yy} = 0$$

however it is possible to recreate this method with the KPII equation, but in this form one can include the effects of surface tension in the hopes of reproducing the capillary forces seen in Milweski's Boussinesq solutions [26] that were difficult to obtain with the KdV methods used earlier.

Now to begin, assume a change of dependent variable as $u = u_0 + 2\frac{\partial^2 \log f(x,t)}{\partial x^2}$, for which the

variable R from the KdV system is still unchanged, but this time assume the function f to be of the form

$$f = e^{-p_1(\zeta - ay)} + \delta_1 \cos(p(\zeta + by)) + \delta_2 e^{p_1(\zeta - ay)} \quad (4.9)$$

as is suggested in paper [20] for each of p_1 , p , a , b , δ_1 and δ_2 as constants to be determined to give the solution for this system. Therefore, substituting this f ansatz into the change of dependent variable u , then back into the modified form of equation 4.2 gives an equation of coefficients for powers of $e^{p_1(\zeta - ay)}$, and so grouping coefficients for each power of this, e.g. for $e^{-p_1(\zeta - ay)}$, e^0 and $e^{p_1(\zeta - ay)}$, and setting them to 0 as per the KP equation gives a system of five equations that can be used to find the values of the six constants needed. The prior sentence has a glaring issue, however, in that there are too many unknowns to solve explicitly for each in the current state; therefore if one assumes that $p_1 = p$ for simplicity then the system can be solved for the remaining constants to give

$$\delta_1 = \pm 2 \left(\frac{(2a^2 - (1 + 6u_0) - b^2)\delta_2}{2b^2 - (1 + 6u_0) - a^2} \right)^{\frac{1}{2}}$$

$$ab = -(1 + 6u_0)$$

$$p^2 = \frac{b^2 - a^2}{4}$$

where the latter two mean $|b| > |a|$ and gives an explicit form for a in terms of b . The result of this is that a , b , δ_2 and the constant u_0 from the start can be chosen to be anything that matches these requirements.

Therefore we choose to set u_0 such that $1 + 6u_0 \neq 0$ (so that both a and b are non-zero) and choose δ_2 such that δ_1 is real. This means that for $u_0 < \frac{-1}{6}$, it means $a^2 > 1 + 6u_0$, and vice versa for $u_0 > \frac{-1}{6}$. Using all of these above results in the ansatz for f given in equation 4.9 results in two solutions depending on the choice of u_0 relative to $\frac{-1}{6}$ (the sign of the δ_1 term) given in [20] by

$$f(\zeta, y) = 2\sqrt{\delta_2} \cosh \left(p \left(\zeta + \frac{1 + 6u_0}{b} y \right) + \frac{1}{2} \log(\delta_2) \right) + \delta_1 \cos(p(\zeta + by))$$

The solution u then follows by again substituting back into the defining equation for the f re-parameterisation, and given that the second derivative of $\log G(x)$ is $\frac{\partial}{\partial x} \frac{G'(x)}{G(x)} = \frac{G''(x)G(x)-G'^2(x)}{G^2(x)}$ for $G(x)$ as functions of $\cosh \zeta$ and $\cos \zeta$.

This still leaves a general δ_2 term, which can be set equal to 1 to make the $\log \delta_2$ terms equal to 0, which simplifies the equation by making the original function f have a $e^{p_1(\zeta-ay)}+e^{-p_1(\zeta-ay)}=2 \cosh(p_1(\zeta-ay))$ term, which cancels terms in the solutions for u_2 (the negative δ_1 case).

This leaves the solution as the periodic function

$$u(\xi, y) = u_0 + \frac{2p^2(m_0 - 2m_1 \sinh(p\zeta + p\frac{1+6u_0}{b}y) \sin(p\zeta + pby))}{(\cosh(p\zeta + p\frac{1+6u_0}{b}y) - m_1 \cos(p\zeta + pby))^2}$$

$$m_0 = \frac{12p^2}{4p^2 - (1 + 6u_0) + b^2}, \quad m_1 = \sqrt{\frac{a^2 - (1 + 6u_0) - 4p^2}{4p^2 - (1 + 6u_0) + b^2}}$$

Plotting this solution appears as a series of two-dimensional sech functions, known in the literature as lump solitons, all in a line with the same vector form as the single line soliton solutions found prior

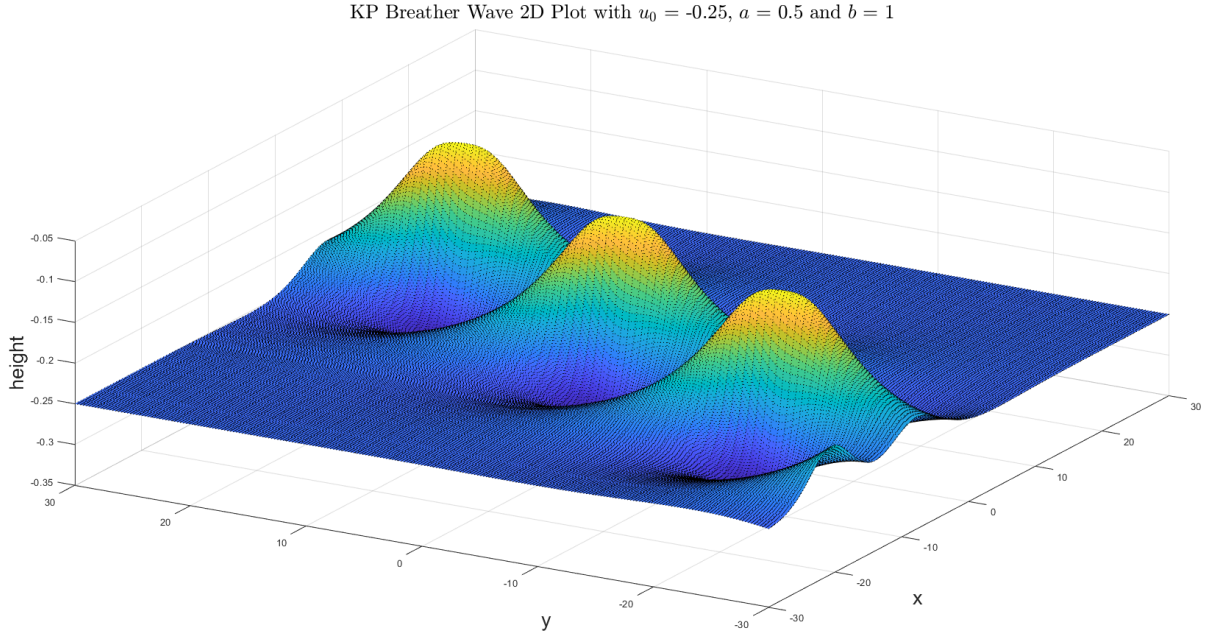


Figure 43: Surface Plot of Hirota's Bilinear Method ($x, y, height$) for the Breather Solution at $t = 0$

To finish the model, the parameter p was defined to control the periodicity of the solution, hence taking the limit as the periodicity tends to ∞ will cause the formation of a standalone wave, as the next will form at infinity, which is what we want to model since rogue waves are defined to be much larger than the rest of their group, and therefore won't be succeeded by waves of equal amplitude. This is done by looking at the periodic term in $\cos(p(\zeta + by))$ and saying the period is given by 2π divided by the coefficient of the spatial term in the subject of \cos , which here is p , so we take the limit as it tends to 0. Notably, increasing the value of p will tend towards the soliton solution for the KP equation derived previously, which further affirms that this change will isolate a singular waveform rather than the group.

Applying both of these conditions to the equation for u_2 results in the KP Breather solution for rogue waves

$$u(\xi, y) = u_0 + \frac{16(6R - (\zeta + \frac{1+6u_0}{b}y)(\zeta + by))}{((\zeta + \frac{1+6u_0}{b}y)^2 + (\zeta + by)^2 + 8R)^2} \quad (4.10)$$

for parameter $R = \frac{1}{b^2 - (1+6u_0)}$ and $\zeta = x + t$, where notably the condition $p = \sqrt{\frac{b^2 - a^2}{4}}$ means $b \approx a$ for p tending to 0.

This model is of two waves combining, as is defined by the exponential terms in the definition of f given what is known about introducing multiple-soliton solutions using Hirota's method.

The wave is travelling in the negative x direction, which means the wave hits the point $(-1, 0)$ at time $t = 1$, where t is time relative to a specific point, rather than from first instability.

This solution can be plotted for both snapshots in space (for x since it is centred around $y = 0$) and time, however this surface looks identical to the two-dimensional surface plot due to the parameter $\zeta = x + t$ being the only relevance of the terms x and t , hence showing how time and space when on a similar scale have the same effect on the surface, which appears as such

KP Breather Wave 2D Plot with $u_0 = -0.5$, $b = 1.4142$

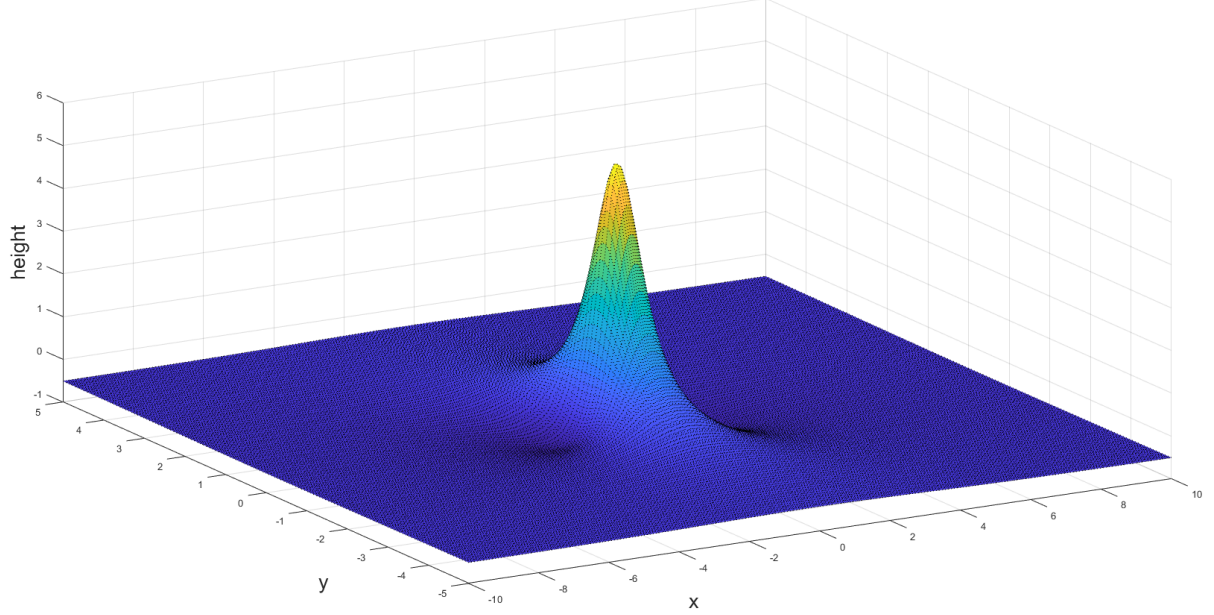


Figure 44: Surface Plot of Hirota's Bilinear Method (x, y, h) for the Breather Solution at $t = 0$

Which shows that along $y = 0$, the envelope of the wave dips below the equilibrium level before quickly rising to a peak and decreasing back down, again dipping below equilibrium before levelling off. This is exactly what Milewski showed for the Boussinesq solution with surface tension in paper [26] by recalling figure 8

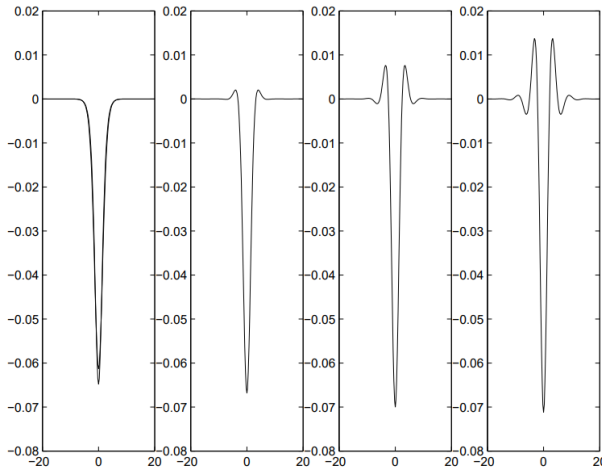


Figure 45: Plots from paper [26] of u_x vs x for varying parameter $B = \frac{\gamma}{h^2}$

Which is directly comparable to a cross-sectional plot of the above surface at a given time

and y cut, such as in

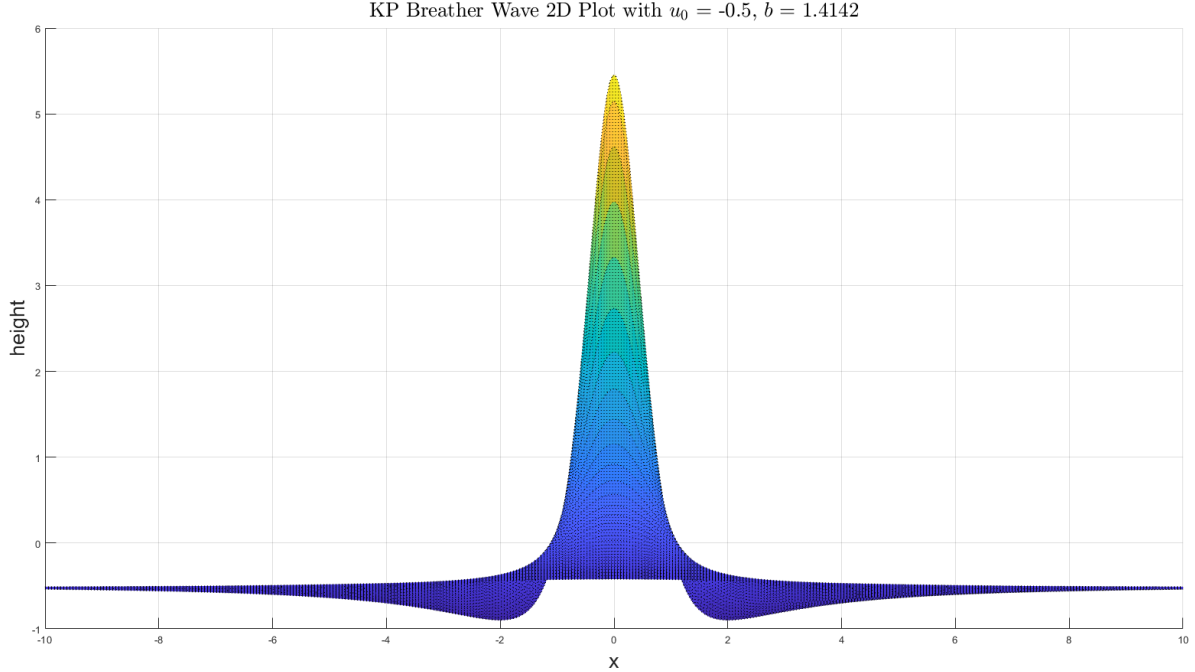


Figure 46: Plot of x vs height for fixed $y = 0$ for a wave moving in the negative x direction

The dips seen before and after the wave hits this point are symptomatic of the inclusion of a small amount of surface tension in the definition of the KPI form of equation 4.2 for the negative u_{yy} term with an inner KdV equation with positive $6uu_x$ term, which is called Capillary Action. Increasing the force further would introduce further oscillations in the farfield away from the instability, which dampen the further away they get. If this force wasn't present, then the envelope of the wave would remain at equilibrium before and after the soliton passes, but this is unrealistic of intuitive knowledge of how large waves interact with the surrounding body of water. It is also possible to recreate these capillary dips either side of the wavefront using other, non-periodic functions f , such as those explored in paper [52]. Therefore further investigation is needed to identify the necessary factors in the ansatz f in Hirota's method that can lead to oscillatory motion off the leading envelope wave.

Notably, if one instead takes the periodicity to 0, and so there are infinitely many lump soliton solutions in a row, this means taking the term p to ∞ and so leaves the solution as

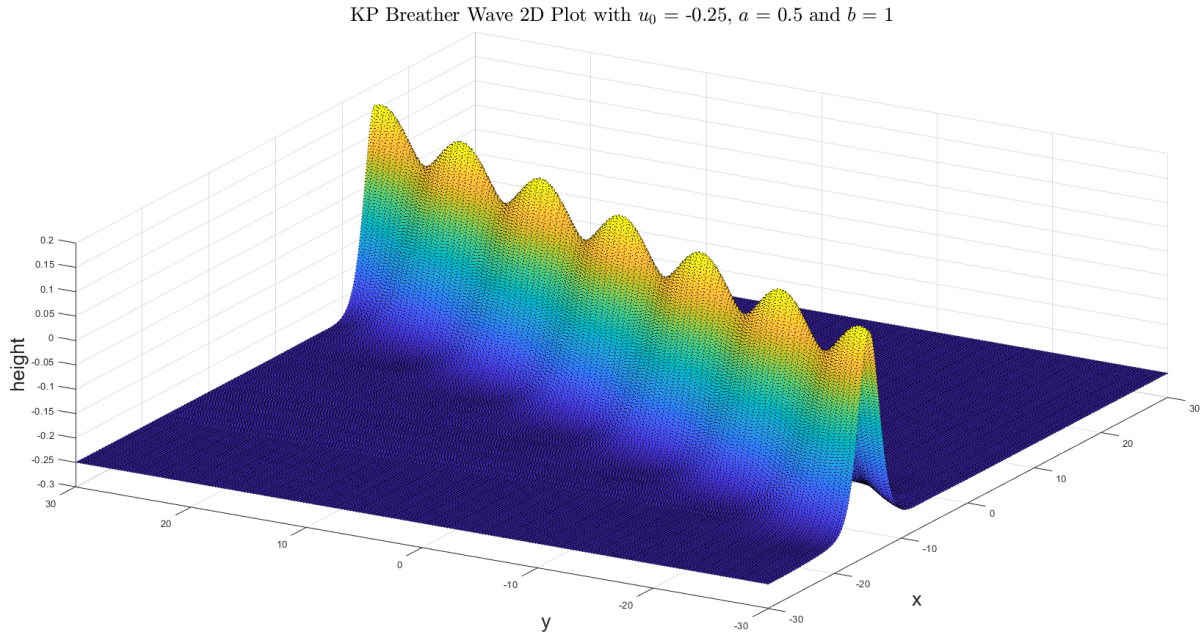


Figure 47: Surface Plot of Hirota's Bilinear Method (x, y, height) for the Breather Solution at $t = 0$ as periodicity tends to 0

Which shows how the new solution ansatz relates to the original line-soliton solution found by using $f(x, y, t) = 1 + \sum_{n=1}^{\infty} \epsilon^n f_n(x, y, t)$, and so each soliton solution type can be found using a multitude of different solution ansatz forms, where those used thus far are just two instructive examples. This allows for us to attain line-soliton solutions with realistic surface tension effects by taking the limit of this solution. This has a profound impact on the current interpretation which parameters impact the farfield oscillations of the system, where if one desires greater oscillations away from the leading wavefront then it is better to change the periodic ansatz function f than to change the derived surface tension parameter γ for the KdV systems investigated, however further investigation is required for higher-order KdV systems. Now returning to the original lump soliton form, the value for u_0 was specifically chosen to match closer to the expected waveform, and its effect is to both slim and raise the amplitude of the waveform with the more negative the value gets. This representation also keeps the assumption that $a = b$ due to the period being infinite, but that isn't necessary for the general Breather solution, and can be plotted using the solution u attained before the last step. The effect of these terms is to change the angle of approach of the wave, while direction itself

remains fixed in the negative x direction. Therefore for this value of u_0 , setting $b \approx 0$ or $b \approx \pm\sqrt{2}$ causes the wave to approach head on (hence the choice of arbitrarily small b for a stereotypical wavefront), while perturbations to these values of b will cause a lean in the positive/negative y direction.

This choice of u_0 and b (and by extension a) produces an accurate representation, but to create larger waves one must decrease u_0 enough to raise the amplitude, at the cost of wave width. This also means the value of b to make the wavefront face forwards changes, which is evident in the choice $u_0 = -1$ with the original $b = \sqrt{2}$ giving the top-down view of the surface plot as

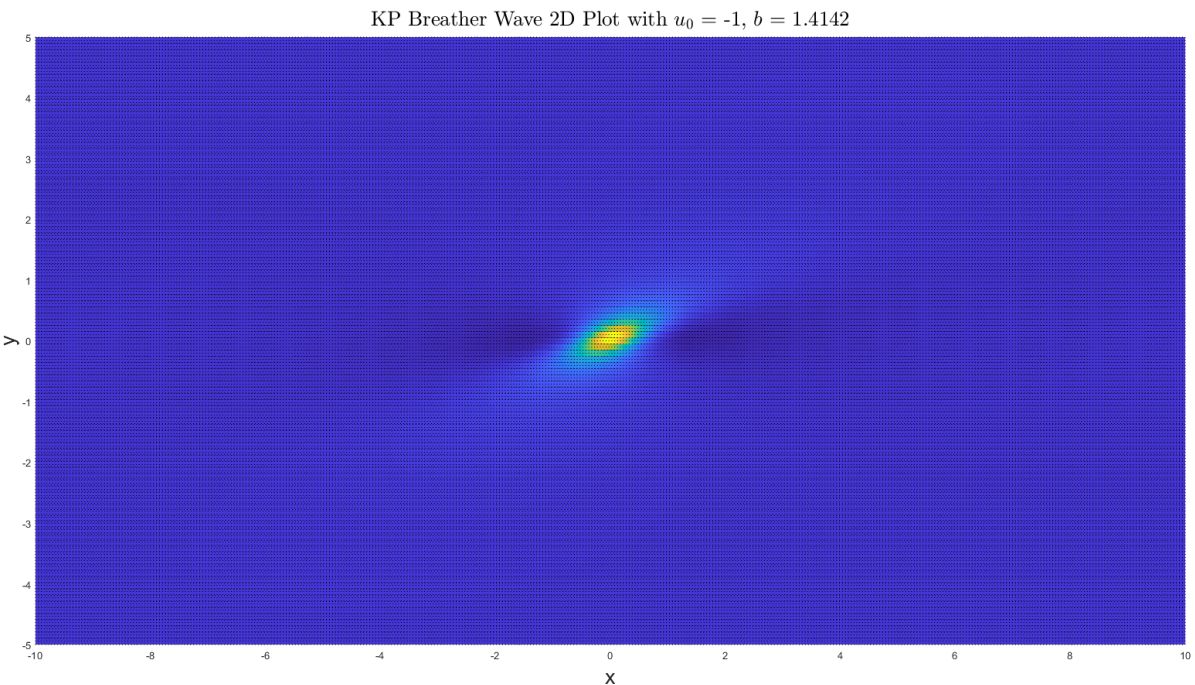


Figure 48: Hirota's Bilinear Method for the Breather Solution at $x = -1$

Which means the wave has a leading edge, as the wave peak still reaches $(0, -1)$ at the same time, but the wave is at peak in the surrounding y at different times, since it travels at an angle to the direction of motion which is still along the vector $(-1, 0)$. Changing to $b = \sqrt{5}$ however will give the forward-facing waveform, as shown in

KP Breather Wave 2D Plot with $u_0 = -1$, $b = 2.2361$

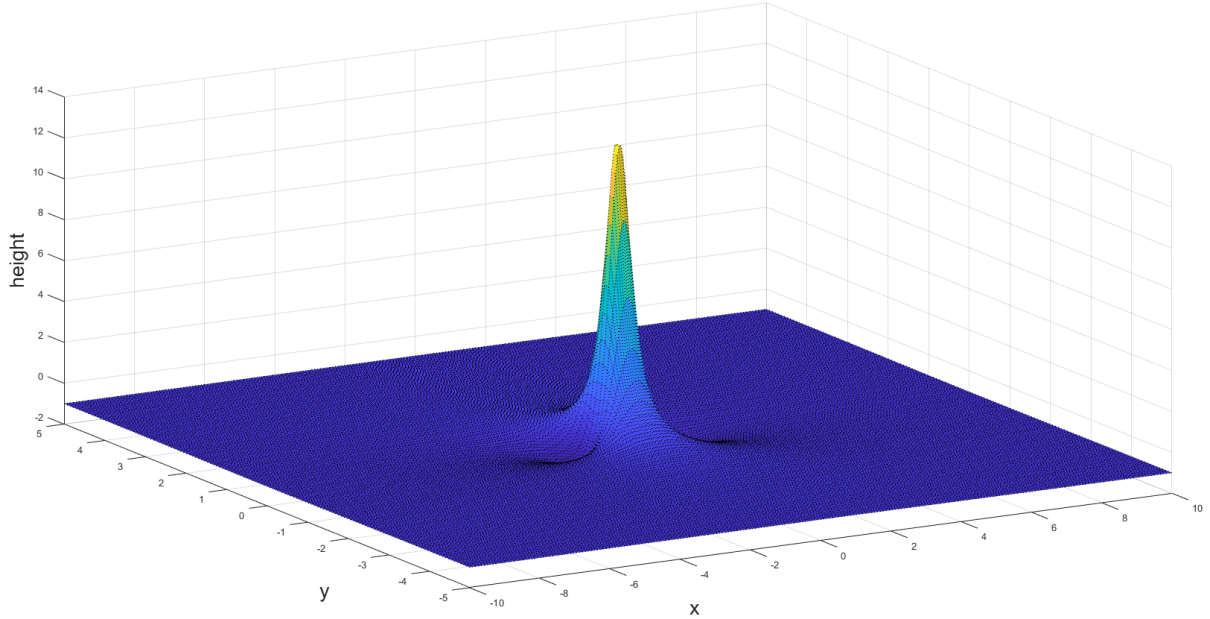


Figure 49: Hirota's Bilinear Method for the Breather Solution at $x = -1$

Which is a considerably taller waveform, which gives motivation that to rescale the Breather solution to match a given problem, one must rescale multiple parameters to keep the wavefront shape consistent.

One can also plot the reverse of this, such as $u_0 = \frac{-1}{6}$ and b arbitrarily small (either positive or negative), so that the central lump is wide enough that it resembles the original line soliton solution also, which looks like

KP Breather Wave 2D Plot with $u_0 = -0.16667$, $b = 0.1$

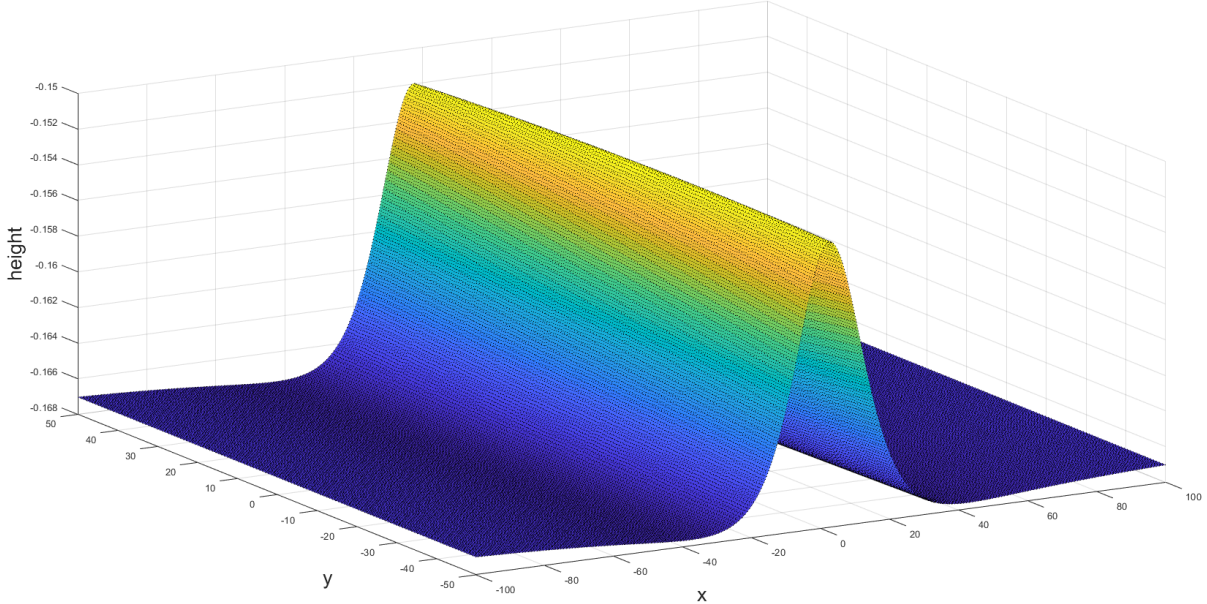


Figure 50: Hirota's Bilinear Method for the Breather Solution at $t = 1$

Which shows a mostly symmetrical wavefront travelling in the negative x direction where the positive y side travels slightly further ahead of the negative side. This solution is very unstable to perturbations in either variable, but does portray a three-dimensional wavefront of significant amplitude travelling in a uniform direction, which could be used for tsunami wave modelling, where changes in the parameters above can affect the height and angle of the leading wavefront, but notably increasing the y scale far enough will show the central height of the soliton gradually decreases to background level, which can be argued to be a more realistic representation of a large scale tsunami wave at sea.

4.6 Application of KdV-Type Systems to the Real World

The solitons investigated so far have been models that appear to represent the generic shapes of Freak Waves, using both analytical and numerical solutions for the KdV and KP equations, but even for the certain circumstances that these models are suited for, they aren't universally applicable in the real world for realistic rogue wave modelling; even for situations that match their initial conditions. This analysis will be based on a KdV approximation to a real world

event, but the assumptions used are also used in the formation of the KP equation, and hence it follows the same way.

Using the previous definitions

$$\mu = \frac{h}{\lambda_x} \text{ and } \epsilon = \frac{a}{h}$$

and that the KdV system was valid for $\epsilon = O(\mu^2)$, this means

$$\frac{\epsilon}{\mu^2} = \frac{a \times \lambda_x^2}{h \times h^2} = O(1)$$

and expanding in terms of h and λ_x for the defined limits of the 'big O' notation given by

$$O(1) \rightarrow > \frac{1}{10} \text{ and } < 10$$

gives an inequality based on orders of magnitude for the value of the wavelength [22]

$$\frac{h^3}{10a} \leq \lambda_x^2 \leq \frac{10h^3}{a} = \frac{10h^2}{\epsilon} \quad (4.11)$$

Where the values of h and a can be chosen based on realistic values taken at normal times before a rogue wave or tsunami.

As an example of such an event, the 1960 Chilean Tsunami, as detailed in article [24], was a tsunami caused by a modulational instability of an earthquake shortly before. The approximate spread of this tsunami can be seen in the following figure, and we will compare this to the predicted range given by the KdV model.

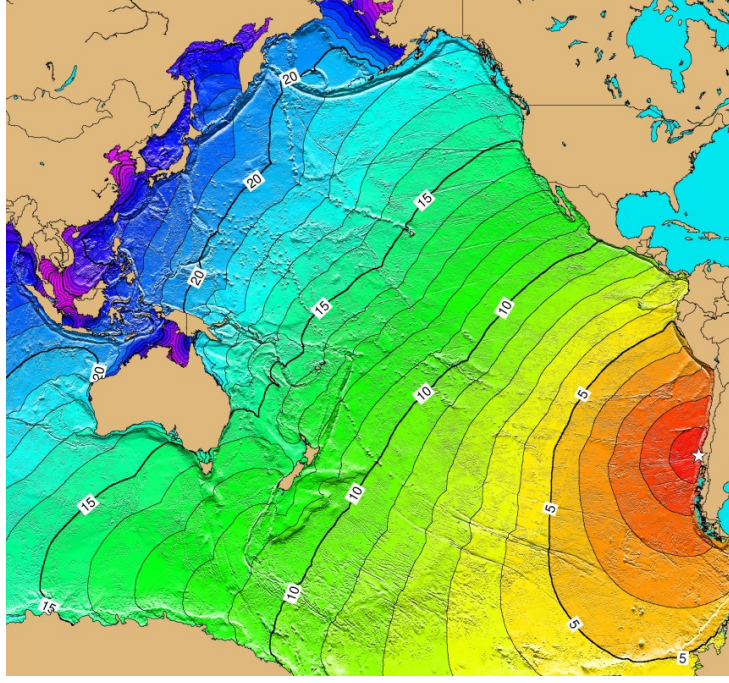


Figure 51: 1960 Chilean Tsunami Map From Article [24]

The area around the point of instigation has an ocean depth of $h = 4300\text{m}$ (which is also mostly uniform to match to prior assumptions in section 3.1) and has a typical wave amplitude of $a = 0.4\text{m}$ as suggested in book [23] to give bounds of 140,000 and 1,400,000 metres, which is as expected for regular waves. Now to calculate the wavelength for the rogue wave itself, finding choices of the parameter a is difficult in a real world setting, so we ideally want to substitute this out for a known parameter, such as the maximum distance travelled by the wave, x_{max} , which for this tsunami is known, since it was detected as far away as the coast of Hawaii, which is of the order 10^4km away. To do this, we keep h_0 the same but try to eliminate a by remembering that the travelling wave parameter $\zeta = x' - t'$ (still primed at this stage by non-dimensionalisation) and the time parameter $\tau = \epsilon t$ are both $O(1)$. Therefore, dimensionalising ζ using the terms from section 3.1 of $x = \lambda_x x'$ and $t = \frac{\lambda_x}{c_0} t'$ for x' and t' as the variables in question here, which means

$$\zeta = x' - t' = \frac{x}{\lambda_x} - \frac{c_0 t}{\lambda_x} = O(1)$$

and by the parameter τ :

$$\tau = \epsilon t' = \frac{\epsilon c_0 t}{\lambda_x} = O(1)$$

which means since only terms of equal order can be added, that

$$\frac{x}{\lambda_x} = O\left(\frac{1}{\epsilon}\right) = O\left(\frac{h}{a}\right)$$

which can be subbed into 4.11 to get

$$\begin{aligned} x &= O\left(\frac{\lambda_x h}{a}\right) < x_{max} \\ \lambda_x^2 &\leq \frac{10h^2}{\epsilon} = \frac{10h^2 x}{\lambda_x} \\ \lambda_x^3 &\leq 10h_0^2 x_{max} \end{aligned} \tag{4.12}$$

Now using an approximate maximum length of $x_{max} = 10^4$ km in the above inequality gives an upper bound for the wavelength in the x direction of $\lambda_x < 200,000$ m, which doesn't match experimental results that give it at least $\lambda_x = 500$ km ([23]). This means that despite the Chilean Tsunami of 1960 matching the requirements of shallow-depth, long wavelength and a uniform lower limit etc, it is unlikely to be an accurate model for this tsunami Wave.

This result supports the concept that effective rogue wave modelling comes from applying the correct model to the correct scenario, and so to support the KdV and KP models proposed, I will now introduce a third model, in the form of the Nonlinear Schrödinger Equation, that doesn't rely on the shallow-water assumptions used prior which invalidated the use of the prior methods in the Chilean Tsunami case.

5 The Nonlinear Schrödinger Equation

The Nonlinear Schrödinger equation is an equivalent model to the KdV-type equations, but is instead valid for deep water systems (and so doesn't rely on the troublesome $\epsilon = \frac{a}{h}$ parameter seen to cause issues above) which allows systems to have theoretically infinite depth, and is a useful system to model rogue waves for when the wave length-to-depth ratio is outside the

range of the KdV equation. However the main difference is in what is represented, since the KdV equation portrays the peaks and troughs of the water waves with oscillatory motion; whereas the NLS equation models the envelope of the wave. The envelope is simply the lines formed along the peaks and troughs of the waves, without any intermediate changes. Therefore, this is a good model for the group velocity (horizontal movement of the wave), but is less effective at modelling phase velocities, since it only shows the peak and trough values; which is best represented by images of the following form



Figure 52: Model of the Envelope of a Wave from book [58], with the wavefront as a solid line and the envelope dotted

Despite these differences, the NLS equation can be derived directly from the general form of the linear part of the KdV equation, given in equation 3.9, where u represents the displacement from the equilibrium. This is done by taking an asymptotic expansion of u in powers of ϵ , but by ignoring the leading order ϵ^0 to account for small amplitude oscillations relative to wave depth. Therefore taking the KdV equation to leading order with this substitution leads to $u_{0,t} + u_{0,xxx} = 0$ as a representation of derivatives of the $O(\epsilon)$ term in the expansion. This yields solutions of the form $u_0 = A(X, T) \exp i\theta$ for $T = \epsilon t$, $X = \epsilon x$ as slow variables, and $\theta = kx - \omega t$ as the fast variable with the envelope represented by the variable $A(X, T)$. Additionally, this solution has an extra complex conjugate term (notated c.c. as follows), and has to consider the mean term $M(X, T)$ as a displacement to this, as suggested in the derivation from source [1], which also retains the dispersion relationship for this being $\omega = -k^3$ for k still as the wavenumber in the x direction and ω as the wave frequency, as seen previously in derivations of first order terms in the bookkeeping variable for Hirota's Bilinear Method examined prior. This mean and complex conjugate solution form can be considered similarly to solving a cubic with one root, where there will be one strictly real solution (the mean in this case) and the two imaginary complex conjugate solutions.

Considering these, and the secular terms that arise by carrying out the asymptotic expansion, a solution ansatz is suggested to minimise the workload in translating between KdV and NLS, but a longform method of the direct conversion follows simply by using the chain rule with the new variables to get $\partial_t = -\omega\partial_\theta + \epsilon\partial_T$ and $\partial_x = k\partial_\theta + \epsilon\partial_X$, then expanding in powers of ϵ to solve secularity.

This solution form, as given in [1], is

$$u_0 = \epsilon[A(X, T) \exp i\theta + c.c. + M(X, T)] + \epsilon^2(\alpha \exp 2i\theta + c.c.) + \dots \quad (5.1)$$

Which avoids secularity with the exponentials to power 1, and can then be applied to every term in the linear KdV equation using the aforementioned chain rule derivatives to give a solution system, where coefficients of each $\exp(in\theta)$ are set to 0 to avoid singularity at each power, e.g. setting the coefficients of $e^{i\theta}$ and M to 0, and summing the coefficients of the $e^{2i\theta}$ terms up to $O(\epsilon^2)$ gives the equation

$$\epsilon^2(2ik^3\alpha + 6ikA^2 - 8ik^3\alpha) = 0 \quad (5.2)$$

to give $\alpha = \frac{A^2}{k^2}$, and removing the mean terms that cause secular instabilities results in $M = O(\epsilon)$, and so to leading order

$$M_T + 6\epsilon(|A|^2)_x \approx 0 \quad (5.3)$$

Now with another change of variables to use a moving reference frame, e.g. $\partial_T = \epsilon\partial_T - \omega'\partial_\zeta$ and $\partial_X = \partial_\zeta$, the above leading order term becomes $M \approx -\frac{2\epsilon|A|^2}{k^2}$. Using this relation for M , and removing $e^{i\theta}$ secular terms from the expanded KdV equation and ignoring higher order ϵ terms leads to

$$A_T - 3k^2A_x - \frac{12i\epsilon|A|^2}{k}A + O(\epsilon) = 0 \quad (5.4)$$

then similarly to the KdV equation, transforming to the moving frame using the variable $\epsilon = X - \omega'(k)T$ and time rescaling $\tau = \epsilon T$ gives the Nonlinear Schrödinger Equation in

canonical form

$$iA_\tau + \frac{\omega''(k)}{2} A_{\epsilon\epsilon} + \frac{6}{k} |A|^2 A = 0 \quad (5.5)$$

This is the most generally used form of the NLS Equation, but much like the KdV and KP equations, the coefficients can be changed without having a profound effect on the overall outcome, therefore some sources such as in paper [32] refer to a simplified form given by

$$iA_t + A_{xx} + 2|A|^2 A = 0 \quad (5.6)$$

Where each variable A , x and t has undergone a transformation to achieve this form, but for brevity sake these transformations will not be explored or mentioned unless necessary.

5.1 Linear Schrödinger Equation: The Inverse Scattering Transform

There is also an equivalent method that can be used to derive the NLS from the KdV equation, which is called the Inverse Scattering Transform, which will be explored here to provide motivation for the existence of and the scope of research into providing multiple equivalent methods of derivation.

This is done by introducing a Miura transformation of the form $u = -v^2 - \partial_x v$ as suggested later in the work by [8], such that it satisfies the mKdV equation, where the nonlinear term changes from $6uu_x$ to $-6v^2v_x$. This equation can be linearised using the transformation $v = \frac{w_x}{w}$ for a new variable w alongside the above equation for v to find $u = -\frac{w_x^2}{w} - \partial_x \frac{w_x}{w}$ and using the quotient rule on the latter term leads to cancellation with the first, and thus results in $w_{xx} + uw = 0$.

From this, a property of the KdV equation can be explored, since substituting $x + 6\lambda t$ in for x in the KdV equation 3.9 yields a translated result $u = u + \lambda$, and so a solution that satisfies the above equation must also satisfy $w_{xx} + uw = -\lambda w$, which is the Linear form of the Schrödinger equation derived previously.

This gives motivation for an alternate derivation from the KdV system, but solutions of which will not be explored further, as the non-linear case provides is more widely used in most literature.

5.2 Rogue Waves as NLS Solutions

Given that the Nonlinear Schrödinger Equation can be used as a model for deep water Stokes waves, it can also be used to model rogue waves under specific circumstances. There exist solutions to the NLS equation that closely resemble that of the lump soliton we've encountered prior, and these can be attained by taking a limiting case of two different solution forms, the Akhmediev and Ma Breathers. The following comprises an overview of the research with references to the methods used included, but does not provide a new account of the derivations for the solutions as it is included to simply provide motivation for the existence of lump soliton solutions for this equation.

The Akhmediev Breather solutions were discovered by Nial Akhmediev and referenced in papers [19, 56], where he discovered a spatially-periodic lump soliton solution form for the simplified form of the NLS equation given prior, where the general solution is given by

$$A(x, t) = \left((-1)^N + \frac{G_N(x, t) + ixH_N(x, t)}{D_N(x, t)} \right) e^{ix}$$

For polynomials G , H and D .

This is derived from equation 5.6 in paper [49] by decomposing the solution A into real and imaginary parts by $A = u + iv$, with $u = a_0(t)v(x, t) + b_0t$, following a series of reparameterisations to get to a function in the form $A = (Q(x, t) + i\delta(t))e^{i\phi(t)}$, which can be substituted back into the original equation to yield two equations that will undergo a series of integrations. The rest of the derivation is omitted for brevity, but taking a special case limit of the resulting function for all real solutions leads to what is known as the Peregrine Breather.

One could also take the limit of the solution presented by Ma in paper [32], where the Ma solution is instead periodic in time rather than space like the Akhmediev solution, where the alternative derivations are explored in detail in multiple sources, such as [33, 51, 49, 57].

Regardless, the resulting analytical solution is called the Peregrine Breather, whose solution to equation 5.5 from papers [19] and [49] is

$$A(x, t) = \left(4 \frac{1 + 2ix}{1 + 4x^2 + 4t^2} - 1 \right) e^{ix}$$

which is notably a fixed surface plot in 1D space which shows a peak around the centre of +3 on top of the background level, with dips in space at any given time either side; so it is expanded to a general solution for a modified form of the NLS equation by Dysthe in paper [31] to be

$$A(x, t) = a \left(1 - 4 \frac{1 - ia^2 t}{1 + 8a^2 x^2 + a^4 t^2} \right) e^{-i \frac{a^2 t}{2}}$$

for amplitude $a > 0$, which looks like

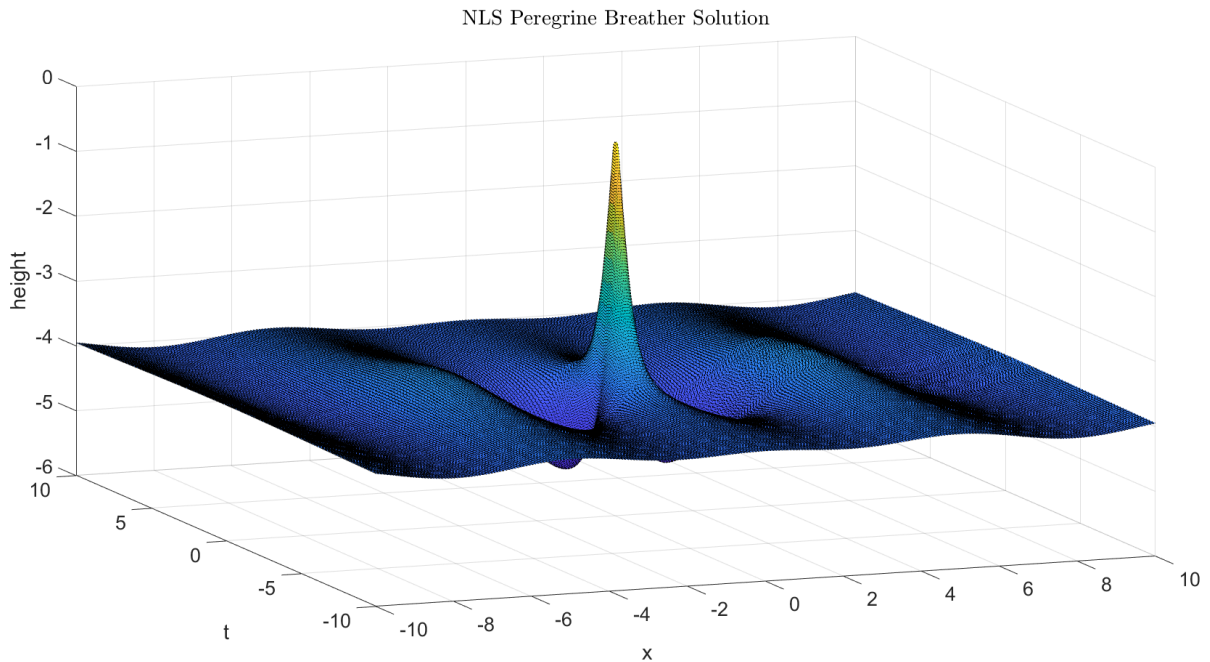


Figure 53: First Order Peregrine Solution for the Nonlinear Schrödinger Equation

This is very similar to the Breather wave solution found for the KP equation in section 4.5 under the periodic f function ansatz, therefore despite this being a rather simplistic and unrealistic representation of real world rogue waves, it shows how deep water wave approximations can yield equivalent models for rogue waves as shallow water systems, and provides a baseline which is found in more complicated systems.

However this solution is rather generic, and contains a consistent peak of three times the surrounding wave height. It also follows a very basic uniform oscillating pattern when viewed at each time step, as shown below

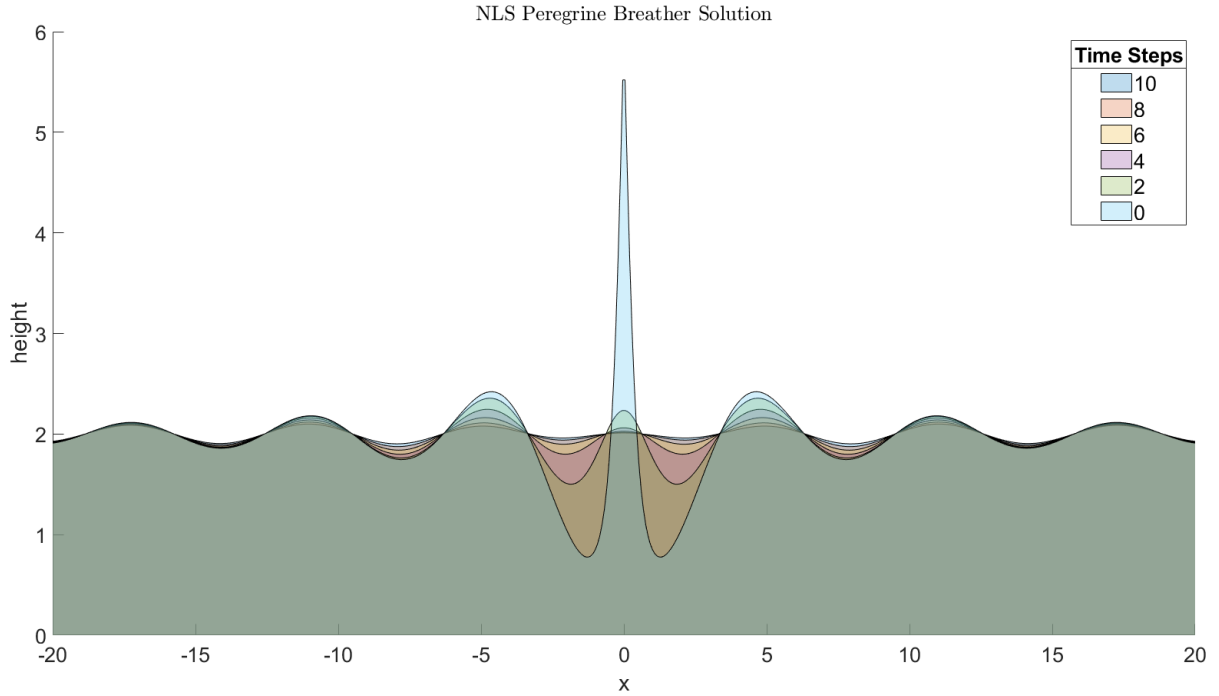


Figure 54: Plot of x vs $height$ at different time snapshots for the First Order Peregrine Solution

Which looks unnaturally uniform when compared to the real-world stochastic oscillations in the farfield, however when compared to the previous surface tension investigation from paper [37], mentioned first in section 3.4 and whose results are shown in figure 11, these effects are much closer to the observed oscillations than those of including surface tension for KdV, and include oscillations further out than is seen for the periodic lump soliton case of the KP equation.

Therefore lump-soliton solutions for the NLS equation already incorporate effects similar to the inclusion of surface tension by virtue of its natural periodicity.

Comparisons of these solutions to simulations of freak wave events, such as in paper [33] where they apply perturbations to a Stokes wavetrain initial condition of

$$q(x, t = 0) = q_0 \left(1 + \epsilon e^{i\psi} \cos \left(\frac{x}{2N} \right) \right)$$

For small ϵ , number of waves in one period N and ψ as an "arbitrary constant phase" shows

great correlation to the predictions given by all of the time-periodic Ma Breather, the space-periodic Akhmediev Breather, and the limiting solution of both in the Peregrine Breather shown above.

There are also other relevant solutions outside of the breather waves for rogue wave models, such as the envelope soliton, presented in paper [31] as

$$A(x, t) = ae^{-ia^2t/4} \operatorname{sech}(ax)$$

Which shares some similarities with the KdV-type solutions, but looks completely different in shape due to the NLS equation being a model of the envelope of the wave, rather than the wavefront itself, and therefore this solution looks like

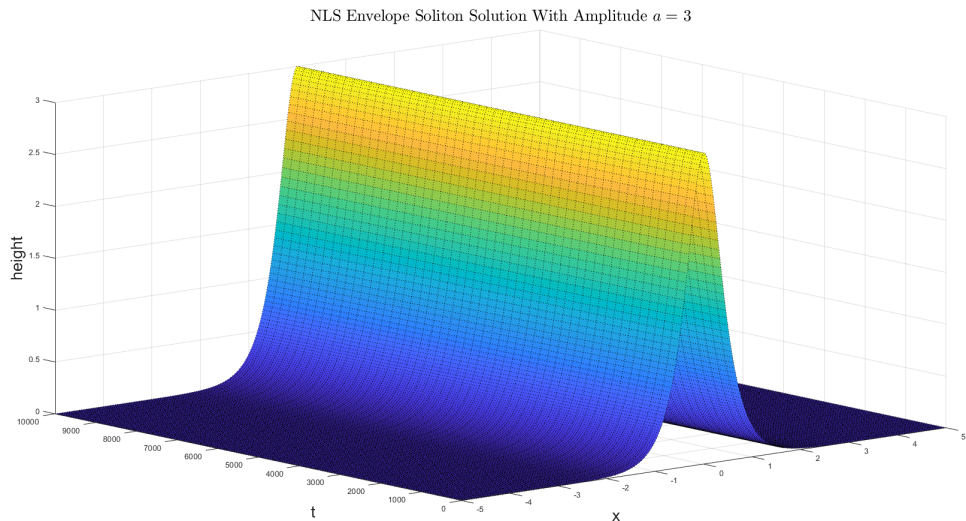


Figure 55: NLS Envelope Soliton Solution for Amplitude $a = 3$

When taking the plot of the absolute value of the solution, which shows no variation in time, whereas just taking the real part of the solution leads to a time-oscillatory solution that portrays the shape of the envelope as time progresses at a fixed point in space (x, y) , as shown in

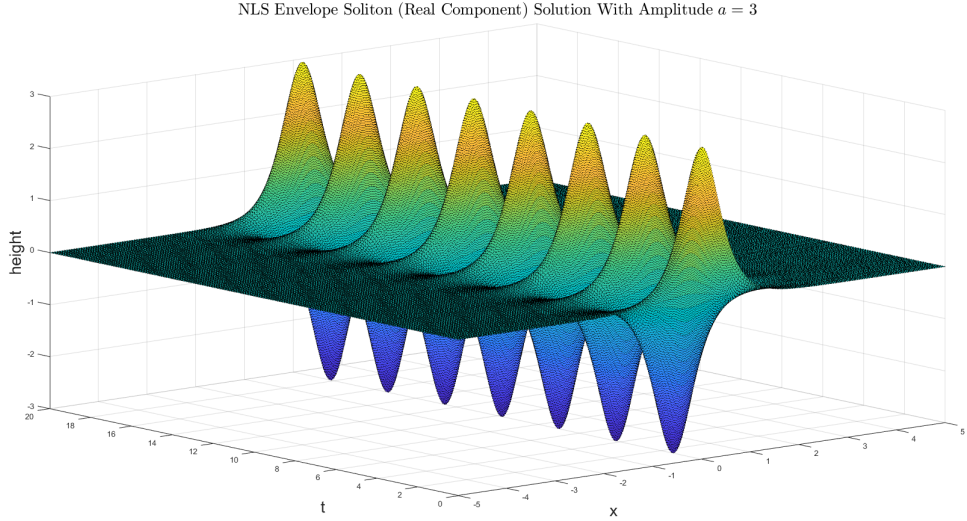


Figure 56: NLS Envelope Soliton (Real Component) Solution for Amplitude $a = 3$

Where taking the periodicity to ∞ and isolating one soliton will give a solution that looks like a KdV lump soliton solution, but without any capillary forces as in paper [26] and interestingly with a depressive soliton of the same size immediately succeeding each elevation wave.

5.3 Statistical Analysis

As an alternative to differential models of the waves themselves, methods of probabilistic modelling of wave occurrences as mentioned previously are explored in recent research, such as in paper [5]. This paper explores different methods of predicting future rogue waves using previous data in that area. The paper finds that more straightforward methods such as measuring Kurtosis (volume of outliers based on normal distribution) are no more likely to correctly predict waves than background after around three wavefronts have passed. This happens for both sample (individual data) and quantile spreads, where the latter should be a more robust predictor in the sense of anomalies. Instead, the paper finds that crest-trough correlation, (a parameter dependent on the angular frequency, wave spectral density, n-th moment and spectral mean period, as defined in the methods section of paper [53]) is the most efficient predictor, with the ratio of wave steepness (peak wavenumber scaled by average wave height) and spectral bandwidth (the wave width at half amplitude) in the Benjamin-Feir

Index being less accurate but still useful indicators for shallow water simulations. However, for an introduction to rogue wave statistics, we will explore specifically the Benjamin-Feir Index and its relation to the excess Kurtosis, known as the change in distribution from the baseline Gaussian distribution. For a comparison of the effectiveness of predictions between the Benjamin-Feir Index and the Crest-Trough Correlation, see paper [53] and the extended literature in the statistical field.

The Gaussian distribution itself is also widely regarded as an insufficient probabilistic model for rogue wave occurrences, where other models such as the Weibull and Jonswap γ distributions match better to the real world dynamics of rogue wave occurrences, as will be briefly detailed below.

Finally, another parameter that is of interest is the excess kurtosis, which is defined in paper [5] as the "proneness to outliers of sea surface elevation", and is posited in the paper to be both a predictive tool and a result of the presence of rogue waves, and is only effective as a predictive measure in the short time before a rogue wave instance. However, for the purpose of this paper we will treat an increase in excess Kurtosis simply as the increased likelihood of rogue waves in a sea state, irrelevant of time. This When comparing the excess kurtosis to the BFI, investigations into the Benjamin-Feir Index should also verify the bisecting angles of incident solitons at which maximum amplification is expected so as to compare these to the KP solution, however first we will compare the different probabilistic methods that are widely used in the field.

5.4 Probability Distributions

The above statistical analysis leads to the belief that as long as waves are sufficiently steep (wave steepness), narrow-banded (spectral bandwidth) and long crested, then applying a modulational instability to them can form rogue waves. However, it is also possible to take a sample dataset of wave occurrences in a region and match it to a multitude of generic probabilistic models that are used for rogue wave frequency measurement; with the two most notable of these being the Jonswap Gamma distribution and certain parameter choices of the Weibull distribution.

The Jonswap Gamma distribution is a variant of the more general Pierson-Moskowitz distribution as a more well-fitted approximation to rogue wave frequencies, by using the eponymous scaling factor γ as shown in its spectral density as a function of wave frequency form in [44]. This is a commonly used distribution for randomly occurring waves, and is commonly referenced in use alongside the Benjamin-Feir Index.

The Weibull distribution is a variable probability model that can be adapted to match a known dataset according to multiple parameters; namely the shape, scale and location parameters, but in this case the function is used without the latter. The general Weibull 2-parameter probability density function can be found in the associated article [15] to be

$$f(T) = \frac{\beta}{\alpha} \left(\frac{T}{\alpha} \right)^{\beta-1} e^{-(\frac{T}{\alpha})^\beta}$$

for shape parameter β and scale parameter α , which can be extended to the cumulative density function for the probability of a wave being a rogue wave model ([14]) by

$$F(c_r) = F\left(\frac{c_r}{H_s}\right) = 1 - e^{-\frac{c_r^\beta}{\alpha}} \quad (5.7)$$

for crest height c and significant wave height H_s , where it is found in the same source ([14]) that for their dataset, values for α and β of approximately 0.37 and 1.75 respectively give a sufficiently accurate model, with small variations depending on the amount of directional spreading. However, these parameters can depend largely on the sea state concerned, therefore multiple scholars have proposed their own choices of parameters that best predict rogue wave occurrences.

The two most prominent and widely applicable of these are the Rayleigh and Forristall distributions, as stated in paper [54], where Rayleigh suggests that for sufficiently deep waves with a narrow spectrum that choices of $\alpha = 0.5$ and $\beta = 2$ provide an accurate distribution, whereas Forristall noted that based on their data that slight alterations to the values to be $\alpha = 0.5263$ and $\beta = 2.126$ provided a better approximation. To test these distributions, paper [54] used measurements from buoys across the North Sea (which is notably the same region as the famous Draupner wave) and plotted the exceedance probabilities, which is done by

plotting $1 - F(c_r)$ against the crest height $c_r = \frac{H}{H_s}$, where any point shows the probability y of that x value being surpassed, so is always a decreasing function (so here shows the chance of any wave from a given sample being greater than the given c_r ratio). Plotting the sample data against the Rayleigh and Forristall predictions in this manner gives

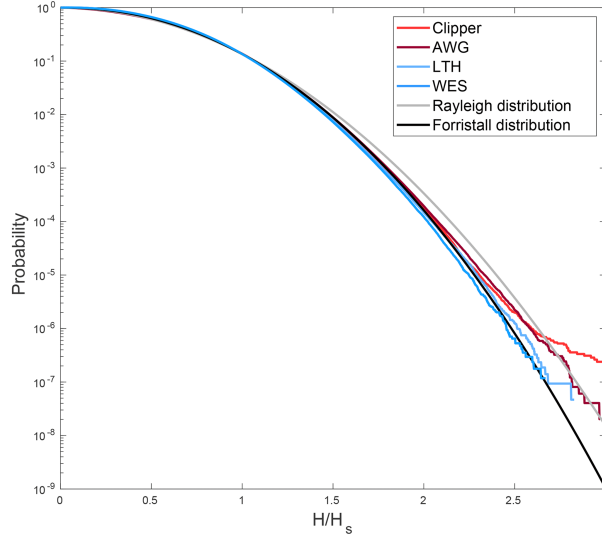


Figure 57: Cumulative Probability Plot from Paper [54] of Rayleigh and Forristall Distributions Against Sample Data From The North Sea

Showing that, since rogue waves occur at $\frac{H}{H_s} = 2$, that rogue waves are expected to occur once in every 10^4 waves, and that the data match closest to the Forristall distribution up to that limit, before the data for the Clipper and AWG nodes (which are closer to the UK than Norway) tend to be better predicted by the original Rayleigh distribution.

5.5 Benjamin-Feir Index for One-Dimensional NLS

As mentioned above, one of the indicators for the probability of a rogue wave occurring is known as the Benjamin-Feir Index, and is defined in paper [14] as

$$BFI = \frac{\frac{1}{2}k_0 H_s}{\frac{\Delta\omega}{\omega_0}}$$

for subscript 0 being the value at peak, so wavenumber of the peak k_0 and peak frequency ω_0 , alongside $\Delta\omega$ being the "halfwidth at half maximum of the spectrum" ([40]). Also, H_s

is a scaling term that represents the height of a significant wave in the area, which can vary wildly from around 5 to 6 metres such as that given by Rosenthal and Lehner in paper [16], and 2.6 metres in the Black Sea as given by Dysthe in paper [31]; and so the numerator of the BFI represents the wave "steepness" (wavenumber \times average waveheight), and the denominator the "frequency spectral bandwidth", which is a measure of the wave frequency and is the more commonly analysed portion of the BFI for a specific scenario with a given wave steepness, as will be seen later. A method to calculate H_s for a given weather scenario is by taking measurements of surface elevation (η from the KdV derivation) and take the standard deviation scaled up by 4, as suggested by [21]; which is the definition used to define the above Rayleigh and Forristall distributions ([54]). However, there are differing values used in its place, such as $H_{\frac{1}{3}}$, which is calculated as the mean of the top third band of wave-heights, for which it is generally smaller than H_s , which causes the threshold for rogue Waves, $> 2H_s$, to be more lenient.

This model is sufficient for long-crested, surface gravity waves, and so is more related to the Nonlinear Schrödinger Equation, from which it is generally derived, but is valid for all rogue wave scenarios. This derivation begins by taking the NLS equation of the form

$$A_t + \frac{\omega_0}{2k_0}\nu A_x + \frac{\omega_0 i}{8k_0^2}\alpha A_{xx} + \frac{\omega_0 k_0^2 i}{2}\beta A|A|^2 = 0$$

as given in paper [17], which is of a similar form to the derived equation 5.5, where the term ν relates to the group velocity, A the envelope, and α and β the water depth, dominant wavenumber k_0 , and that wavenumber's corresponding angular frequency ω_0 , as the equivalent for the peak values given above.

Now finding the BFI is similar to finding the Reynold's number when given the Navier Stokes equation with suitable parameters, where we take the non-dimensionalised form of the equation, where A has dimensions $\frac{1}{a}$ for amplitude a , x has dimensions of the change in wavenumber, and t has dimensions $\frac{\omega_0 \Delta k^2 \alpha}{8k_0^2}$, since angular frequency has units of time, and the rest of the parameters cancel in units of length. Now substituting this, and taking the coefficient of

the non-linear term gives

$$BFI = \frac{2k_0 a}{\frac{\Delta\omega}{\omega_0}} \nu \sqrt{\frac{|\beta|}{\alpha}}$$

Which also uses the $\frac{\Delta\omega}{\omega_0} = \frac{\nu \Delta k}{2k_0}$ property from the definition of ν given on page 615 in paper [18] as

$$\nu = 1 + 2 \frac{k_0 h}{\sinh(2k_0 h)}$$

This version of the Benjamin-Feir index applies for Stokes waves, which are valid for deep water situations, as opposed to the KdV and KP models derived above that are sufficient for shallow water scenarios. This form of the BFI is suitable for the single-wave scenario, where another form will later be derived similarly for a coupled system of waves.

Some sources refer to what is known as the Benjamin-Feir Instability (e.g. [31]), which refers to performing a modulational instability (like an earthquake or wind-speed change) and applying it to a periodic system like that suggested prior with the Peregrine solutions for the NLS equation in paper [56]. Provided that the spectral bandwidth is less than the spectral steepness (as defined above), then this instability causes the system to spiral into producing ever greater oscillations, which culminates in a spike, like a rogue wave occurrence. This suggests what values of the BFI will correlate well to rogue wave situations, where $BFI \approx 1$ will start to see rapidly increasing oscillations.

This is shown by analysing the Kurtosis, as defined previously but can also be defined as the sharpness of the Gaussian distribution curve, which means higher Kurtosis results in an increase in the number of outliers, which in this case is a defining feature of rogue waves.

Now using the Benjamin-Feir Index, the Kurtosis spread of the distribution governing the appearance of freak waves has been found to depend on the BFI in paper [36] in the equation $C_4 = \tau^2 (BFI)^2 (1 - R)$ for dimensionless slow-time variable $\tau = \omega_0 \frac{\sigma_\omega}{\omega_0} t$, BFI defined as $\frac{\epsilon \sqrt{2} \omega_0}{\sigma_\omega}$ with steepness ϵ and R defined using the parameters $R = \frac{1}{2} \frac{(\sigma_\theta \omega_0)^2}{\sigma_\omega^2}$ with σ 's as frequency and angular widths. This is notable since the Kurtosis parameter C_4 was defined to be the difference of the current distribution from the predictive Gaussian (normal) distribution, where $C_4 > 0$ means the probability of there being a rogue wave event is higher than the Gaussian model predicts, and vice versa for < 0 .

This form shows how the directional effects that govern the term R (σ_θ) will affect the Kurtosis, and hence the probability of a rogue wave occurring, given that for $\sigma_\theta \omega_0 < \sqrt{2}\sigma_\omega$ that gives $R > 1$ and so $C_4 < 0$ so rogue waves are more likely than the standard Gaussian distribution of wave heights would predict.

Regarding the Kurtosis as a function of the Benjamin-Feir Index, there have also been studies into the dynamic effect of wave instabilities on the excess Kurtosis value as given above, such as in paper [42] and how as the limit is taken in large-time then the resultant relation tends towards

$$C_4 = (BFI)^2 \frac{\pi}{3\sqrt{3}}$$

for their Benjamin-Feir Index

$$BFI = \frac{\mu\sqrt{2}}{\nu}$$

For $\mu = k_0\sigma$ wave steepness and ν spectral bandwidth, however this will not be explored further here.

5.6 Benjamin-Feir Index for Two Interacting NLS Solitons

The above results are valid for singular soliton forms of the Nonlinear Schrödinger Equation given in equation 5.5, however to compare the results of this to the previous analysis done to the two-soliton KdV equation, we must extend the NLS model to a multiple soliton case, and hence investigate what is known as the coupled analogue to the Benjamin-Feir Index.

There are many examples of coupled equations for the NLS equation, as shown in section 5 of paper [51], however the one that will be used is the one-dimensional Zakharov equation as defined in paper [50] as it appears in paper [41], which itself is a result of the work by Zakharov in their series of papers surrounding using the inverse scattering transform to solve the NLS equation, which will not be derived here for brevity.

The result of this research is the final system for the evolution of the envelope complex amplitude of the first line-soliton wave A

$$\frac{\partial A}{\partial t} + i\frac{\omega(\kappa)}{8\kappa^2} \beta \frac{\partial^2 A}{\partial x^2} + i\frac{1}{2}\omega(\kappa)\kappa^2 (1 + \gamma) A|A|^2 = 0$$

for parameters: $\kappa = \sqrt{k^2 + m^2}$, $\beta = k^2 - 2m^2$

$$\gamma = \frac{2k^5 - 2k^3m^2 - 6km^4 - 4k^4\kappa + 4k^2m^2\kappa + 4m^4\kappa}{(k - 2\kappa)\kappa}$$

which is equivalent to the second line-soliton wave given complex amplitude B (with swapped amplitudes A and B in the above system), where equivalence of A and B is met by making the same choice of incident vectors as in section 4.4 of (k, m) and $(k, -m)$, which as has been made clear prior, results in incident line-solitons of the same amplitude. Notably this is just an extension of the previous form in equation 5.5 $iA_\tau + \frac{\omega''(k)}{2}A_{\epsilon\epsilon} + \frac{6}{k}|A|^2A = 0$ but for two equations.

Now the coupled BFI can be found similarly to the one-dimensional case, where a non-dimensionalisation of the equation is taken, and the coefficient terms will be grouped to produce the singular BFI coefficient, similarly to the Reynold's number for the Navier-Stokes equations. To begin, the parameters that require dimensional analysis are the complex amplitude A , the spatial parameter x and the time parameter t . Therefore one can reuse the parameters used in the derivation of the BFI as seen previously in this paper when referring to paper [17], but with slight alterations, such as paper [39] using $A' = \frac{1}{\sqrt{2}a}A$ and $t' = \frac{\omega(\kappa)\Delta k^2\beta}{8\kappa^2}t$ in their representation. This means that after substituting in the non-dimensional variables to get

$$\frac{\omega(\kappa)\Delta k^2\beta\sqrt{2}a}{8\kappa^2}\frac{\partial A'}{\partial t'} + i\frac{\omega(\kappa)}{8\kappa^2}\beta\Delta k^2\sqrt{2}a\frac{\partial^2 A'}{\partial x'^2} + i\frac{1}{2}\omega(\kappa)\kappa^2(1 + \gamma)2a^2A'|A'|^2 = 0$$

one can note that the coefficients for both of the linear terms are equivalent, hence one can rearrange the system such that the dimensional coefficients are grouped in front of the nonlinear $A'|A'|$ term to give a singular constant that depends on the dimensions of the problem, which in this case is our coupled Benjamin-Feir Index

$$\text{BFI} = \frac{2\sqrt{2}\kappa a}{\frac{\Delta k}{\kappa}}\sqrt{\frac{\gamma + 1}{\beta}}$$

Where again the property ν derived in paper [18] can be used to convert the denominator from a relation on the change in wavenumber into one of the spectral bandwidth $\frac{\Delta\omega}{\omega_0}$ using

$\frac{\Delta\omega}{\omega_0} = \frac{\nu\Delta k}{2k_0}$, and so the index appears as before with the ratio of steepness and spectral bandwidth, where γ and β are functions dependent on the two incident vectors $(k, \pm m)$, and since κ is just a measure of the incident vector length, that means changes in the incident angle between vectors given by α prior only affects the latter root term. Notably, extending this coupled index to multiple dimensions, as will be seen below, is quoted in paper [39] as being the exact same, but with changes to the parameters β and γ .

After attaining the analogue of the Benjamin-Feir Index for the coupled equations, the relevance of the index comes with its relationship with the kurtosis as defined prior, where now paper [39] found this relationship to now be

$$C_4 = \frac{\pi}{\sqrt{3}}(BFI)^2 + 24\epsilon^2 + 3$$

Where ϵ again refers to the wave steepness. This shows how the overt relationships to the ω_0 angular width and σ frequency are now more subtly reliant on their definition in the new BFI.

5.7 Two-Dimensional NLS

Now for the inclusion of transverse variations, there is a change in the initial Zakharov equation(s) used to derive the incident waves, which will not itself be derived but stated as follows as it appears in papers [43] and [41] for a singular soliton with envelope amplitude A alongside the interaction effect with another soliton of the same form with amplitude B

$$i \left(\frac{\partial A}{\partial t} + C_x \frac{\partial A}{\partial x} + C_y \frac{\partial A}{\partial y} \right) + \alpha \frac{\partial^2 A}{\partial x^2} + \beta \frac{\partial^2 A}{\partial y^2} + \gamma \frac{\partial^2 A}{\partial x \partial y} - \xi |A|^2 A - 2\zeta |B|^2 A = 0 \quad (5.8)$$

for constants

$$C_x = \frac{\omega k}{2\kappa^2}, \quad C_y = \frac{\omega m}{2\kappa^2}$$

And α and β are the reciprocal equivalent of the previous β multiplied by $\frac{\omega}{8\kappa^4}$, the new $\gamma = \frac{-3\omega mk}{4\kappa^4}$, $\xi = \frac{\omega \kappa^2}{2}$ and ζ being the previous γ multiplied by $\frac{\omega}{4\kappa}$.

Now as in paper [43], assuming a perturbed solution form with amplitude $A_0 + \epsilon A_1$ for small ϵ , and performing linear analysis on some spatially independent solutions of the above system,

which can be found by neglecting derivatives in space and just including time dependencies and solving as an exponential function that satisfies

$$i\frac{\partial A}{\partial t} - \xi|A|^2 A - 2\zeta|B|^2 A = 0$$

and so solutions come in the form of $iA_t = (\xi|A|^2 + 2\zeta|B|^2)A$, so if one takes $A = A(t)$, then dividing through by A and integrating both sides in terms of t leaves $\int \frac{A'}{A} dt = \log(A)$, and so solutions of this type come in the exponential form of the right-hand side bracket, $A = A_0 e^{i(\xi|A_0|^2 + 2\zeta|B_0|^2)t}$.

Given that solutions of this form are perfectly reasonable solutions to the above system, that means taking a linear perturbation on the solution such that $A_0 \rightarrow A_0 + \epsilon A_1$, separating the real and imaginary parts, then Fourier transforming with parameters K and L for the spatial wavenumbers and Ω for the wave frequency results in the equation as stated in paper [43]. The result of this is a dispersion relation equation relating these Fourier modes using the coefficients from equation 5.8 which depend on the original wave-vectors k and l , which can be converted to the same angular representation as before using $\alpha_{12} = 2 \arctan\left(\frac{m}{k}\right)$. The results they found were less precise than those of the analytical KP angle, but showed an amplification of more than twice the incident soliton amplitudes when at an angle of intersection of $\alpha_{12} \approx 22^\circ$, whereas an angle of $\approx 45^\circ$ produced no significant amplification. They ([43]) explained this using analysis of their coefficient for the $\frac{\partial^2 A}{\partial x^2}$ term, $\alpha = \frac{\omega(2m^2 - k^2)}{8\kappa^4}$, where this parameter changing sign triggers a change from a focussing to a defocussing equation, and so shifts from constructive to destructive interference. Now most importantly from this is that the shift occurs for $2m^2 = k^2$ and so $\frac{m}{k} = \frac{1}{\sqrt{2}}$ and so $\alpha_{12} = 35.3^\circ$, which falls within a reasonable bound of the result found in section 4.4, however it must be noted that this result is based on a non-dimensionalised system with infinite depth, and so the angle of amplification in this case is an approximation, but the growth of amplification up to a value before decreasing still indicates a similarity to the KP result.

This is corroborated by paper [55], where they performed experimental and numerical investigations using the same coupled system as derived above for the spatially independent solution but retaining the second order spatial term $\alpha \frac{\partial^2 A}{\partial x^2}$, except their numerical solution followed by

an argument similar to the derivation of the KdV system, where they took an irrotational, inviscid and incompressible fluid that satisfies the Laplace equation, but with an infinite depth $h = -\infty$. This then resulted in what they refer to as the kinematic and dynamic boundary conditions that can be solved by applying a Fourth-Order Runge-Kutta method like prior, and they considered systems of up to perpendicular angles of bisection between the incident solitons (k, m) and $(k, -m)$. The results of this numerical experiment were that increasing the angle of intersection linearly up to 40° resulted in an increase in Kurtosis, which is the same as saying the number of rogue wave occurrences increases, and the system then remains constant between 40° and 60° before becoming stagnant for values beyond that, as shown in the following figure extracted from the source for the numerical solution form given by the circular results at each increment of 10°

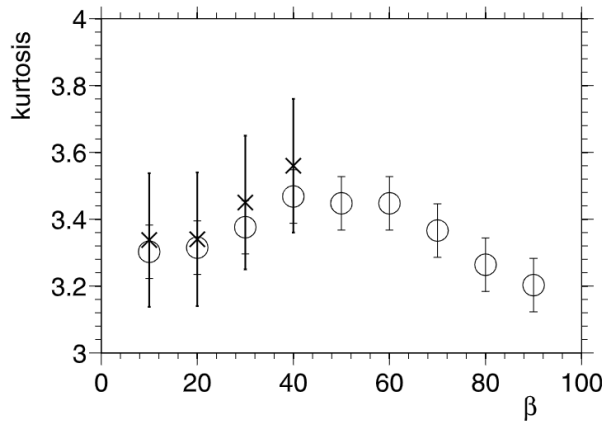


Figure 58: Maximum Kurtosis as a function of the angle $\alpha_{12} = 2 \arctan \left(\frac{m}{k} \right)$ (here β) from paper [55]. Circles represent the Runge-Kutta Numerical Solution under consideration

These results are excellent news in the context of the results from section 4.4, since it means the typical wave scenario that reaches a maximum amplitude at $\approx 36^\circ$ (with $H_s = 1.8$ and $h = 50$) is corroborated by results here that not only does the maximum amplitude increase, but the frequency of rogue waves in the sea state also increases as a result; which is to be expected in a situation of peak amplitude waves.

6 Conclusions

In this paper, the main aims were to provide an introduction to the Korteweg de Vries equation types, provide examples of their application to real world events, to extend them using more realistic parameters like surface tension and finally to provide motivation for equations that extend the existing models to improve their accuracy further, and show that alternate models can be used to complement existing models.

In regards to the inclusion of surface tension effects, the Bernoulli condition in the general non-dimensional KdV equation was extended to include a surface tension parameter, which was solved analytically to discover that the inclusion of surface tension for the one-dimensional KdV equation results in the transformation from an elevation $+\operatorname{sech}^2$ wave into a depressive $-\operatorname{sech}^2$ wave. This was found to not match the expected result of surface tension observed in the real world and for analytical solutions for higher order equations such as the Boussinesq equation as given in papers [37] and [26] respectively. The latter detailed how increasing surface tension is expected to initially reduce the width of the soliton, and then beyond the limit of $\gamma > B_0 = \frac{1}{3}$ the inclusion of surface tension results in transforming the soliton into a depressive wave, where increasing surface tension effects further will increase the width of the depressive soliton; however, wave tank simulations also found how increasing surface tension will impact the farfield (area outside the wavefront) and develop ripples that act similarly to a dissipating sinusoidal function. To match this, a new numerical solution form was introduced using the fourth order Runge-Kutta method, where incorporating surface tension up until the limit given by $\gamma = B_0$ before was shown to introduce such oscillations, but not beyond that limit, and would reach unrealistic levels of oscillations far from the incident soliton(s) as the system approached that limit, so further investigations are needed into re-applying these methods to higher order KdV equations, such as the Sawada-Kotera or Kaup-Kupershmidt models, to see how the introduction of the analytical surface tension effects will impact the resulting sech^2 soliton waves. In a similar vein to this, the KdV system could also be tested with a new numerical solution type other than the fourth-order Runge-Kutta to see if the original high surface-tension form of $u_t - 6uu_x + u_{xxx} = 0$ can be effectively represented numerically. However, it was found that by applying a new method known as Hirota's Bilinear method to

the unsimplified non-dimensional form of the KdV equation with a periodic solution ansatz, that the solution can be made to exhibit the correct surface tension effects, which was again the case for inclusion of surface tension for the KP equation. This showed how inclusion of surface tension can be more effectively achieved by applying a sinusoidal solution ansatz in Hirota's method instead of incorporating surface tension in the analytical solution form. Further research in this field is highly recommended to find which parameters from both the periodic and linear ansatz for the function f in Hirota's method contributed the most towards the farfield oscillations, and whether these can be applied to higher-order KdV systems of equations.

Applying a periodic solution ansatz in the two-dimensional extension to the KdV equation was also shown to permit a new solution type, known as the Breather wave, where taking periodicity to ∞ resulted in an isolated lump soliton, which proved to be a very effective means of representing a rogue wave, whereas taking periodicity to 0 resulted in the original line-soliton, proving how versatile this solution form is. This wasn't found to be exclusive to periodic solutions, however, since the associated literature also suggests solution forms of simply linear equations in x , y and t can achieve similar results, and so this must be investigated further to find which parameters in the Hirota f ansatz are necessary to produce both line/lump solitons and surface tension effects in the farfield.

The introduction of Hirota's form also had other benefits, such as isolating the amplification factor of interacting solitons, and so the different situations that lead to destructive and constructive interactions could be explored better. This allows a model for the maximum amplification to be found, which was later compared to the Coupled Non-Linear Schrödinger equation to find that for a standard rogue wave inducing scenario, both the maximum amplification and probability of a rogue wave occurring (based on excess kurtosis from the Gaussian model) happen at around a 35° to 40° angle bisecting the two incident wavefronts. This research can be extended further to find whether this occurs for different wave states, and whether other models such as the Benney-Luke, Sawada-Kotera or Kaup-Kuperschmidt exhibit the same effects, and what amplification these models suggest happens there.

This focus on the NLS equation also resulted in the discovery of a prediction parameter for

the appearance of rogue waves in the form of the Benjamin-Feir Index, which can be applied given knowledge of datum such as the significant wave height and wave frequencies to give an indication of the probability of the occurrence of a rogue wave when compared to the standard Gaussian distribution of wave heights. This index was extended to the coupled system of equations, but not to other predicting parameters; namely the crest-trough correlation being the most popular, with many others being suggested in the referenced literature, which allows for further research from the perspective of a statistical overview.

In summary, this paper has introduced the most famous models concerning rogue waves, alongside different solution forms, methods of introducing surface tension, and explored notable interactions between solitons and why these effects happen, alongside providing motivation for expansion in theoretical research for both the introduction of surface tension without introducing a tension force, and in comparisons between maximum amplification angles for different models.

A Modifications to Referenced Code

A.1 KdV Solitons Using Fourth Order Runge-Kutta (MatLab)

This is the modified code from book [2] to incorporate surface tension effects on a surface plot.

```
N=256;  
dt=0.4/N^2;  
x=(2*pi/N)*(-N/2:N/2-1)';  
A=40;  
B=30;  
clf;  
drawnow  
u=3*A^2*sech(.5*(A*(x+2))).^2+3*B^2*sech(.5*(B*(x+1))).^2;  
v=fft(u);  
k=[0:N/2-1 0 -N/2+1:-1]';  
ik3=1i*k.^3;  
  
tmax=0.03;  
nplt=floor((tmax/25)/dt);  
nmax=round(tmax/dt);  
udata=u;  
tdata=0;  
h=waitbar(0,'please wait..');  
for n=1:nmax  
    t=n*dt;  
    g=-0.1i*dt*k;  
    E=exp(dt*ik3/2);  
    E2=E.^2;  
    a=g.*fft(real(ifft(v)).^2);
```

```

b=g.*fft ( real( ifft (E.* (v+a/2))).^2);
c=g.*fft ( real( ifft (E.* v+b/2)).^2);
d=g.*fft ( real( ifft (E2.*v+E.*c)).^2);
v=E2.*v+(E2.*a+2*E.* (b+c)+d)/6;
if mod(n, nplt)==0
    u=real( ifft (v));
    waitbar(n/nmax);
    udata=[udata u];
    tdata=[tdata t];
end
surf(x, tdata, udata , "linestyle ", ":"), view(-20,15)
xlabel x, ylabel t, axis([-pi pi 0 tmax -1000 3000]), grid off
set(gca, 'ztick ',[0 2000]), close(h), pbaspect([1 1 .13]);
title(['Plot for $u_t+(\frac{1}{10}uu_x)+u_{xxx}=0$ with $K=40$ and $30$']);

```

References

- [1] Ablowitz, M. J.; Nonlinear Dispersive Waves: Asymptotic Analysis and Solitons; Cambridge: Cambridge University Press; 2011.
- [2] Trefethen, L. N.; Spectral Methods in MATLAB; Philadelphia, Pa.: Society for Industrial and Applied Mathematics, 2000.
- [3] Johnson, R. S.; A Modern Introduction to the Mathematical Theory of Water Waves. Cambridge, New York, N.Y.: Cambridge University Press, 1997.
- [4] Mouassom, L. F.; Nkomom, T. N.; Mvogo, A.; Mbane, C. B.; Effects of viscosity and surface tension on soliton dynamics in the generalized KdV equation for shallow water waves. Communications in Nonlinear Science and Numerical Simulation, Volume 102. Journal.: Elsevier, 2021.
- [5] Häfner, D.; Gemmrich, J.; Jochum, M.; Real-world rogue wave probabilities. Sci Rep 11, 10084 (2021). <https://doi.org/10.1038/s41598-021-89359-1>
- [6] Kraaiennest; Images; [https://en.wikipedia.org/wiki/Dispersion_\(water_waves\)](https://en.wikipedia.org/wiki/Dispersion_(water_waves)); Accessed 24/4/23.
- [7] Serio, M.; Onorato, M.; Osborne, A.; Janssen, P.; (2005). On the computation of the Benjamin-Feir Index. Nuovo Cimento della Societa Italiana di Fisica C. 28. 893-903. 10.1393/ncc/i2005-10134-1.
- [8] Meylan M.; Nonlinear PDE's Course. University of Newcastle, New South Wales, Australia. (2022). https://wikiwaves.org/Introduction_to_KdV. Accessed 3/12/22
- [9] Ablowitz, M. J.; Baldwin, D. E.; Nonlinear shallow ocean-wave soliton interactions on flat beaches; Department of Applied Mathematics, University of Colorado, USA; 2012; <https://journals.aps.org/pre/abstract/10.1103/PhysRevE.86.036305>; Accessed 9/12/22
- [10] Anco, S.; Willoughby, M. R.; KdV Solitons; Brock University, Canada; 2022; http://lie.math.brocku.ca/_sanco/solitons/kdv_solitons.php; Accessed 5/12/22.

- [11] Wazwaz, A. M.; Multiple-soliton solutions for the KP equation by Hirota's bilinear method and by the tanh–coth method; *Applied Mathematics and Computation*, Volume 190, Issue 1, 2007, Pages 633-640, ISSN 0096-3003, <https://doi.org/10.1016/j.amc.2007.01.056>. (<https://www.sciencedirect.com/science/article/pii/S0096300307000975>); Accessed 9/12/22.
- [12] Hereman, W.; Nuseir, A.; Symbolic methods to construct exact solutions of nonlinear partial differential equations; Department of Mathematical and Computer Sciences, Colorado School of Mines, Colorado, USA.; (1997); Elsevier. <https://www.sciencedirect.com/science/article/pii/S0378475496000535>; Accessed 9/12/22.
- [13] King, T.; Ong, C. T.; Isa, M.; (2006). Two-Soliton Solutions Of The Kadomtsev-Petviashvili Equation. *Jurnal Teknologi*. 44. 10.11113/jt.v44.365. https://www.researchgate.net/publication/239768652_Two-Soliton_Solutions_Of_The_Kadomtsev-Petviashvili_Equation; Accessed 26/1/23.
- [14] Bitner-Gregersen, E. M.; Toffoli, A.; On the probability of occurrence of rogue waves, *Nat. Hazards Earth Syst. Sci.*, 12, 751–762, <https://doi.org/10.5194/nhess-12-751-2012>, 2012. <https://nhess.copernicus.org/articles/12/751/2012/>; Accessed 28/1/23.
- [15] Reliability Hotwire eMagazine; Issue 14 (April 2002); ReliaSoft Corporation; <https://www.weibull.com/hotwire/issue14/relbasics14.htm>; Accessed 28/1/23.
- [16] Rosenthal, W.; and Lehner, S.; (June 6, 2008); "Rogue Waves: Results of the MaxWave Project." *ASME. J. Offshore Mech. Arct. Eng.* May 2008; 130(2): 021006. <https://doi.org/10.1115/1.2918126>; Accessed 28/1/23.
- [17] Serio, M.; Onorato, M.; Osborne, A.; Janssen, P.; (2005).; On the computation of the Benjamin-Feir Index. *Nuovo Cimento della Societa Italiana di Fisica C*. 28. 893-903. 10.1393/ncc/i2005-10134-1; https://www.researchgate.net/publication/233414477_On_the_computation_of_the_Benjamin-Feir_Index; Accessed 29/1/23.

- [18] Mei, C. C.; The Applied Dynamics of Ocean Surface Waves; John Wiley, New York; 2000; p615.
- [19] Akhmediev, N.; (2021); Waves that Appear From Nowhere: Complex Rogue Wave Structures and Their Elementary Particles. *Front. Phys.* 8:612318. doi: 10.3389/fphy.2020.612318; Accessed 30/1/23
- [20] Zhenhui, X.; Hanlin, C.; Zhengde D.; Rogue wave for the (2+1)-dimensional Kadomtsev–Petviashvili equation; *Applied Mathematics Letters*, Volume 37, 2014, Pages 34-38, ISSN 0893-9659; <https://www.sciencedirect.com/science/article/pii/S0893965914001463>; Accessed 31/1/23.
- [21] Kristian Dysthe, K.; Krogstad, H.; Müller, P.; Oceanic Rogue Waves; 2008; Journal Article; Annual Review of Fluid Mechanics; 287-310 <https://www.annualreviews.org/doi/abs/10.1146/annurev.fluid.40.111406.102203>; Accessed 4/2/23.
- [22] Stuhlmeier, R.; (2009); KDV theory the chilean tsunami of 1960; *Discrete and Continuous Dynamical Systems-series B - DISCRETE CONTIN DYN SYS-SER B.* 12. 623-632. 10.3934/dcdsb.2009.12.623.; https://rstuhlmeier.github.io/publications/My_Publications/KdVChileanTsunami_2009.pdf; Accessed 4/2/23.
- [23] Bryant, E.; Tsunami: The underrated hazard; Springer-Praxis books, Springer, Berlin; 2008.
- [24] National Oceanic and Atmospheric Administration; 'Southern Chile Earthquake and Tsunami, 22 May 1960'; Article; National Centers for Environmental Information (NCEI); E/NE42 325 Broadway, Boulder, Colorado USA 80305 <https://www.ngdc.noaa.gov/hazard/22may1960.html>; Accessed 11/2/23.

- [25] Yoneyama, T.; The Korteweg-de Vries Two-Soliton Solution as Interacting Two Single Solitons, Progress of Theoretical Physics, Volume 71, Issue 4, April 1984, Pages 843–846; <https://doi.org/10.1143/PTP.71.843>; Accessed 24/3/23.
- [26] Milewski, P.; (2005); Three-dimensional Localized Solitary Gravity-Capillary Waves; Comm. Math. Sci.. 3. 10.4310/CMS.2005.v3.n1.a6; https://www.researchgate.net/publication/38327194_Three-dimensional_Localized_Solitary_Gravity-Capillary_Waves; Accessed 25/3/23.
- [27] Kumar, S.; Mohan, B.; Partial Differential Equations in Applied Mathematics; A novel and efficient method for obtaining Hirota's bilinear form for the nonlinear evolution equation in (n+1) dimensions; Journal; 2023; <https://www.sciencedirect.com/journal/partial-differential-equations-in-applied-mathematics>; Accessed 26/3/23.
- [28] Hirota, R.; (2004); The direct method in soliton theory (No. 155); Cambridge University Press.
- [29] Peterson, P.; Soomere, T.; Engelbrecht, J.; van Groesen, E; Soliton interaction as a possible model for extreme waves in shallow water; Nonlin. Processes Geophys.; 10, 503–510, <https://doi.org/10.5194/npg-10-503-2003>, 2003; Accessed 22/4/23.
- [30] Kumar, S.; Mohan, B.; A study of multi-soliton solutions, breather, lumps, and their interactions for kadomtsev-petviashvili equation with variable time coefficient using hirota method; Published 24 November 2021; IOP Publishing Ltd; Physica Scripta, Volume 96, Number 12; Phys. Scr. 96 125255; DOI 10.1088/1402-4896/ac3879; Accessed 22/4/23.
- [31] Dysthe, K.; Krogstad, H.; Müller, P.; (2008); Oceanic Rogue Waves; Annual Review of Fluid Mechanics; 40. 287-310; <https://www.annualreviews.org/doi/pdf/10.1146/annurev.fluid.40.111406.102203>; Accessed 23/4/23.
- [32] Ma, Y. C.; (1979); The Perturbed Plane-Wave Solutions of the Cubic Schrödinger Equation; Studies in Applied Mathematics, 60, 43-58; <https://doi.org/10.1002/sapm197960143>; Accessed 24/4/23.

- [33] Dysthe, K.; Trulsen K.; (1999); Note on Breather Type Solutions of the NLS as Models for Freak-Waves. *Physica Scripta*. T82. 48. 10.1238/Physica.Topical.082a00048; Accessed 25/4/23.
- [34] Choi, J.; Bokhove, O.; Kalogirou, A.; Kelmanson, M. A.; (2022); Numerical Experiments on Extreme Waves Through Oblique–Soliton Interactions; *Water Waves*, 4(2), 139–179; <https://doi.org/10.1007/s42286-022-00059-3>; Accessed 26/4/23.
- [35] Peterson, P.; Groesen, E.; (2001); Sensitivity of the inverse wave crest problem; *Wave Motion*. 34. 391-399. 10.1016/S0165-2125(01)00076-2; Accessed 26/4/23.
- [36] Peter Janssen, P.; Bidlot J. R.; (2009); On the extension of the freak wave warning system and its verification; ECMWF Technical Memoranda, 588, 42; <https://www.ecmwf.int/node/10243>; 10.21957/uf1sybog; Accessed 26/4/23.
- [37] Falcon, E.; Laroche, C.; Fauve, S.; (2002); Observation of Depression Solitary Surface Waves on a Thin Fluid Layer; Physical review letters. 89. 204501. 10.1103/PhysRevLett.89.204501; <https://journals.aps.org/prl/abstract/10.1103/PhysRevLett.89.204501>; Accessed 27/4/23.
- [38] Peterson, P.; van Groesen, E.; (2000); A direct and inverse problem for wave crests modelled by interactions of two solitons; *Physica D: Nonlinear Phenomena*, Volume 141, Issues 3–4, 2000, Pages 316-332, ISSN 0167-2789; <https://www.sciencedirect.com/science/article/pii/S0167278900000373>; Accessed 3/5/23.
- [39] Liu, S.; Zhang, X.; A modified Benjamin-Feir index for crossing sea states; 35th International Workshop on Water Waves and Floating Bodies; State Key Laboratory of Ocean Engineering, Shanghai Jiao Tong University, China; http://www.iwwwfb.org/Abstracts/iwwwfb35/iwwwfb35_27.pdf; Accessed 5/5/23.
- [40] Bitner-Gregersen, E. M.; Toffoli, A.; (2014); Occurrence of rogue sea states and consequences for marine structures; *Ocean Dynamics*. 64. 1457-1468. 10.1007/s10236-

014-0753-2; <https://link.springer.com/article/10.1007/s10236-014-0753-2>; Accessed 5/5/23.

- [41] Onorato, M.; Osborne, A. R.; Serio, M.; (2006); Modulational Instability in Crossing Sea States: A Possible Mechanism for the Formation of Freak Waves; Journal, Phys. Rev. Lett., volume 96, issue 1; American Physical Society; <https://link.aps.org/doi/10.1103/PhysRevLett.96.014503>; Accessed 5/5/23.
- [42] Fedele, F.; (2015); On the kurtosis of deep-water gravity waves; Journal of Fluid Mechanics (submitted); 10.1017/jfm.2015.538; <https://www.cambridge.org/core/services/aop-cambridge-core/content/view/7DE34CF393A3E9A928208A48ACA2C05D/S0022112015005388a.pdf/on-the-kurtosis-of-deep-water-gravity-waves.pdf>; Accessed 7/5/23.
- [43] Shukla, P.; Kourakis, I.; Eliasson, B.; Marklund, M.; Stenflo, L.; (2006); Instability and evolution of nonlinearly interacting water waves; Phys Rev Lett 97:94501; doi:10.1103/PhysRevLett. 97.094501; <https://journals.aps.org/prl/pdf/10.1103/PhysRevLett.97.094501>; Accessed 7/5/23.
- [44] Stewart, R; Ocean Wave Spectra; Introduction to Physical Oceanography; New Zealand Institute of Mathematics and its Applications; https://wikiwaves.org/Ocean-Wave_Spectra; Accessed 9/5/23.
- [45] Hietarinta, J.; Introduction to the Hirota bilinear method; Integrability of Nonlinear Systems, pages 95–103; Springer Berlin Heidelberg; <https://arxiv.org/abs/solv-int/9708006>; Accessed 10/5/23.
- [46] Alquran, M.; Alhami, R.; (2022); Analysis of lumps, single-stripe, breather-wave, and two-wave solutions to the generalized perturbed-KdV equation by means of Hirota's bilinear method; Nonlinear Dyn 109, 1985–1992; <https://doi.org/10.1007/s11071-022-07509-0>; Accessed 10/5/23.
- [47] Anker, D.; Freeman, N; (1978); Interpretation of three-soliton interactions in terms of resonant triads; Journal of Fluid Mechanics, 87(1), 17-31;

doi:10.1017/S0022112078002906; <https://www.cambridge.org/core/journals/journal-of-fluid-mechanics/article/interpretation-of-threesoliton-interactions-in-terms-of-resonant-triads/A9D233F6337DB746A9C63986C1471A85>; Accessed 11/5/23.

- [48] Wazwaz, A. M.; (2020); Two new integrable Kadomtsev–Petviashvili equations with time-dependent coefficients: multiple real and complex soliton solutions; Waves in Random and Complex Media, 30:4, 776–786; DOI: 10.1080/17455030.2018.1559962; <https://www.tandfonline.com/doi/full/10.1080/17455030.2018.1559962>; Accessed 12/5/23.
- [49] Akhmediev, N. N.; Eleonskii, V. M.; Kulagin, N. E.; (1987); Exact first-order solutions of the nonlinear Schrödinger equation; Theor Math Phys 72, 809–818; <https://doi.org/10.1007/BF01017105>; <https://people.physics.anu.edu.au/nna124/TMF1987.pdf>; Accessed 12/5/23.
- [50] Zakharov, V. E.; (1972); Stability of periodic waves of finite amplitude on the surface of a deep fluid; Journal of Applied Mechanics and Technical Physics, 9(2), 190–194; <https://doi.org/10.1007/bf00913182>; <https://www.scinapse.io/papers/2090885565>; Accessed 13/5/23.
- [51] Uthayakumar, T.; Al Sakkaf, L.; Al Khawaja, U.; (2020); Peregrine Solitons of the Higher-Order, Inhomogeneous, Coupled, Discrete, and Non-local Nonlinear Schrödinger Equations; Frontiers in Physics, Volume 8; <https://www.frontiersin.org/articles/10.3389/fphy.2020.596886>; Accessed 13/5/23.
- [52] Ma, W. X.; (2015); Lump solutions to the Kadomtsev–Petviashvili equation; Physics Letters A, Volume 379, Issue 36, Pages 1975–1978, ISSN 0375-9601; <https://doi.org/10.1016/j.physleta.2015.06.061>; <https://www.sciencedirect.com/science/article/pii/S0375960115005800>; Accessed 13/5/23.
- [53] Gemmrich, J.; Cicon, L.; Generation mechanism and prediction of an observed extreme rogue wave; Sci Rep. 2022 Feb 2;12(1):1718; doi:

10.1038/s41598-022-05671-4. PMID: 35110586; PMCID: PMC8811055.;
<https://www.ncbi.nlm.nih.gov/pmc/articles/PMC8811055/>; Accessed 13/5/23.

- [54] Teutsch, I.; Weisse, R.; Moeller, J.; Krueger, O.; (2020); A statistical analysis of rogue waves in the southern North Sea; Nat. Hazards Earth Syst. Sci., 20, 2665–2680; <https://doi.org/10.5194/nhess-20-2665-2020>; <https://nhess.copernicus.org/articles/20/2665/2020/>; Accessed 13/5/23.
- [55] Toffoli, A.; Bitner-GregerSEN, E. M.; Osborne, A. R.; Serio, M.; Monbaliu, J.; Onorato, M; (2011); Extreme waves in random crossing seas: Laboratory experiments and numerical simulations; Geophys. Res. Lett., 38, L06605; <https://agupubs.onlinelibrary.wiley.com/doi/epdf/10.1029/2011GL046827>; Accessed 13/5/23.
- [56] Chabchoub, A.; Hoffmann, N.; Onorato, M.; Akhmediev, N.; (2012); Super Rogue Waves: Observation of a Higher-Order Breather in Water Waves; Phys. Rev. X Journal, volume 2, issue 1, pages 011015, numpages 6; American Physical Society; <https://journals.aps.org/prx/pdf/10.1103/PhysRevX.2.011015> ; Last Accessed 14/5/23.
- [57] Chabchoub, A.; Hoffmann, N. P.; Akhmediev, N.; (2011); Rogue Wave Observation in a Water Wave Tank; Phys. Rev. Lett. Journal, volume 106, issue 20; American Physical Society; <https://journals.aps.org/prl/pdf/10.1103/PhysRevLett.106.204502>; Last Accessed 14/5/23.
- [58] Dingemans, M. W.; (2000); Water Wave Propagation Over Uneven Bottoms: Linear wave propagation; Part 1, isbn 9789810239947, Advanced series on ocean engineering; World Scientific Pub.; <https://books.google.co.uk/books?id=vlwzIFk1ETIC>; Accessed 14/5/23.